

DIPYRIDOPHENAZINE COMPLEXES OF RUTHENIUM(II) AS
LUMINESCENT REPORTERS OF DNA

Thesis by
Yonchu Jenkins

In Partial Fulfillment of the Requirements
for the Degree of
Doctor of Philosophy

California Institute of Technology
Pasadena, California

1996

(Submitted January 19, 1996)

ACKNOWLEDGEMENT

I am leaving Caltech with many fond memories and so I wish to thank those responsible for making my time here such a pleasant one. First of all, I would like to express my gratitude to my research advisor, Prof. Jackie Barton. In addition to all of the great science I learned while in her laboratory, more importantly, I acquired confidence in myself and my ability to accomplish things. I owe much of this to Jackie's constant support and encouragement. When I started graduate school, I really didn't think myself capable of finishing. Thanks to Jackie, I am leaving with much more than a Ph.D.

I would like to thank my undergraduate advisor, Prof. Tetsuo Otsuki, at Occidental College for his enthusiasm and his dedication to teaching science. It was Dr. O who first showed me that research is fun. Prof. Frank DeHaan, my general chemistry professor, I am also indebted to. His love of teaching is what first drew me into chemistry and even now, he still continues to serve as a role model for me.

The members of the Barton group, past and present, I would like to thank for their friendship, their persistent willingness to help me, and for overlooking the fact that I am a less than average softball player. I have had a lot of fun being in the Barton group and although I don't think that I will miss being at Caltech, I will miss being with the group.

Susanne Lin I would like to thank for spending so much of her time helping me with the computers. Dr. Cathy Murphy showed me around when I started and then she kept the HPLCs running so that I could keep working. After Cathy left, Michelle Arkin took over the thankless job of tending the HPLCs and I know that I have pulled her away from her own experiments many times. Michelle I also have to thank for many helpful discussions. Without Michelle's help, some of my work would not have been possible. I also want to thank my coffee and ice cream break partner, Ai Ching Lim, for always cheerfully agreeing to play hooky for a little bit. To Mo Renta, I am grateful for making my life run a bit more smoothly.

Outside of the Barton group, I wish to thank Jerome Claverie, Jack Mizoguchi, Gary Mines, and Don Low for all of the wonderful times that we've shared. I will miss them all immensely. I thank Dian Buchness for always being so friendly and for her ever present smile.

I will always be grateful to my parents. None of this would have been possible without the love and support which they've provided in abundance. I could never say enough about how much they mean to me.

Last but not least, I wish to thank Toshi for his continuous love and support and for always being there.

ABSTRACT

The search for novel diagnostics for DNA detection has generated interest in the potential applications of polypyridyl complexes of ruthenium(II). Recently, it was reported that dipyridophenazine complexes of ruthenium(II) may serve as molecular light switches for DNA. These complexes, which bind DNA avidly through intercalation, show no luminescence in aqueous solutions. Upon intercalation into double-helical DNA and the concomitant protection of the phenazine ring from quenching by interaction with water, intense photoluminescence is apparent. The light switch effect as a function of nucleic acid sequence and conformation was examined for $[\text{Ru}(\text{phen})_2\text{dppz}]^{2+}$ and $[\text{Ru}(\text{bpy})_2\text{dppz}]^{2+}$. The emission properties of these complexes were found to be extremely sensitive to the nature of the intercalation environment with strong correlations between the luminescence parameters and the level of water protection afforded by the double helix. In order to impart sequence specificity to the light switch effect, various methods have been developed for appending a functionalized $[\text{Ru}(\text{phen})_2\text{dppz}]^{2+}$ to the 5' terminus of oligonucleotides, both on the solid support and in solution. Assays for analyzing the structural integrity of the resulting conjugates are described. These ruthenated oligonucleotides can serve as enzyme substrates, enabling the construction of long metalated oligonucleotides not easily prepared using chemical synthesis. In order to evaluate their utility as useful DNA diagnostics, a series of ruthenated oligonucleotides were synthesized and their photophysical properties characterized. Biochemical analysis of oligonucleotide duplexes containing ruthenated strands showed no significant structural perturbation of the duplex as a result of the ruthenium modification. The overall results of this investigation suggest that an oligonucleotide functionalized with a dppz complex of ruthenium may be used to target single-stranded DNA in a sequence-specific fashion and that this derivative could be extremely valuable in the development of novel hybridization probes for both heterogeneous and homogeneous assays.

TABLE OF CONTENTS

ACKNOWLEDGEMENT.....	ii
ABSTRACT.....	iv
TABLE OF CONTENTS.....	v
LIST OF FIGURES.....	ix
LIST OF TABLES.....	xiii
LIST OF SCHEMES.....	xiv

Chapter 1:

The Development of Ruthenium(II) Polypyridyl Complexes as Spectroscopic Probes for DNA.....	1
1.1. Introduction	1
1.2. Binding of $[\text{Ru}(\text{phen})_3]^{2+}$ to DNA.....	2
1.2.1. Studies Based Upon Properties of the Metal Complex.....	6
1.2.2. Changes Observed in DNA Resulting From Complex Binding.....	13
1.2.3. Enantioselectivity in Binding.....	14
1.2.3. Structural Studies Based Upon $^1\text{H-NMR}$	19
1.3. Development of Ruthenium Probes Targeted Against Specific DNA Conformations.....	24
1.4. Dppz Complexes of Ruthenium(II)	
Molecular Light Switches for DNA.....	32
References	36

Chapter 2:

Characterization of the Interactions of Dppz Complexes of Ruthenium(II) with Nucleic Acids	40
2.1. Introduction	40
2.2. Experimental	42
2.3. Results	44
2.3.1. Unwinding of Supercoiled DNA.....	44
2.3.3. Anionic Quenching of Ruthenium Complexes in the Presence of DNA	52
2.3.4. Sequence Dependence of the Emission.....	56
2.3.5. Cleavage of pUC18 Restriction Fragments By $^1\text{O}_2$ Generated From Photoexcited $[\text{Ru}(\text{phen})_2\text{dppz}]^{2+}$	58
2.3.6. Variation in Emission Characteristics with Double Helical Conformation	66
2.3.7. Binding to a Triple Helix	70
2.3.8. Binding to tRNA^{Phe}	73
2.4. Discussion	73
2.4.1. Mode of Binding to DNA for Dppz Complexes of Ruthenium(II).....	73
2.4.2. Sequence-specificity of $[\text{Ru}(\text{phen})_2\text{dppz}]^{2+}$	75
2.4.3. Comparison of Luminescent Parameters for $[\text{Ru}(\text{phen})_2\text{dppz}]^{2+}$ and $[\text{Ru}(\text{bpy})_2\text{dppz}]^{2+}$	75
2.4.4. Correlation of Conformational Luminescence Parameters with Water Protection.....	76
2.5. Conclusions.....	79
References	81

Chapter 3:

Synthesis and Characterization of Ruthenium-Oligonucleotide Conjugates	84
3.1. Introduction	84
3.2. Experimental	87
3.3. Results and Discussion.....	95
3.3.1. Synthesis of the Functionalized Ruthenium Complex, [Ru(phen') ₂ dppz] ²⁺	95
3.3.2. Synthetic Strategies.....	101
3.3.3. Characterization of Oligonucleotides Appended at the 5' Terminus With [Ru(phen') ₂ dppz] ²⁺	113
3.3.4. Generation of Longer Ruthenated Oligonucleotides.	122
3.4. Conclusion.....	125
References	129

Chapter 4:

Biochemical and Photophysical Characterization of Oligonucleotide Duplexes Covalently Modified By [Ru(phen') ₂ dppz] ²⁺	131
4.1. Introduction	131
4.2. Experimental	132
4.3. Results and Discussion.....	133
4.3.1. Examination of the Structural Integrity of Ruthenated Duplexes.....	133
4.3.2. Luminescence Characterization of Ruthenated Oligonucleotides.....	149
4.3.3. Ru-NH(CH ₂) ₆ OPO ₂ AGTGCCAAGCTTGCA-3' as a Novel Hybridization Probe.....	167
4.4. Implications for Diagnostic Application.....	177

	viii
4.5. Conclusion.....	179
References.....	180

LIST OF FIGURES

Chapter 1:

1.1. Structures of Λ - and Δ -[Ru(phen) ₃] ²⁺	3
1.2. Binding Modes of Octahedral Coordination Complexes to B-form DNA.....	4
1.3. Stereoselectivity in Binding to B-form DNA of Λ - and Δ -[Ru(phen) ₃] ²⁺	7
1.4. Luminescence Spectra of [Ru(phen) ₃] ²⁺ and its Enantiomers in the Presence of DNA.....	9
1.5. EPR Spectrum of [Ru(phen) ₂ phen-TEMPO] ²⁺ in the Presence of DNA.....	12
1.6. CD Spectra of [Ru(phen) ₃] ²⁺ After Equilibrium Dialysis Against B- and Z-form DNA.....	15
1.7. Luminescence Quenching by Ferrocyanide and Steady-State Luminescence Polarization of [Ru(phen) ₃] ²⁺ Enantiomers Bound to DNA.....	17
1.8. ¹ H-NMR Spectra of d(GTGCAC) ₂ in the Absence and Presence of Racemic [Rh(phen) ₃] ²⁺	22
1.9. Variation in Chemical Shift for Oligonucleotide Proton Resonances Upon Titration of d(GTGCAC) ₂ With [Ru(phen) ₃] ²⁺ Enantiomers.....	23
1.10. Structures of A-, B-, and Z-DNA.....	25
1.11. Structure of [Ru(DIP) ₃] ²⁺	27
1.12. Structure of [Ru(TMP) ₃] ²⁺ and Equilibrium Dialysis of [Ru(TMP) ₃] ²⁺ Bound to B- and A-form Nucleic Acids.....	30
1.13. Structure of [Ru(bpy) ₂ dppz] ²⁺ and Emission Spectra of [Ru(bpy) ₂ dppz] ²⁺ in the Absence and Presence of B-DNA.....	34

Chapter 2:

2.1. Structures of $[\text{Ru}(\text{phen})_2\text{dppz}]^{2+}$ and $[\text{Ru}(\text{bpy})_2\text{dppz}]^{2+}$	41
2.2. Unwinding of pBR322 DNA by $[\text{Ru}(\text{bpy})_2\text{dppz}]^{2+}$ After Incubation With Topoisomerase I.....	46
2.3. Luminescence Quenching of $[\text{Ru}(\text{phen})_2\text{dppz}]^{2+}$ in Acetonitrile By H_2O and D_2O	49
2.4. Luminescence Quenching of $[\text{Ru}(\text{phen})_3]^{2+}$ and $[\text{Ru}(\text{phen})_2\text{dppz}]^{2+}$ in the Presence of DNA By Ferrocyanide	54
2.5. $^1\text{O}_2$ Mediated Photocleavage of pUC18 140 Base Pair Restriction Fragment By $[\text{Ru}(\text{phen})_2\text{dppz}]^{2+}$ and Its Enantiomers.....	60
2.6. $^1\text{O}_2$ Mediated Photocleavage of pUC18 180 Base Pair Restriction Fragment By $[\text{Ru}(\text{phen})_2\text{dppz}]^{2+}$ and Its Enantiomers.....	62
2.7. Histograms of 180mer Photocleavage Gel.....	64
2.8. Schematic Diagram of $[\text{Ru}(\text{bpy})_2\text{dppz}]^{2+}$ Bound to Different Oligomers.....	71
2.9. Luminescence of $[\text{Ru}(\text{bpy})_2\text{dppz}]^{2+}$ Bound to tRNA^{Phe} on Titration With $[\text{Rh}(\text{phen})_2\text{phi}]^{3+}$	74
2.10. Models Illustrating Intercalation By $[\text{Ru}(\text{phen})_2\text{dppz}]^{2+}$ Into DNAs of Different Conformations.....	77

Chapter 3:

3.1. Representative Ruthenated Oligonucleotide.....	85
3.2. Structure of $[\text{Ru}(\text{phen}')_2\text{dppz}]^{2+}$	96
3.3. ^1H -NMR Spectra of the Three Isomers of $[\text{Ru}(\text{phen}')_2\text{dppz}]^{2+}$	99
3.4. Structures of Aminoalkyl Phosphodiester and Aminoalkyl Carbamate Linkers.....	102
3.5. HPLC Chromatograms of FPLC and non-FPLC Purified Coupling	

Reactions	110
3.6. Absorption Spectra of Ru-NH(CH ₂) ₆ NHCO ₂ AGAAGGCCTGGT-3' and [Ru(phen') ₂ dppz] ²⁺	114
3.7. HPLC Chromatograms of Ru-NH(CH ₂) ₉ NHCO ₂ -AGTCTAGGCCTATCGT-3' and Unmodified Oligonucleotide After Incubation With Snake Venom Phosphodiesterase and Alkaline Phosphatase.....	117
3.8. ESI-MS of Ru-NH(CH ₂) ₉ NHCO ₂ AGTGTATATAAACGT-3'	119
3.9. MALDI-TOF Mass Spectrum of Ru-NH(CH ₂) ₉ CO ₂ -AGTCTTATATAAAATATCGT-3'.....	120
3.10. Extension of Ru-NH(CH ₂) ₆ NHCO ₂ AGAAGGCCTGGT-3' Using Sequenase.....	123
3.11. Ligation of Ru-NH(CH ₂) ₆ NHCO ₂ AGAAGGCCTGGT-3' to Phosphorylated Oligonucleotide.....	126

Chapter 4:

4.1. Hybridization of Ru-NH(CH ₂) ₉ NHCO ₂ AGTCTGTAAACATCGT-3' to Complementary Strand.....	134
4.2. Hybridization of Ru-NH(CH ₂) ₉ NHCO ₂ AGTGTATATAAACGT-3' to Both Complementary Strand and 5'-Rhodium Labeled Complementary Strand.....	137
4.3. Hybridization of Ru-NH(CH ₂) ₉ NHCO ₂ -AGTCTAGGCCTATCGT-3' to Both Complementary Strand and 5'-Rhodium Labeled Complementary Strand	139
4.4. Thermal Denaturation Profiles of Duplex Containing Ru-NH(CH ₂) ₉ NHCO ₂ AGTGCGAAG-3', Noncovalent Analogue, and Unmodified Duplex.....	143

4.5. Luminescence Titrations of Free $[\text{Ru}(\text{phen})_2\text{dppz}]^{2+}$ Into Duplex Containing Ru-NH(CH ₂) ₉ NHCO ₂ AGTGTATATAACGT-3' and Unmodified Duplex.....	147
4.6. Luminescence Titrations of Free $[\text{Ru}(\text{phen})_2\text{dppz}]^{2+}$ Into Duplex Containing Ru-NH(CH ₂) ₉ NHCO ₂ AGTCTAGGCCTATCGT-3' and Unmodified Duplex.....	148
4.7. Luminescence of Ru-NH(CH ₂) ₆ NHCO ₂ AGAAGGCCTGGT-3', Ruthenated Duplex, and Noncovalently Bound Analogues at 26°C 37°C.....	169
4.9. Emission Spectra of Ru-NH(CH ₂) ₆ OPO ₂ - AGTGCCAAGCTTGCA-3', Hybridized Duplex, and in the Presence of a Noncomplementary Strand.....	171
4.10. Dilution of Ruthenated 15mer Duplex.....	173
4.11. Luminescence Titrations of Free $[\text{Ru}(\text{phen})_2\text{dppz}]^{2+}$ Into Duplex Containing Ru-NH(CH ₂) ₆ OPO ₂ AGTGCCAAGCTTGCA-3' and Unmodified Duplex.....	175

LIST OF TABLES

Chapter 1:

Table 1.1.....	20
----------------	----

Chapter 2:

Table 2.1.....	51
----------------	----

Table 2.2.....	57
----------------	----

Table 2.3.....	67
----------------	----

Chapter 4:

Table 4.1.....	153
----------------	-----

Table 4.2.....	154
----------------	-----

Table 4.3.....	159
----------------	-----

Table 4.4.....	161
----------------	-----

Table 4.5.....	164
----------------	-----

Table 4.6.....	165
----------------	-----

Table 4.7.....	176
----------------	-----

LIST OF SCHEMES**Chapter 3:**

Scheme 3.1.....	97
Scheme 3.2.....	104
Scheme 3.3.....	106
Scheme 3.4.....	107

Chapter 4:

Scheme 4.1.....	150
-----------------	-----

Chapter 1: The Development of Ruthenium(II) Polypyridyl Complexes as Spectroscopic Probes for DNA.

1.1. Introduction

Numerous studies have been undertaken on the interactions of small molecules with DNA in an attempt to 1) delineate factors that contribute to recognition of specific sites by proteins,¹ to 2) rationally design small molecules for the sequence-specific or conformation-specific recognition of DNA,² and to 3) develop novel diagnostics for DNA detection.³ Our laboratory has utilized the rich coordination chemistry of transition metals to synthesize new DNA binding molecules. Complexes based upon transition metals can expand the repertoire of DNA-binding interactions available for a single molecule; recognition in three-dimensions can be accessed by the variety of molecular shapes provided by the coordination geometries of different transition metals, as opposed to the single binding mode available to most organic molecules. In addition, reactivity, either redox or spectroscopic, can be conferred to the complex by the metal center.

Our efforts have focused, in part, on the development of polypyridyl complexes of ruthenium(II) as sensitive, noncovalent probes of nucleic acids. These positively charged complexes are water soluble, coordinatively saturated, and substitutionally inert. These structural features provide these molecules with a unique three-dimensional architecture which determines the nature of their interactions with the double helix. The binding of these complexes to nucleic acids can be readily perturbed by modifying the shape of the molecule. The manner in which these complexes interact with DNA can be monitored by the spectroscopic properties imparted by the ruthenium center. Polypyridyl complexes of ruthenium(II) are intensely colored owing to a well-characterized, localized metal-to-ligand charge transfer (MLCT) transition.⁴ Importantly, this transition is perturbed upon binding to DNA, providing a sensitive spectroscopic handle for interactions with nucleic acids.

This chapter will serve to review the binding studies, both photophysical and

structural, carried out on tris(phenanthroline) complexes of ruthenium(II) and their derivatives. It will chronicle the development, based upon the initial studies performed with $[\text{Ru}(\text{phen})_3]^{2+}$, of $[\text{Ru}(\text{TMP})_3]^{2+}$ and $\Lambda\text{-}[\text{Ru}(\text{DIP})_3]^{2+}$, ruthenium complexes sensitive to alternate conformations of DNA (TMP = 3,4,7,8-tetramethyl-1,10-phenanthroline and DIP = 4,7-diphenyl-1,10-phenanthroline). The novel luminescence properties of dppz complexes of ruthenium(II) (dppz = dipyridophenazine), molecular light switches for DNA, will also be described.

1.2. Binding of $[\text{Ru}(\text{phen})_3]^{2+}$ to DNA

Early studies performed on the simple polypyridyl complex tris(phenanthroline)-ruthenium(II) (Figure 1.1) identified several modes of interaction of this complex with the double helix. Figure 1.2. illustrates our model for the different binding modes of $[\text{Ru}(\text{phen})_3]^{2+}$ to B-form DNA. This binding paradigm served as the basis for the subsequent design of complexes targeted against different conformations and specific sequences. It has been found that $[\text{Ru}(\text{phen})_3]^{2+}$ associates with the helix primarily through intercalation and surface binding. These binding modes are commonly observed in the noncovalent interactions of natural products with DNA.⁵ Surface binding, in which the ligands are associated with the minor groove of DNA, arises from a combination of electrostatic and hydrophobic effects. Intercalation involves the stacking of one of the aromatic heterocyclic ligands of the metal complex between adjacent base pairs of the DNA duplex. The effect of this interaction upon DNA is lengthening and unwinding of the helix in order to accommodate the intercalating molecule. For $[\text{Ru}(\text{phen})_3]^{2+}$, only partial stacking of one of the phenanthrolines with the bases occurs due to the presence of the ancillary ligands.

Because these complexes are positively charged, they can also associate electrostatically with DNA, as shown by the green $[\text{Ru}(\text{bpy})_3]^{2+}$ molecule in Figure 1.2.

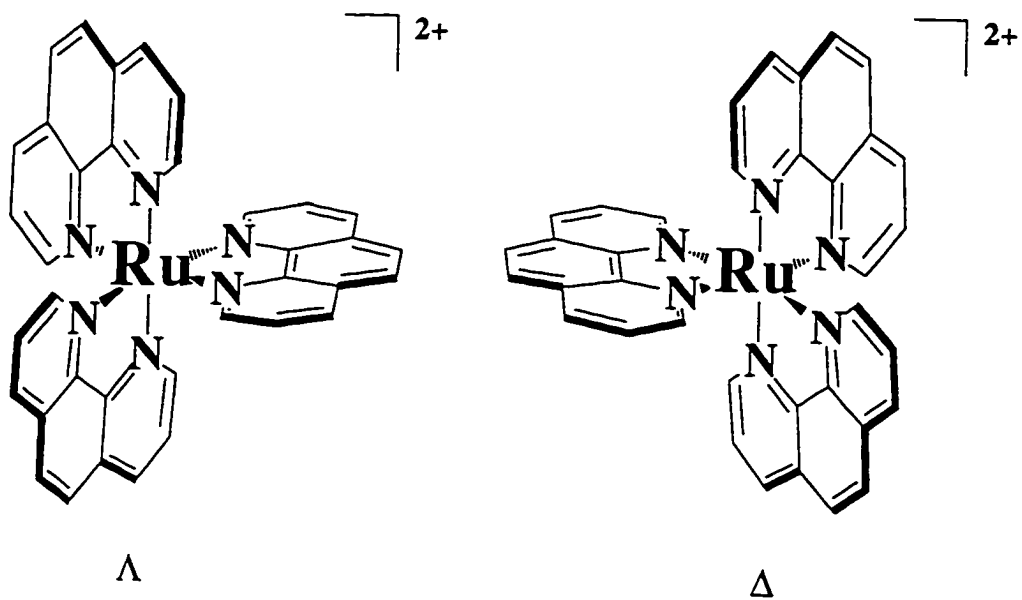
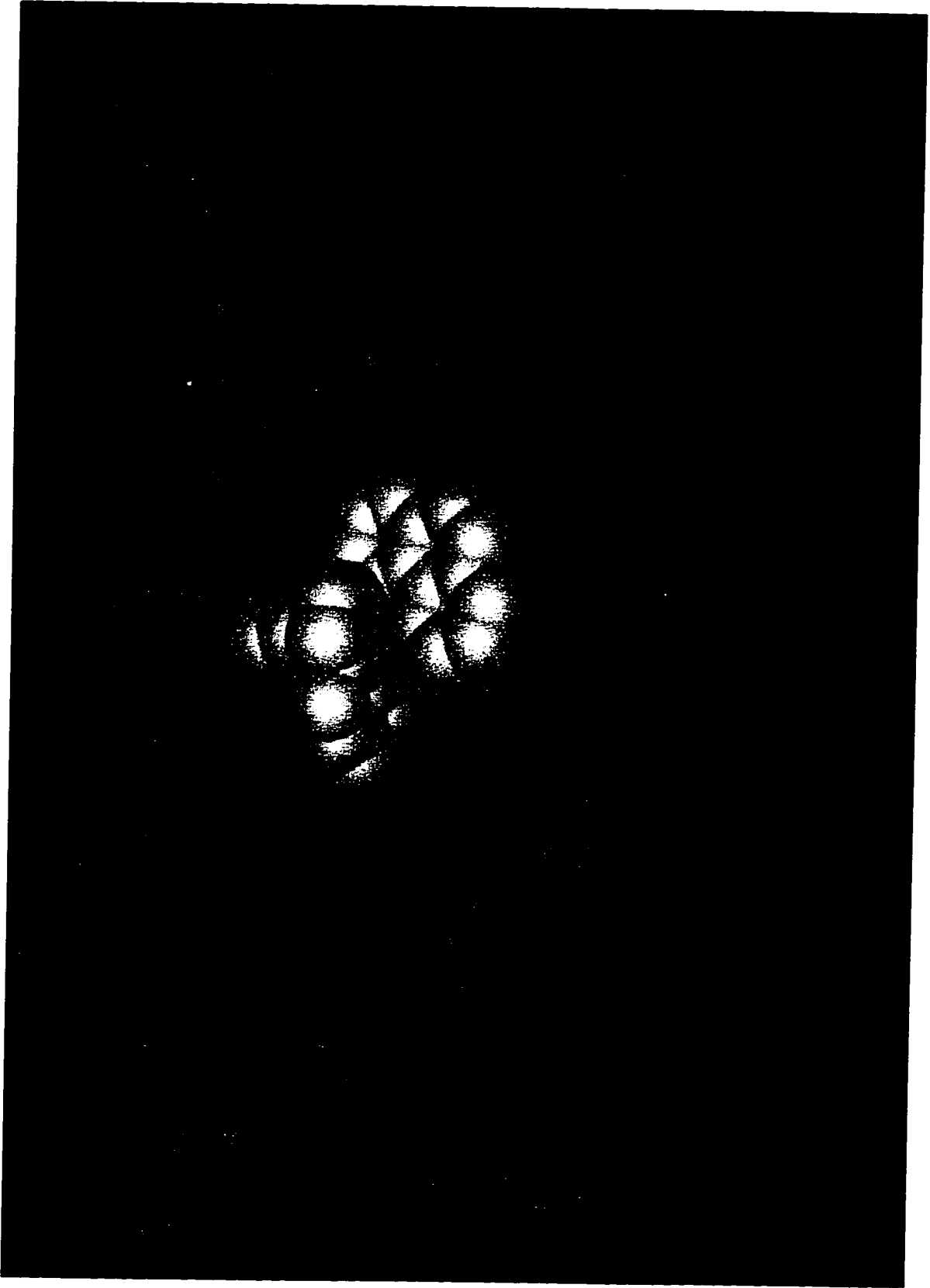


Figure 1.1. Structures of Λ - $[\text{Ru}(\text{phen})_3]^{2+}$ (left) and Δ - $[\text{Ru}(\text{phen})_3]^{2+}$ (right).

Figure 1.2. Model illustrating the different binding modes of ruthenium complexes to B-form DNA (base-pairs in blue, sugar-phosphate backbone in purple). Electrostatic binding to the helix is demonstrated by the green $[\text{Ru}(\text{bpy})_3]^{2+}$; Δ - $[\text{Ru}(\text{phen})_3]^{2+}$ (yellow) is intercalated in the major groove; and Λ - $[\text{Ru}(\text{phen})_3]^{2+}$ (red) is surface-bound against the minor groove. Figure taken from reference 11.



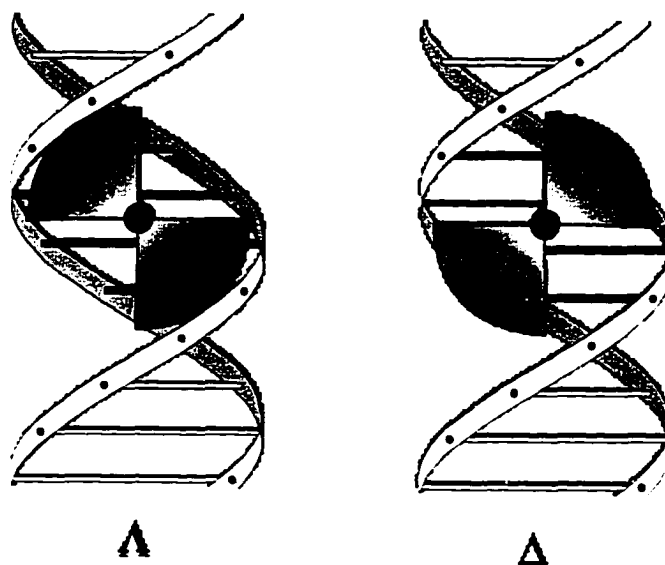
Binding based solely upon electrostatic interactions has been found to be weak and does not change the photophysical properties of the metal complex. The partitioning of these complexes between surface binding and intercalation is heavily influenced by the ligands.⁶ For example, complexes containing ligands with an extended aromatic surface such as phenanthrenequinonediimine are more likely to bind via intercalation than complexes containing TMP, a ligand which precludes intercalative binding.

Ruthenium(II) polypyridyl complexes are chiral, with Δ and Λ isomers that can be readily separated.⁷ Because DNA itself is also a chiral molecule, these complexes can interact with DNA in an enantioselective manner. Partitioning of the binding into surface association and intercalation may differ between the two enantiomers depending upon the symmetry of the complex with respect to the helix. Comparison of the groove dimensions relative to the overall dimensions of the metal complex suggests that enantioselective discrimination may be observed for intercalation (Figure 1.3). The right-handed Δ enantiomer matches the symmetry of the right-handed double helix; the direction of the ancillary ligands of the complex parallels the direction of the major groove. The ancillary ligands of the Λ enantiomer, however, are disposed contrary to the direction of the groove, leading to steric clashes with the phosphate backbone. For the surface-bound mode, the opposite enantioselectivities are apparent. It is evident that in order to design complexes for recognition of particular DNA sites or conformations, it is important to identify how these complexes are bound to the polymer.

1.2.1. Studies Based Upon Properties of the Metal Complex

Changes in UV-visible Absorption. The binding of small molecules to DNA can be followed by monitoring the changes in the drug absorption as DNA is added to the solution. Addition of DNA to racemic $[\text{Ru}(\text{phen})_3]^{2+}$ results in both hypochromism (~17%) and a slight red shift in the charge transfer band of the complex (2 nm).⁸ The

Figure 1.3. Schematic representation of the enantiomers of $[\text{Ru}(\text{phen})_3]^{2+}$ intercalated in B-form DNA. The Δ isomer fits easily within the right-handed groove whereas steric interactions are observed between the sugar-phosphate backbone and the ancillary ligands of the Λ isomer, illustrating how shape complementarity can be used as the basis for stereoselectivity in binding.

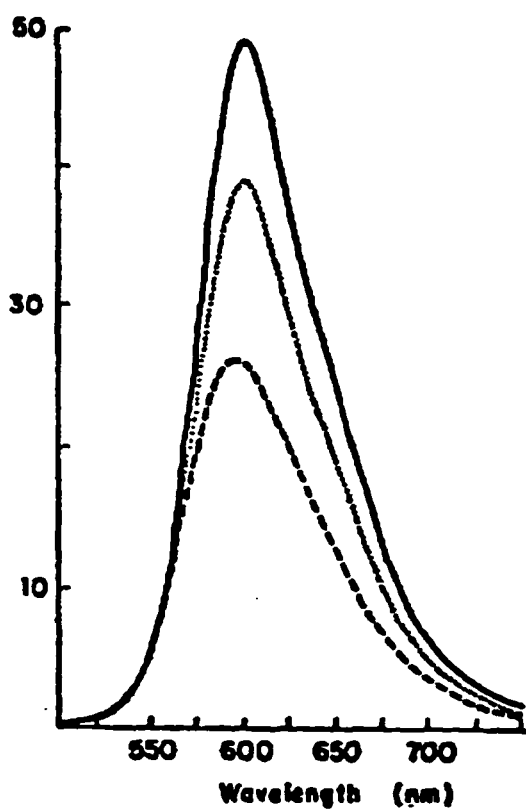


observed changes in the transition are consistent with a mode of interaction which involves a stacking interaction between an aromatic chromophore and the base pairs of DNA. The spectral changes are small compared to those observed for other intercalators; this could reflect the weakness of the stacking interaction for this particular molecule.⁶ Equilibrium dialysis of this complex to calf thymus DNA yielded a binding constant of about $6 \times 10^3 \text{ M}^{-1}$. No significant differences between the two enantiomers were observed via this method.

Time-resolved/Steady state Luminescence. Excitation into the MLCT transition results in long-lived luminescence which is sensitive to the local ligand environment. Intercalation often leads to enhancements in the emission intensity due to the decreased motion of the molecule upon binding. Figure 1.4 shows the emission spectra of free $[\text{Ru}(\text{phen})_3]^{2+}$ and of the individual enantiomers bound to calf thymus DNA. Emission enhancements of 48% and 87% are observed respectively for Λ - and Δ - $[\text{Ru}(\text{phen})_3]^{2+}$. In addition, a red shift of 2 nm in the emission wavelength for both enantiomers occurs.

Measurements of the time-resolved luminescence decay for the separate enantiomers bound to calf thymus DNA yielded identical excited state lifetimes of 0.6 μs and 2 μs . The short lifetime is identical to the lifetime of the free complex in aerated solution. The longer lived component has been assigned to the intercalated species; an increase in the lifetime of the excited state is expected for an intercalative interaction due to the increased rigidity of the bound complex, resulting in less vibrational deactivation. No enhancement in emission is expected for complexes that are surface-bound; the complex, in a surface-bound mode, would be relatively free to diffuse along the groove surface, and thus its excited state lifetime may be indistinguishable from that of free metal complex in solution. The similarity of the time-resolved luminescence decay for the two enantiomers indicates that equivalent binding modes are used by the two enantiomers. The greater steady-state enhancement observed for the Δ enantiomer simply reflects a higher proportion of bound Δ -isomer, rather than differences in the modes of

Figure 1.4. Luminescence spectra of free (---) $[\text{Ru}(\text{phen})_3]^{2+}$ and of Λ - $[\text{Ru}(\text{phen})_3]^{2+}$ (---) and Δ - $[\text{Ru}(\text{phen})_3]^{2+}$ (—) in the presence of DNA (0.3 mM phosphate). Ruthenium concentrations are 10 μM . Excitation is at 447 nm. Intensity (y-axis) is reported in arbitrary units.



association with the helix.

Luminescence Quenching Experiments. The luminescent excited state of the ruthenium complex can be efficiently quenched in buffered solution by the anionic quencher ferrocyanide (K_{SV} about $5 \times 10^3 \text{ M}^{-1}$).⁹ Due to its high charge, ferrocyanide can not efficiently quench ruthenium complexes intimately associated with the helix. Stern-Volmer plots for the luminescence quenching of the ruthenium complex when bound to DNA are nonlinear, indicating the presence of more than one species in solution. The source of the ruthenium species being discriminated in solution by ferrocyanide quenching is currently a point of contention. According to Barton and coworkers,⁸ the Stern-Volmer slopes for *both* regimes of the nonlinear plot are smaller than the K_{SV} for the free molecule by at least a factor of two. This decreased efficiency of quenching is used as support for the presence of the surface-bound mode, the smaller quenching constant being due to protection of the metal complex by the negatively charged backbone. Results from another laboratory show no significant difference in the larger quenching rate constant, suggesting that the source of nonlinearity is the dissociation of the ruthenium complex from DNA caused by the increase in ionic strength from the added quencher.¹⁰ What is clear is the intimate association of the long lifetime component with the double helix, consistent with an intercalative interaction.

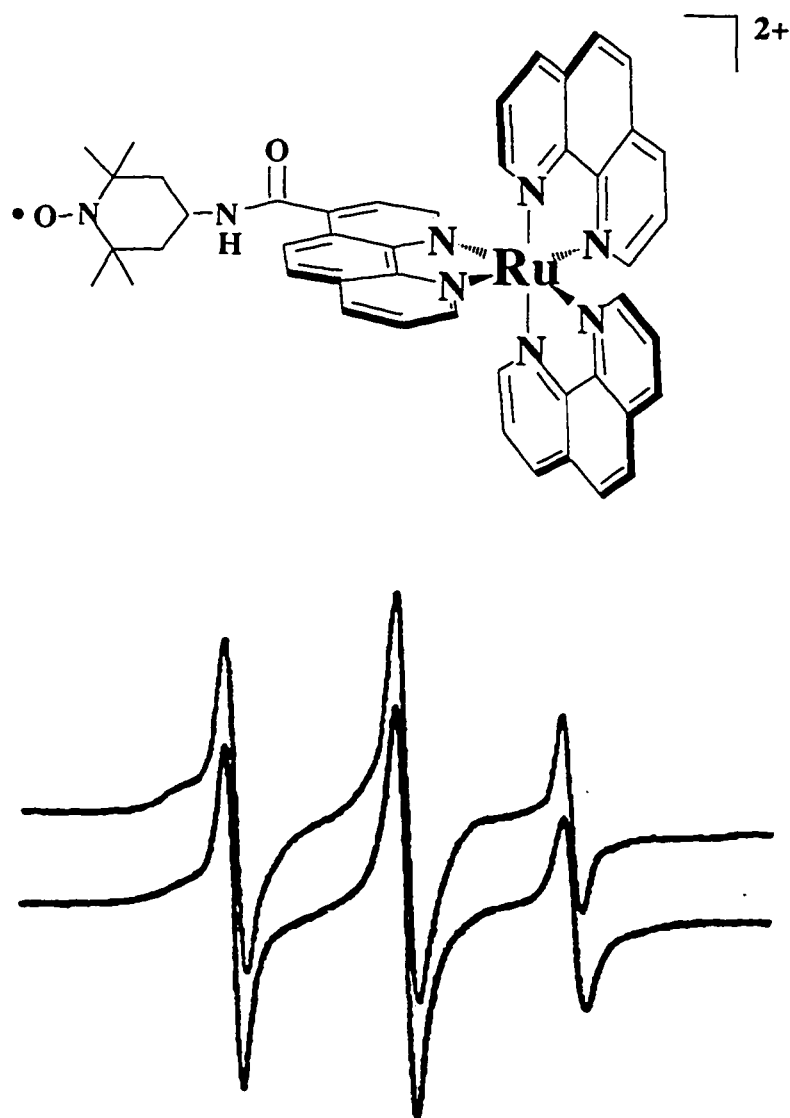
Luminescence Polarization. Steady-state luminescence experiments performed using polarized light yields information on the rotational dynamics of complexes bound to DNA. In order to maintain polarization, the complexes have to be rigidly oriented on the timescale of the measurement. Emission polarization probes the intercalated species exclusively; the surface-bound species can not be detected due to its greater motion. Free metal complexes in solution have a polarization value, P , of about 0.003.¹¹ Upon addition of calf thymus DNA, increases in polarization are observed for both Δ - and Λ -[Ru(phen)₃]²⁺, with greater polarization observed for the Δ isomer than the Λ (0.0367 versus 0.0258). Here it is evident from the greater polarization that the Δ isomer is

preferred over the Λ for intercalation into calf thymus DNA. All experiments described thus far demonstrate greater intercalative binding for the Δ isomer over the Λ isomer, consistent with the predictions made from shape-selection.

EPR Study Using a Nitroxide Derivative of $[\text{Ru}(\text{phen})_3]^{2+}$. The binding of a derivative of $[\text{Ru}(\text{phen})_3]^{2+}$, $[\text{Ru}(\text{phen})_2\text{phen-Tempo}]^{2+}$, to calf thymus DNA was studied using electron paramagnetic resonance (EPR) spectroscopy.¹² The structure of $[\text{Ru}(\text{phen})_2\text{phen-Tempo}]^{2+}$, where Tempo (2,2,6,6-tetramethylpiperidine-N-oxyl) is a stable nitroxide moiety, is shown in Figure 1.5. This study was undertaken in order to support and confirm the results of previous photophysical studies.

The resulting EPR data was best simulated by the addition of *three* components with characteristic features: component A is distinguished by fast [$(\tau)^{13} = 150$ ps, $\tau(\text{parallel}) = 75$ ps, and $\tau(\text{perpendicular}) = 300$ ps] and low anisotropic motion ($N^{14} = 4$), component B displays slower motion [$(\tau) = 2.25$ ns, $\tau(\text{parallel}) = 1.12$ ns, and $\tau(\text{perpendicular}) = 4.5$ ns] of low anisotropy ($N = 4$), while component C displays slow motion [$(\tau) = 3$ ns, $\tau(\text{parallel}) = 474$ ps, and $\tau(\text{perpendicular}) = 4.5$ ns] which is highly anisotropic (Figure 1.5). The three components are present in a 72:13:15 ratio and have been assigned respectively as the free species, the surface-bound species, and the intercalated species. A ten-fold drop in the correlation time without an increase in anisotropic motion is consistent with an interaction such as surface binding which does not impose great restraints on the rotational orientation of the probe molecule. This is the first direct spectroscopic evidence for a binding mode other than intercalation for $[\text{Ru}(\text{phen})_3]^{2+}$. The results provided by EPR serve to complement and confirm results obtained from photophysical studies of tris(phenanthroline)ruthenium(II). The qualitative agreement between the two experimental techniques supports the notion of two different binding modes for $[\text{Ru}(\text{phen})_3]^{2+}$ which can be distinguished by variations in their relative mobilities and orientational constraints.

Figure 1.5. Structure of $[\text{Ru}(\text{phen})_2\text{phen-Tempo}]^{2+}$ and the experimental (top curve) and simulated (bottom curve, sum of three components) EPR spectra of the complex (50 μM) in the presence of calf thymus DNA (1 mM phosphate) in tris buffer containing 50 mM NaCl. Data taken from reference 12.



1.2.2. Changes Observed in DNA Resulting From Complex Binding

Changes in Thermal Denaturation Profiles. The thermal denaturation profiles of calf thymus DNA in the presence of both $[\text{Ru}(\text{phen})_3]^{2+}$ and $[\text{Ru}(\text{bpy})_3]^{2+}$ were examined.¹⁵ Intercalation alters the thermal denaturation of duplex DNA; an increase in the T_m of the duplex occurs due to stabilization of the duplex form over the single strand.¹⁶ The melting curve in the presence of $[\text{Ru}(\text{bpy})_3]^{2+}$ closely resembles duplex melting in the presence of added Mg^{2+} ; the transition still remains sharp but is shifted to higher temperatures, consistent with electrostatic stabilization of the helix. In contrast, introduction of $[\text{Ru}(\text{phen})_3]^{2+}$ results in a broadened melting profile, with an increased melting temperature. The effects observed for $[\text{Ru}(\text{phen})_3]^{2+}$ closely resemble the results obtained using ethidium, a well characterized intercalator, and are consistent with the reported stabilization of molecules known to bind DNA via intercalation.

Unwinding of Plasmid DNA. The extent of DNA helix unwinding by a noncovalently bound species may be quantitated by examining the change in superhelical density in a plasmid after relaxation of the plasmid in the presence of bound complex with topoisomerase I.¹⁷ Because the base stack has to unwind to accommodate an intercalating molecule, increased unwinding may be reflected in the change in topoisomer distribution after incubation of plasmid with intercalator and topoisomerase.

$[\text{Ru}(\text{phen})_3]^{2+}$ has been shown to unwind pBR322 plasmid DNA with an unwinding angle of $22 \pm 1^\circ$, a value close to that determined for ethidium (26°).¹⁵ Unwinding as a manifestation of intercalative binding has recently been contested; helix unwinding has also been demonstrated, although to much lower extents, for compounds incapable of intercalation such as crystal violet (calculated unwinding angle of 9.8° ¹⁸).

Viscometry. It has been argued, mainly from the results of comparative viscosity studies performed on calf thymus DNA in the presence of both Λ^- and Δ^- $[\text{Ru}(\text{phen})_3]^{2+}$, that only partial intercalation of the two metal complexes occurs.¹⁹ "Classical"

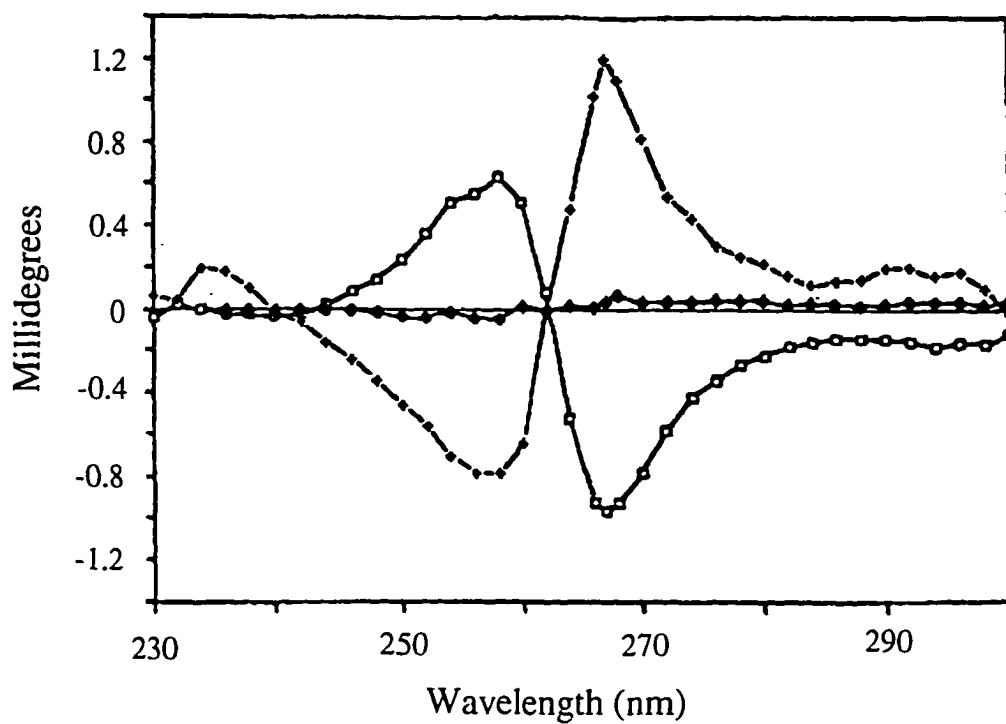
intercalation involves full separation of the base stack due to bound complex, an interaction which results in lengthening of the helix because the intercalating moiety mimics a base pair. An increase in the helix length alters the hydrodynamic properties of DNA in a predictable fashion.

At low binding ratios ($r < 0.1$), Λ -[Ru(phen)₃]²⁺ was found not to affect the viscosity of calf thymus DNA whereas binding of Δ -[Ru(phen)₃]²⁺ actually decreased the viscosity.^{10,19} Given that these experiments were performed at concentrations where the metal complexes were not fully bound, caution should be exercised in the interpretation of the results. The authors of this study propose that only partial intercalation of the metal complex occurs; full intercalation is impeded by the nonintercalating phenanthroline rings. Partial intercalation by [Ru(phen)₃]²⁺ would act as a wedge to pry apart one side of the base pair stack but not fully separate the stack. This interaction may result in a kink or bend in the DNA, and could be responsible for the decreased viscosity observed for Δ -[Ru(phen)₃]²⁺. The results of the viscosity studies are in agreement with results obtained from linear dichroism which suggested changes in the hydrodynamic behavior of DNA upon binding of Δ -[Ru(phen)₃]²⁺.²⁰ That only partial intercalation of [Ru(phen)₃]²⁺ occurs has always been assumed and was first proposed in 1984 by the authors of the original study in question.⁸ Indeed, partial intercalation actually serves to contribute to the enantioselective binding displayed by the two isomers of [Ru(phen)₃]²⁺.

1.2.3. Enantioselectivity in Binding

Discrimination based upon different conformations. Circular dichroism measurements of the dialysate from the equilibrium dialysis of calf thymus DNA with racemic [Ru(phen)₃]²⁺ showed an enrichment in the Λ isomer, indicating preferential binding of the Δ isomer to B-form DNA (Figure 1.6).²¹ That the Δ isomer had a higher affinity for B-form DNA was already evident from the luminescence studies; the greater steady-state luminescence enhancement and the greater contribution of the long

Figure 1.6. Circular dichroic spectra of Δ -[Ru(phen)₃]²⁺ (open squares) and of the dialysate from equilibrium dialysis of racemic [Ru(phen)₃]²⁺ against B-DNA (crosses) and Z-DNA (filled diamonds). Enrichment of the unbound Λ isomer is observed after dialysis against B-DNA. Data taken from reference 8.

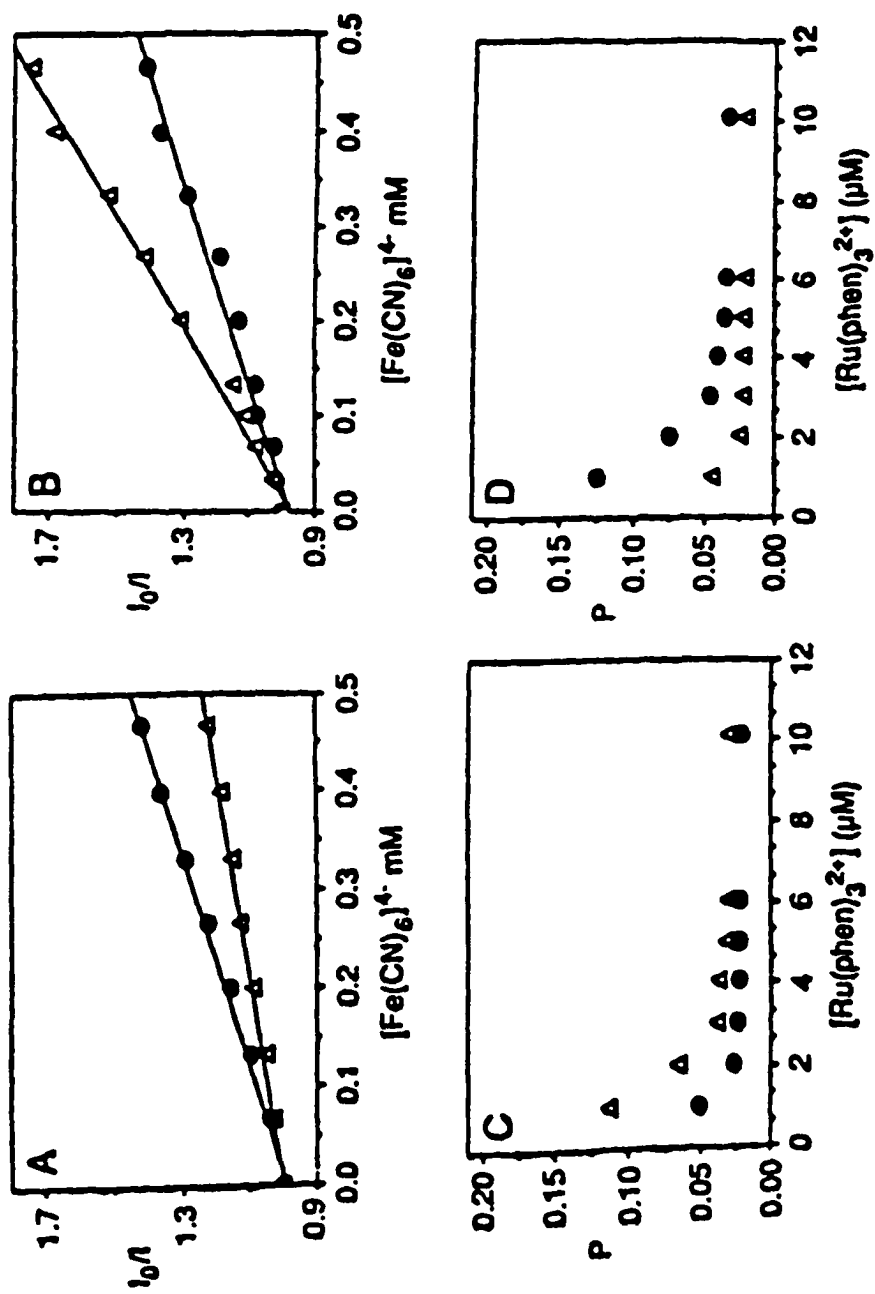


component to the excited-state decay is consistent with a higher proportion of intercalative binding by the delta isomer. This enantioselectivity was expected from shape considerations; the intercalated Δ isomer, with its ancillary ligands disposed along the major groove, complements the symmetry of the B-form helix.

Again, based upon shape considerations, it is conceivable that the enantioselectivity for Z-form, or left-handed DNA, will be opposite that of B-form DNA. The photophysical properties of Δ and Λ pairs for several ruthenium(II) complexes, including $[\text{Ru}(\text{phen})_3]^{2+}$, were studied in the presence of Z-form poly (dG·dC) · poly (dG·dC). The overall emission enhancement was found to be greater for Z-form DNA (50% increase compared to an increase of 20% for calf thymus DNA). It is not known if the greater enhancement is a reflection of higher binding affinity for Z-form or a higher luminescence quantum yield for binding to the Z helix. NMR studies are consistent with increased rigidity of the base pairs in Z-DNA compared to the B-form helix.²² A reversal in the luminescence enhancement was observed upon binding to Z-DNA; greater enhancement is found with the lambda isomer than the delta (a luminescence enhancement of 2.0 versus 1.26). Accordingly, a reversal in the polarization and in ferrocyanide quenching efficiency was also seen, as illustrated in Figure 1.7, indicating tighter binding by the Λ isomer.

It has not been determined conclusively whether the reversal in luminescence properties observed for Δ - and Λ - $[\text{Ru}(\text{phen})_3]^{2+}$ in the presence of Z-DNA is due to differential binding affinities for the Z-form helix as was evident for calf thymus DNA. Preferential binding for the Λ isomer has not been demonstrated; equilibrium dialysis performed on poly (dG·dC) · poly (dG·dC) in the presence of racemic ruthenium complex and 4 M NaCl showed no optical enrichment in the dialysate. However, it is likely that at a salt concentration of 4 M, no binding of ruthenium complex occurred due to the high sensitivity of the binding constant to ionic strength. That the Λ isomer has a higher binding affinity for the Z-conformation is supported by luminescence quenching data

Figure 1.7. Photophysical experiments that demonstrate the reversal of $[\text{Ru}(\text{phen})_3]^{2+}$ enantioselectivity for B- versus Z-DNA. Shown on the top are Stern-Volmer plots of the luminescence quenching of $10\ \mu\text{M}\ \Delta\text{-}[\text{Ru}(\text{phen})_3]^{2+}$ (triangles) and $\Lambda\text{-}[\text{Ru}(\text{phen})_3]^{2+}$ (circles) by ferrocyanide in the presence of $100\ \mu\text{M}$ nucleotide B-form poly (dG·dC) · poly (dG·dC) (panel A) or Z-form poly (dG·dC) · poly (dG·dC) (panel B). Shown on the bottom are steady-state luminescence polarizations of $\Delta\text{-}[\text{Ru}(\text{phen})_3]^{2+}$ (triangles) and $\Lambda\text{-}[\text{Ru}(\text{phen})_3]^{2+}$ (circles) as a function of concentration in the presence of $100\ \mu\text{M}$ nucleotides B-DNA (panel C) and Z-DNA (panel D). Data taken from reference 28.



which indicates greater accessibility of the Δ isomer to the ferrocyanide quencher.

Discrimination based upon different sequences. Changes in the luminescence properties for the two enantiomers of $[\text{Ru}(\text{phen})_3]^{2+}$ based upon differences in DNA sequence were studied by using synthetic polynucleotides varying in GC and AT content (Table 1.1). From the photophysical studies, it was revealed that as the GC content of the polymer was increased, binding of the Δ isomer was favored. For the GC-containing polynucleotide, no photophysical changes in the emission of the Λ isomer occur. The lifetime of Λ - $[\text{Ru}(\text{phen})_3]^{2+}$ in the presence of poly (dG·dC) · poly (dG·dC) is identical to the lifetime of the free metal complex; most likely, the Λ isomer binds solely through surface binding.

The overall effect of increasing the GC concentration on the photophysical properties of Δ - and Λ - $[\text{Ru}(\text{phen})_3]^{2+}$ could be mimicked by increasing the ionic strength of the solution. The enantioselectivity for the Δ isomer tracked with increasing salt concentrations. As the double helix is compressed by neutralization of phosphate-phosphate repulsions, the major groove may narrow and hence become more selective for the Δ isomer. The sequence results may address the relative size of the major groove for AT versus GC containing polymers. Increased major groove dimensions for AT rich sequences may allow greater intercalative binding for Λ - $[\text{Ru}(\text{phen})_3]^{2+}$; increasing the GC content or raising the ionic strength has the effect of compressing the major groove, leading to higher enantioselectivity for Δ isomer binding. A slight preference of the Λ isomer for AT rich sequences and the Δ isomer for GC rich sequences has been reported elsewhere.¹⁰

1.2.3. Structural Studies Based Upon $^1\text{H-NMR}$

Oligonucleotide Duplex d(GTGCAC)₂. The interaction of tris(phenanthroline) complexes of ruthenium(II), cobalt(III), and rhodium(III) with hexamer oligonucleotide duplexes was examined using one-dimensional $^1\text{H-NMR}$.²³ The binding of these

Table 1.1. Features in Binding Ru(phen)₃²⁺ Enantiomers to DNAs of Varying Base Sequences

DNA	% GC	K(0) × 10 ⁻³ , M ⁻¹	Stern-Volmer slope × 10 ⁻³ , M ⁻¹		emission lifetimes, ns			polarization		
			rac	Δ	rac	Δ	Λ	Δ	Λ	
poly[d(AT)]	0	9.2	3.0	3.8	2.0	412 (426) ^a 1076 (487)			0.0199	0.0196
<i>Cl. perfringens</i>	26	9.8	3.7	5.9	4.2	563 (801) 2211 (184)	502 (705) 1587 (284)	539 (741) 1851 (253)	0.0301	0.0267
calf thymus	42	6.2	4.4	2.5	3.7	505 (700) 1233 (245)	559 2137	583 1999	0.0367	0.0258
<i>M. lysodeikticus</i>	74	10.0	3.7	3.8	7.3	509 (807) 1309 (130)	677 1864		0.0206	0.0094
poly[d(GC)]	100	4.0	5.5			581 (690) 708 (270)	531 (1000)		0.0132	0.0060

^a Values in parentheses correspond to the preexponential weighting factors obtained in solving the decay curves as a biexponential. Although not strictly quantitative, these coefficients reflect the amplitude of short- and long-lived components in the ruthenium-DNA samples.

complexes was observed to be in fast exchange, indicative of weak binding.

Enantioselective interactions with the DNA duplex were observed for each complex used. Resonances corresponding to bound Λ - and Δ -[Ru(phen)₃]²⁺ appeared upon addition of the duplex to a solution of *racemic* metal complex, indicating that the duplex can serve as a chiral shift reagent for the discrimination of the two enantiomeric forms (Figure 1.8). Addition of [Co(phen)₃]³⁺ to the oligonucleotide duplex induces rapid racemization of the complex, with enantiomer ratios dependent upon the sequence of the oligonucleotide used. Less Λ - [Co(phen)₃]³⁺ was observed for 5'-pd(CGCGCG)₂ than for d(GTGCAC)₂, consistent with previous results from photophysical studies that attested to increasing affinity for the Δ isomer with increasing GC content.

In contrast to the photophysical studies, it appears that NMR is more sensitive to the surface-bound form of the complex located in the minor groove. The largest chemical shift perturbation observed for the duplex occurs with AH2, a proton located in the minor groove of DNA. There is a slight downfield migration of the major groove thymine methyl protons but the change is not nearly as great as for the AH2 resonance. Λ -[Ru(phen)₃]²⁺ appears to influence the upfield chemical shift of the AH2 proton more than Δ -[Ru(phen)₃]²⁺ whereas the thymine methyl resonances are perturbed more by the Δ isomer. The differential effects caused by binding of the two enantiomers to the duplex on major and minor groove resonances are illustrated graphically in Figure 1.9. Further evidence for enantioselective binding is the difference in relaxation parameters for protons corresponding to the two enantiomers, fully compatible with the notion of different binding modes which differ in their dynamics of association with the helix. In addition, ¹H-NMR studies performed on the same oligonucleotide duplex with Λ - and Δ -tris(phenanthroline) analogues containing the paramagnetic metal centers Ni³⁺ and Cr³⁺ showed selective paramagnetic broadening of the oligonucleotide protons, consistent with preferential association of the Λ isomer of tris(phenanthroline) complexes with the minor groove.¹

Figure 1.8. 300-MHz ^1H NMR spectrum of $\text{d}(\text{GTGCAC})_2$ in the absence (bottom) and presence (top) of $[\text{Rh}(\text{phen})_3]^{3+}$ in D_2O (5 mM sodium phosphate, pH 7.0, 15 mM NaCl). R is the ratio of metal complex per oligomeric duplex. Resonances corresponding to metal complex protons are marked with letters. Note that binding to the oligomer leads to chemical shift differences between the bound enantiomers, as clearly illustrated in the resolution of H4,7 resonances indicated by (a). Data taken from reference 23.

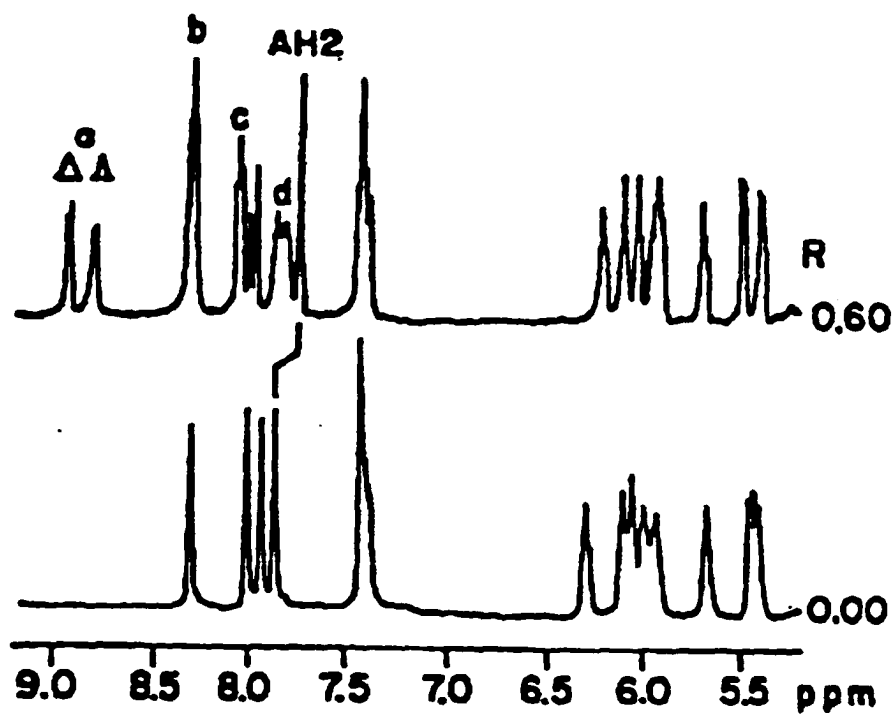
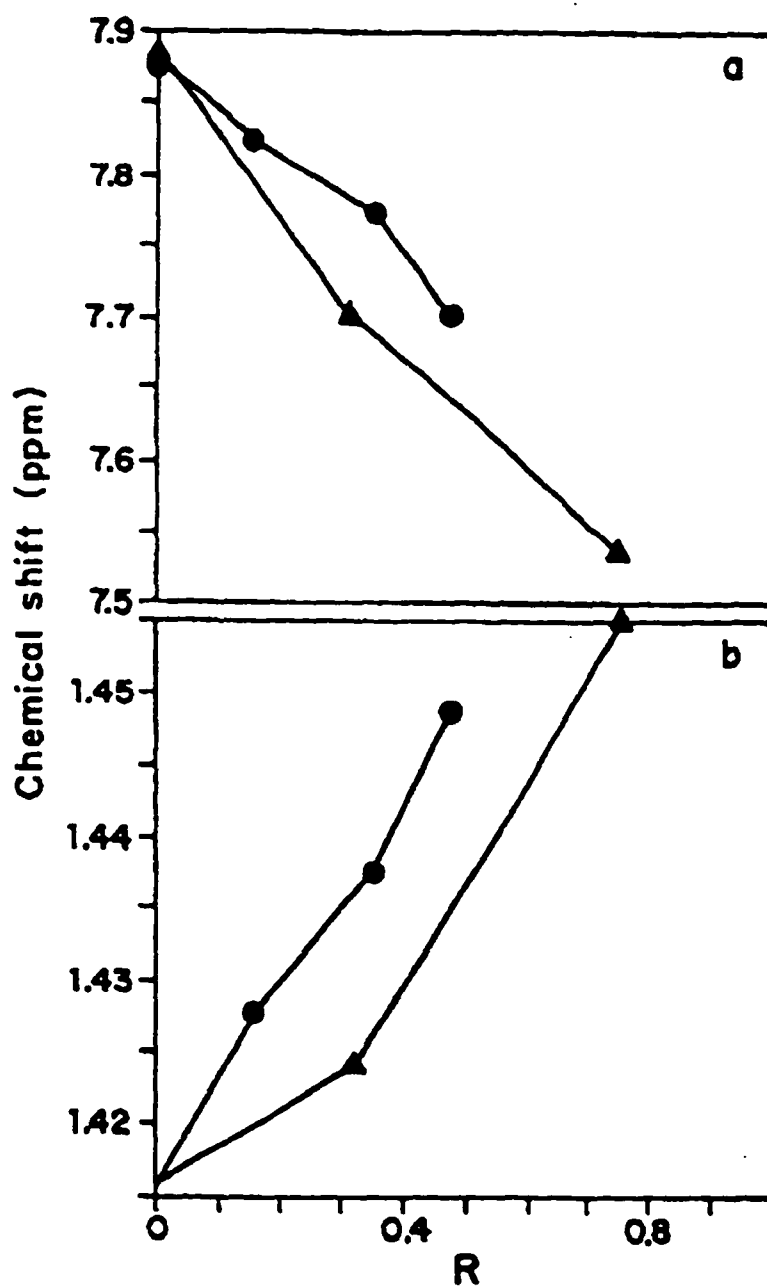


Figure 1.9. Variation in chemical shift observed for AH2 (a) and TMe (b) resonances upon titration with Λ - (triangles) and Δ - (circles) $[\text{Ru}(\text{phen})_3]^{2+}$. The AH2 proton, located in the minor groove, is perturbed more by the Λ -isomer, while the major groove TMe protons are affected more by the Δ -isomer. R denotes the ratio of metal per duplex oligomer. Data taken from reference 23.



The NMR results do not reveal sufficient structural detail to establish intercalation or the surface-bound interaction of these complexes with the helix. Weak binding to the helix, fast chemical exchange, and the low specificity of these complexes precluded further high resolution studies. However, all the results taken together support differential binding of the two enantiomers to the double helix with intercalation favoring the Δ isomer and a surface-bound interaction favoring the Λ isomer.

Oligonucleotide Duplex d(CGCGATCGCG)₂. The binding of the Δ - and Λ -[Ru(phen)₃]²⁺ to the oligonucleotide duplex d(CGCGATCGCG)₂ was studied using 1-D and 2-D ¹H-NMR.²⁵ This study again demonstrates the higher sensitivity of NMR to surface binding than intercalation for tris(phenanthroline) complexes. NOE crosspeaks were observed between duplex protons and the metal complex. Most of the interactions between Δ - and Λ -[Ru(phen)₃]²⁺ and the oligonucleotide duplex appear to be localized in the center of the duplex, on the minor groove side. No evidence for intercalation was obtained from this data but this is not surprising given the negligible sequence-specificity of the complexes. That different crosspeaks with different intensities were observed for each enantiomer provides further support for differential interactions used by the two enantiomers in binding to the double helix.

1.3. Development of Ruthenium Probes Targeted Against Specific DNA Conformations

1.3.1. [Ru(DIP)₃]²⁺: Probe of Z-DNA conformation

The photophysical studies on [Ru(phen)₃]²⁺ identified the binding modes and enantioselectivities for the two isomers. Based upon these findings, novel ruthenium complexes with different ligands were designed to probe alternate DNA conformations. Z-DNA is distinguished from B-form primarily by its left-handed helicity (Figure 1.10). In contrast to the well-defined major and minor grooves of B-form, the region of Z-DNA corresponding to the major groove of B-form is sufficiently shallow and wide to be

Figure 1.10. The three conformational families of DNA: the A-conformation (left) is commonly observed for double-helical RNA and mixed DNA/RNA hybrids, canonical B-form (center), and Z-form (right) which is adopted under particular ionic strength conditions.

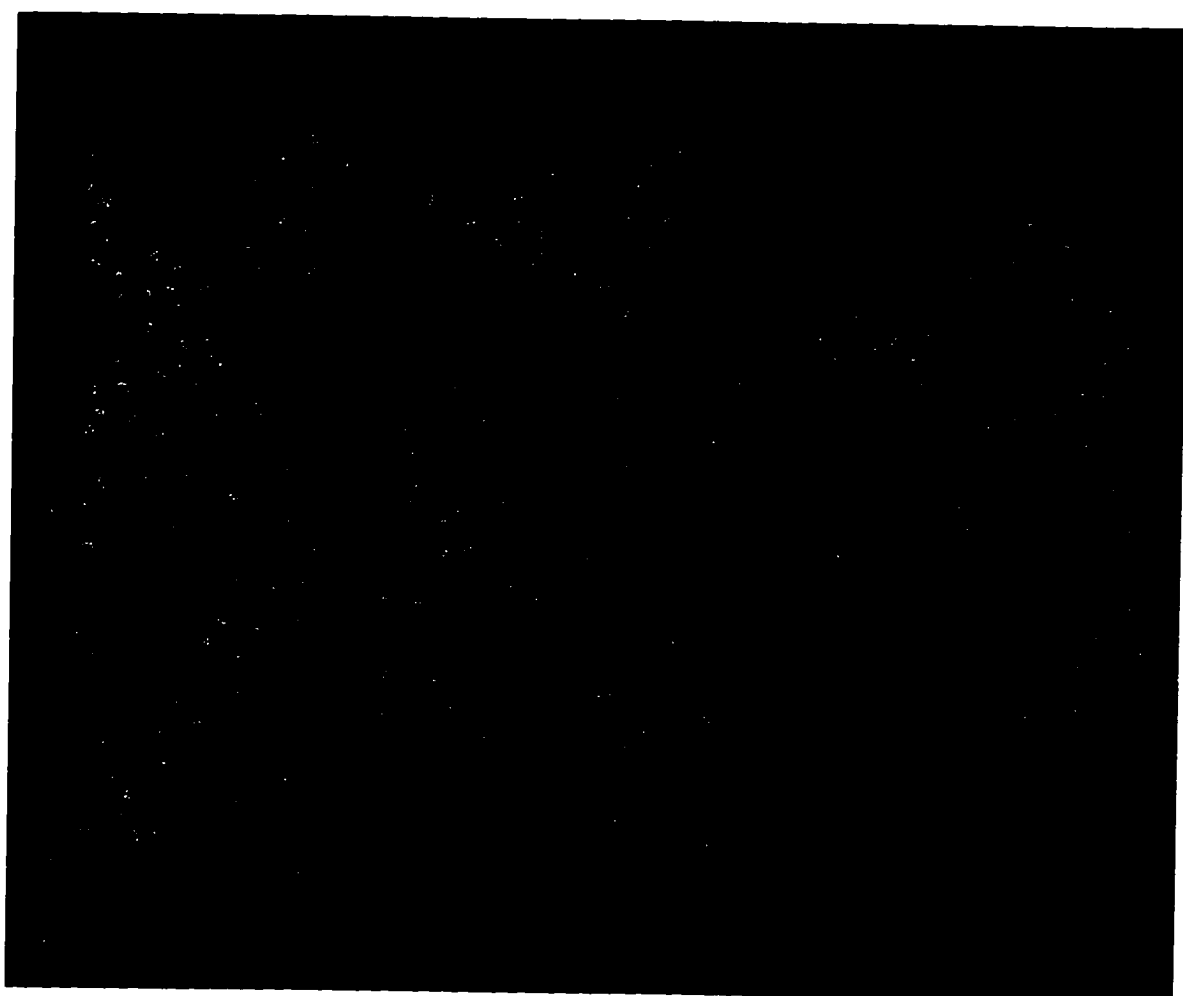
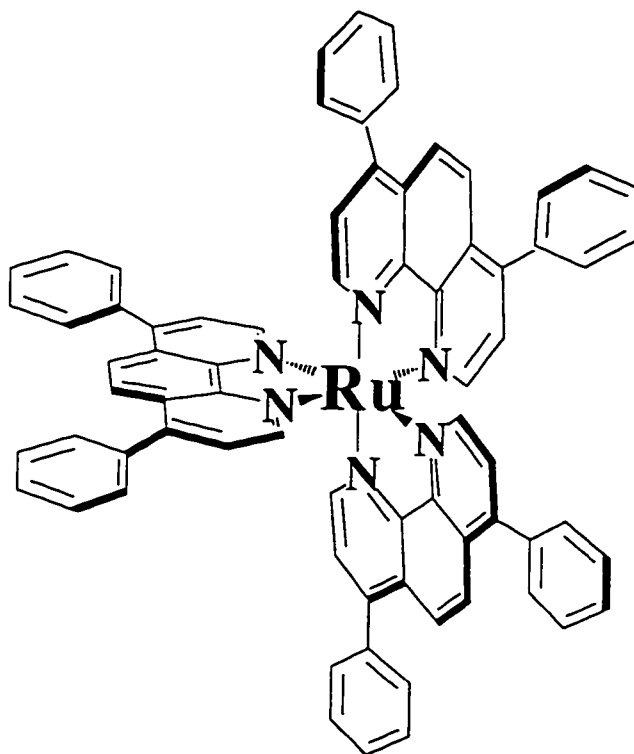


Figure 1.11. Structure of $[\text{Ru}(\text{DIP})_3]^{2+}$.



essentially a hydrophobic surface without a groove. A very narrow helical groove in the region comparable to the minor groove of B-DNA is present.

Visible absorption titrations of racemic $[\text{Ru}(\text{DIP})_3]^{2+}$ (Figure 1.11) with either B-form poly (dG-dC) · poly (dG-dC) or Z-form poly (dG-dC) · poly (dG-dC) showed hypochromicity and a red shift of two nanometers in the MLCT transition.²⁶ Greater hypochromicity was observed for $[\text{Ru}(\text{DIP})_3]^{2+}$ bound to Z-DNA (17% versus 9% for B-form), suggesting greater affinity of this complex for Z-DNA. This conclusion is supported by equilibrium dialysis studies. A slightly greater luminescence enhancement was found for the racemic complex in the presence of B-DNA than for the Z-form polymer, despite the higher affinity of the complex for Z-DNA.

Photophysical studies on the individual enantiomers of $[\text{Ru}(\text{DIP})_3]^{2+}$ in the presence of calf thymus DNA showed no hypochromicity for the Λ isomer.²⁷ Ferrocyanide quenching confirmed that Λ - $[\text{Ru}(\text{DIP})_3]^{2+}$ did not bind by intercalation to B-form DNA. Placement of phenyl groups at the 4,7 positions of the phenanthroline rings amplifies the chiral discrimination previously observed for $[\text{Ru}(\text{phen})_3]^{2+}$, sterically preventing the Λ isomer of $[\text{Ru}(\text{DIP})_3]^{2+}$ from binding by intercalation. Reversal of the helix chirality, however, allows intercalative binding by the Λ isomer, as evidenced by an increase in the excited state lifetime and in emission polarization.²⁸

No stereoselectivity for the two enantiomers upon binding to Z-DNA is observed. Because of the shallow and very wide character of the major groove in Z-DNA, no steric constraints comparable with that found in B-DNA exist to hinder binding by the Δ isomer. The higher affinity of both Δ - and Λ - $[\text{Ru}(\text{DIP})_3]^{2+}$ may be from greater hydrophobic interactions with the helical surface. Although the Z-form helix can not be used as a template to distinguish the two enantiomers of $[\text{Ru}(\text{DIP})_3]^{2+}$, differential binding by the Λ and Δ isomers can be used advantageously in determining helix chirality.

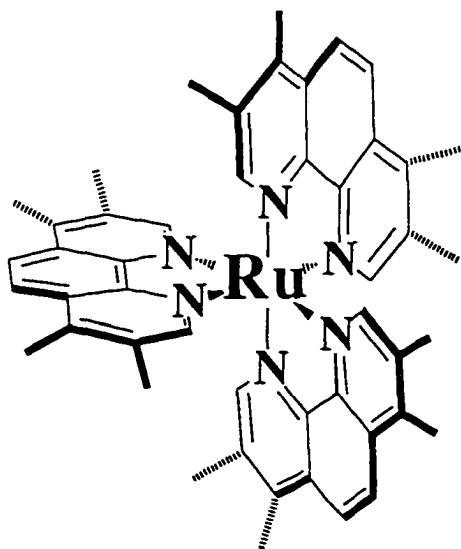
Cleavage studies were performed on pBR322 containing a d(C-G)₁₆ insert using a

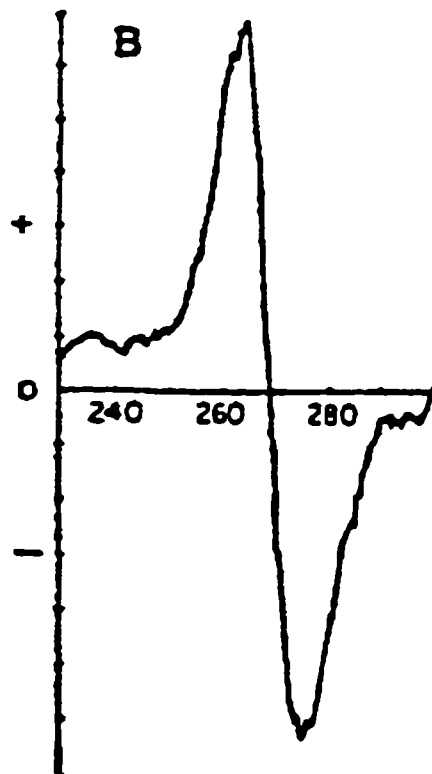
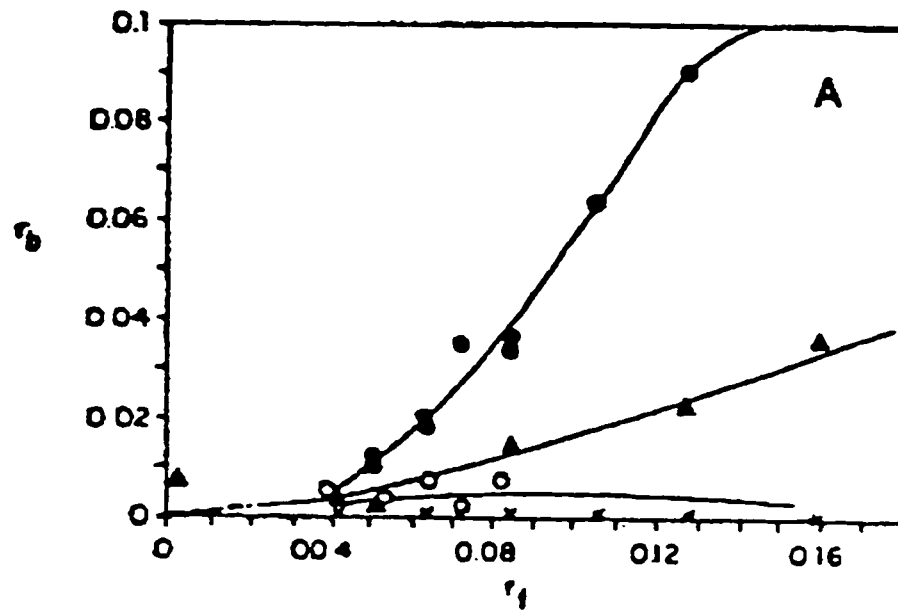
photoactive analog of Λ -[Ru(DIP)₃]²⁺, Λ -[Co(DIP)₃]³⁺.²⁹ It is well known that alternating purine-pyrimidine stretches can adopt the Z conformation under various solution conditions.³⁰ The primary cleavage site for the complex in the mutant plasmid is at the insert. Interestingly, the cleavage sites for the complex in the native pBR322 all correspond to segments of alternating purine-pyrimidines, consistent with selective recognition of the Z conformation by the Λ isomer of tris(diphenylphenanthroline) complexes.

1.3.2. [Ru(TMP)₃]²⁺: Probe of A-DNA Conformation

As illustrated in Figure 1.10, the A form helix is characterized by a shallow and wide minor groove, with a relatively inaccessible major groove that is deep and narrow. The tetramethylated derivative of [Ru(phen)₃]²⁺, [Ru(TMP)₃]²⁺, was prepared so as to maximize interactions in the minor groove of the A conformation³¹; binding to B-form DNA either by intercalation or by surface interactions is precluded by the increase in the dimensions of the complex. The absence of an increase in the luminescence of [Ru(TMP)₃]²⁺ in the presence of double-helical RNA supports this binding model. Equilibrium dialysis of various synthetic polynucleotides in the presence of [Ru(TMP)₃]²⁺ showed cooperative binding to A-form nucleic acids under conditions where little binding is apparent to other nucleic acid forms. Circular dichroism of the dialysate after dialysis of racemic complex against double stranded RNA showed enrichment in the Δ isomer of the complex, indicating preferential binding of the Λ isomer to the nucleic acid (Figure 1.12). The binding specificity of the Δ and Λ isomers of the complex was examined using singlet-oxygen mediated photocleavage of a linear fragment of pBR322. The cleavage of Δ -[Ru(TMP)₃]²⁺ closely resembled that of [Ru(phen)₃]²⁺ and paralleled the intrinsic reactivity of the guanines within the fragment. Specific cleavage of Λ -[Ru(TMP)₃]²⁺ at homopyrimidine/ homopurine stretches was observed. There have been experimental indications from a variety of techniques that

Figure 1.12. Shown below is the structure of $[\text{Ru}(\text{TMP})_3]^{2+}$. On the next page is shown: (A) Binding of $[\text{Ru}(\text{TMP})_3]^{2+}$ to nucleic acids after dialyses of A-form polymers poly (rI) · poly (dC) (filled circles) and poly (rG) · poly (dC) (filled triangles) and B-form calf thymus DNA (open circles) and poly d(GC) (crosses) in buffer with racemic $[\text{Ru}(\text{TMP})_3]^{2+}$ at 25°C; r_b is the ratio of bound ruthenium to nucleotide concentration and r_f is the formal added ratio of metal per nucleotide. Binding of $[\text{Ru}(\text{TMP})_3]^{2+}$ occurs with A-form helices. (B) Circular dichroic spectrum of the dialysate after equilibrium dialysis of poly (rI) · poly (dC) against racemic $[\text{Ru}(\text{TMP})_3]^{2+}$. Preferential binding of the L isomer to the double-helical RNA is observed, leading to a dialysate enriched in the Δ isomer. Data taken from reference 31a.





these stretches may adopt non-B conformations, among them bent, triple, and A-form.³² Regardless of whether these sites are A-like, they are definitely distinctive in their conformation and clearly illustrate the utility of this complex for distinguishing sites of alternate conformation along a DNA segment.

1.4. Dppz Complexes of Ruthenium(II): Molecular Light Switches for DNA

Tris(phenanthroline) complexes of ruthenium(II) and their derivatives possess several features which render them ideal as spectroscopic probes for nucleic acids; upon binding to double-helical DNA, luminescence enhancement is observed owing to intercalative interactions and the recognition properties of these complexes can be altered by variation of the ancillary ligands, enabling the rational design of spectroscopic probes for alternate nucleic acid conformations. For broader application as general nonradioactive nucleic acid probes, several limitations of $[\text{Ru}(\text{phen})_3]^{2+}$ are 1) the background luminescence of the unbound complex, 2) the weak binding affinity for DNA, and 3) the extent of luminescence enhancement upon binding.

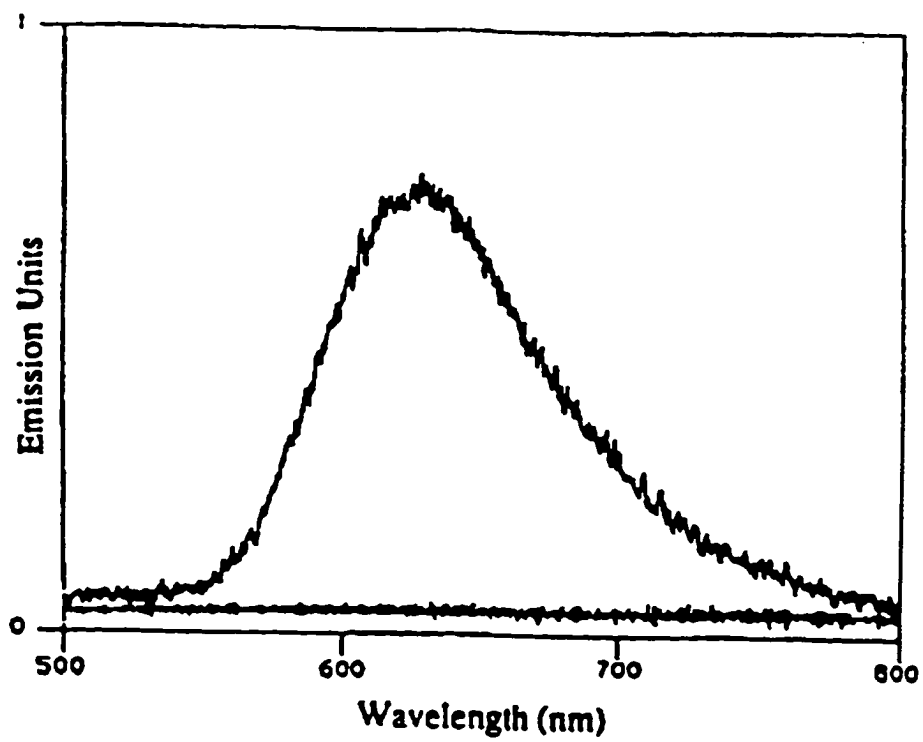
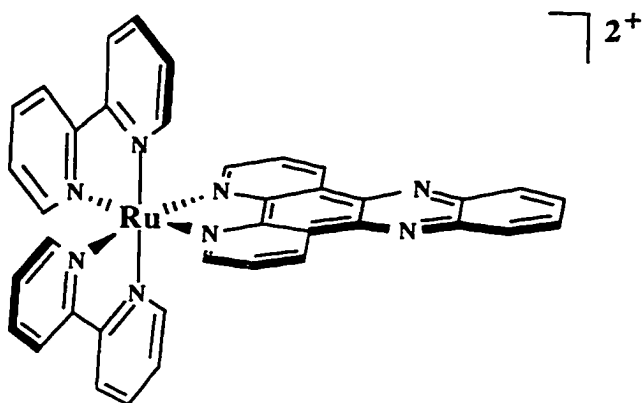
Recent work in our laboratory has focused on using transition metal complexes containing the dppz ligand (dppz = dipyrido[3,2-*a*:2',3'-*c*]phenazine) as novel luminescent reporters for double-helical DNA³³ and to examine electron transfer reactions mediated by the DNA double helix.³⁴ The dipyridophenazine ligand, compared to the parent phenanthroline, has an extended aromatic surface area which facilitates extensive stacking in DNA; complexes containing dppz bind avidly to DNA with binding constants at least three orders of magnitude larger than $[\text{Ru}(\text{phen})_3]^{2+}$ ($\sim 10^7 \text{ M}^{-1}$ compared to $\sim 10^4 \text{ M}^{-1}$). The intercalative form of association is by far the predominant mode of binding of the dppz complexes to the double helix.

Excitation of complexes containing dppz using visible light leads to localized charge transfer onto the dipyridophenazine ligand.³⁵ Because the emission originates

from an excited state centered on the intercalating ligand, the photophysical properties of dppz complexes are very sensitive to the environment. Dppz complexes of ruthenium(II), osmium(II), and rhenium(I)³⁶ possess a rather unique luminescent characteristic. These complexes in water do not emit due to deactivation of the excited state by the aqueous solvent, perhaps via proton transfer³⁷ or hydrogen bonding with the phenazine nitrogens of the dppz ligand. Intercalation of the complex into double helical DNA protects the phenazine nitrogens from solvent water, resulting in intense photoluminescence (Figure 1.13).

Much work has been carried out in our laboratory and in others on characterizing the photophysical properties of dppz complexes in the presence of nucleic acids^{33,38} and also their modes of binding.³⁹ In this thesis, the luminescence properties of dppz complexes of ruthenium(II) as a function of the nucleic acid will be explored. Detailed synthetic methodologies for constructing oligonucleotides modified at the 5' terminus with a ruthenium(II) dppz complex will be outlined as well as their methods of characterization. The properties of one conjugate will be discussed with an emphasis on DNA hybridization technology. In addition, attempts to use these modified oligonucleotides for novel biosensor applications will be described. The experiments performed during the course of this thesis work will attempt to evaluate the potential of ruthenium complexes containing dppz as useful DNA diagnostics.

Figure 1.13. Structure of $[\text{Ru}(\text{bpy})_2\text{dppz}]^{2+}$ ($\text{bpy} = 2,2'$ -bipyridine) and the steady-state emission spectra of $[\text{Ru}(\text{bpy})_2\text{dppz}]^{2+}$ ($10 \mu\text{M}$) in the absence and presence of B form poly (dG·dC) · poly (dG· dC) ($100 \mu\text{M}$ nucleotides). In the absence of DNA, only the base-line spectrum is obtained for the ruthenium complex in 50 mM NaCl, 5 mM Tris, pH 7.0 at 25°C . Data taken from reference 33a.



References

- ^{1a}Steitz, T.A., *Q. Rev. Biophys.*, **1990**, *23*, 205. ^{1b}Harrison, S.C.; Aggarwal, A.K., *Annu. Rev. Biochem.*, **1990**, *59*, 933.
- ²Barton, J.K., *Chem. Eng. News*, **1988**, (26 Sept), 30-42.
- ^{3a}Bannwarth, W.; Schmidt, D.; Stallard, R.I.; Hornung, C.; Knorr, R.; Muller, F., *Helv. Chim. Acta*, **1988**, *71*, 2085. ^{3b}Telser, J.; Cruickshank, K.A.; Schanze, K.S.; Netzel, T.L., *J. Am. Chem. Soc.*, **1989**, *111*, 7221.
- ⁴Juris, A.; Balzani, V.; Barigelletti, F.; Campagna, S.; Belser, P.; von Zelewsky, A., *Coord. Chem. Rev.*, **1988**, *84*, 85.
- ^{5a}Burckhardt, G.; Waehnert, U.; Luck, G.; Zimmer, C., *Stud. Biophys.*, **1986**, *114*, 225.
- ^{5b}Kissinger, K.; Krowicki, K.; Dabrowiak, J.C.; Lown, J.W., *Biochemistry*, **1987**, *26*, 5590. ^{5c}Kopka, M.L.; Yoon, C.; Goodsell, D.; Pjura, P.; Dickerson, R.E., *Proc. Natl. Acad. Sci. U.S.A.*, **1985**, *82*, 1376. ^{5d}Wilson, W.D.; Wang, Y.-H.; Kusuma, S.; Chandrasekaran, S.; Yang, N.C.; Boykin, D.W., *J. Am. Chem. Soc.*, **1985**, *107*, 4989.
- ^{5e}Berman, H.M.; Young, P.R., *Annu. Rev. Biophys. Bioeng.*, **1981**, *10*, 87.
- ⁶Pyle, A.M.; Rehmann, J.P.; Meshoyrer, R.; Kumar, C.V.; Turro, N.J.; Barton, J.K., *J. Am. Chem. Soc.*, **1989**, *111*, 3051.
- ^{7a}Gillard, R.D.; Hill, R.E.E., *J. Chem. Soc. Dalton Trans.*, **1974**, 1217. ^{7b}Yoshikawa, Y.; Yamasaki, K., *Coord. Chem. Rev.*, **1982**, *28*, 205.
- ⁸Barton, J.K.; Danishefsky, A.T.; Goldberg, J.M., *J. Am. Chem. Soc.*, **1984**, *106*, 2172.
- ⁹Barton, J.K.; Goldberg, J.M.; Kumar, C.V.; Turro, N.J., *J. Am. Chem. Soc.*, **1986**, *108*, 2081.
- ¹⁰Satyanarayana, S.; Dabrowiak, J.C.; Chaires, J.B., *Biochemistry*, **1993**, *32*, 2573.
- ¹¹Murphy, C.J.; Barton, J.K., *Methods Enzymol.*, **1993**, *226*, 576.
- ¹²Ottaviani, M.F.; Ghatlia, N.D.; Bossmann, S.H.; Barton, J.K.; Durr, H.; Turro, N.J., *J. Am. Chem. Soc.*, **1992**, *114*, 8946.

¹³ τ is the correlation time for the reorientation motion and is expected to increase upon binding of Ru-Tempo to DNA, thus providing information about the relative strengths of the different binding interactions.

¹⁴N is the ratio of the parallel to the perpendicular components of the diffusional motion tensor.

¹⁵Kelly, J.M.; Tossi, A.B.; McConnell, D.J.; OhUigin, C., *Nucleic Acids Res.*, **1985**, *13*, 6017.

^{16a}Kumar, C.V.; Asuncion, E.H., *J. Am. Chem. Soc.*, **1993**, *115*, 8457. ^{16b}Tarui, M.; Doi, M.; Ishida, T.; Inoue, M.; Nakaike, S.; Kitamura, K., *Biochem. J.*, **1994**, *304*, 271.

^{17a}Keller, W., *Proc. Natl. Acad. Sci. U.S.A.*, **1975**, *72*, 4876. ^{17b}Waring, M., *J. Mol. Biol.*, **1970**, *54*, 247.

¹⁸Wakelin, L.P.G.; Adams, A.; Hunter, C.; Waring, M.J., *Biochemistry*, **1981**, *20*, 5779.

¹⁹Satyanarayana, S.; Dabrowiak, J.C.; Chaires, J.B., *Biochemistry*, **1992**, *31*, 9319.

²⁰Hiort, C.; Norden, B.; Rodger, A., *J. Am. Chem. Soc.*, **1990**, *112*, 1971.

²¹Optical enrichment appears to be the most sensitive technique for detecting preferential binding affinity. Equilibrium dialysis performed on the individual enantiomers with DNA to measure relative binding affinities showed no significant differences between the two isomers.

²²Mirau, P.A.; Behling, R.W.; Kearns, D.R., *Biochemistry*, **1985**, *24*, 6200.

²³Rehmann, J.P.; Barton, J.K., *Biochemistry*, **1990**, *29*, 1701.

²⁴Rehmann, J.P.; Barton, J.K., *Biochemistry*, **1990**, *29*, 1710.

^{25a}Eriksson, M.; Leijon, M.; Hiort, C.; Norden, B.; Graslund, A., *J. Am. Chem. Soc.*, **1992**, *114*, 4933. ^{25b}Eriksson, M.; Leijon, M.; Hiort, C.; Norden, B.; Graslund, A., *Biochemistry*, **1994**, *33*, 5031.

²⁶Barton, J.K.; Basile, L.A.; Danishefsky, A.; Alexandrescu, A., *Proc. Natl. Acad. Sci. U.S.A.*, **1984**, *81*, 1961.

-
- ²⁷Kumar, C.V.; Barton, J.K.; Turro, N.J., *J. Am. Chem. Soc.*, **1985**, *107*, 5518.
- ²⁸Friedman, A.E.; Kumar, C.V.; Turro, N.J.; Barton, J.K., *Nucleic Acids Res.*, **1991**, *19*, 2595.
- ²⁹Barton, J.K.; Raphael, A.L., *Proc. Natl. Acad. Sci. U.S.A.*, **1985**, *82*, 6460.
- ³⁰Pohl, F.M.; Jovin, T.M., *J. Mol. Biol.*, **1972**, *67*, 375.
- ^{31a}Mei, H.-Y.; Barton, J.K., *J. Am. Chem. Soc.*, **1986**, *108*, 7414. ^{31b}Mei, H.-Y.; Barton, J.K., *Proc. Natl. Acad. Sci. U.S.A.*, **1988**, *85*, 1339.
- ^{32a}Wu, H.M.; Crothers, D.M., *Nature (London)*, **1984**, *308*, 509. ^{32b}Arnott, S.; Selsing, E., *J. Mol. Biol.*, **1974**, *88*, 551. ^{32c}Burkhoff, A.M.; Tullius, T.D., *Cell*, **1987**, *48*, 935.
- ^{32d}Boles, T.C.; Hogan, M.E., *Biochemistry*, **1987**, *26*, 367.
- ^{33a}Friedman, A.E.; Chambron, J.-C.; Sauvage, J.-P.; Turro, N.J.; Barton, J.K., *J. Am. Chem. Soc.*, **1990**, *112*, 4960. ^{33b}Jenkins, Y.; Friedman, A.E.; Turro, N.J.; Barton, J.K., *Biochemistry*, **1992**, *31*, 10809. ^{33c}Holmlin, R.E.; Barton, J.K., *Inorg. Chem.*, **1995**, *34*, 7.
- ^{34a}Murphy, C.J.; Arkin, M.A.; Jenkins, Y.; Ghatlia, N.C.; Bossman, S.H.; Turro, N.J.; Barton, J.K., *Science*, **1993**, *262*, 1025. ^{34b}Murphy, C.J.; Arkin, M.A.; Ghatlia, N.D.; Bossman, S.; Turro, N.J.; Barton, J.K., *Proc. Natl. Acad. Sci. U.S.A.*, **1994**, *91*, 5315.
- ^{34c}Stemp, E.D.A.; Arkin, M.A.; Barton, J.K., *J. Am. Chem. Soc.*, **1995**, *117*, 4788.
- ^{35a}Chambron, J.-C.; Sauvage, J.-P.; Amouyal, E.; Koffi, P., *New J. Chem.*, **1985**, *9*, 527.
- ^{35b}Amouyal, E.; Homsy, A.; Chambron, J.-C.; Sauvage, J.-P., *J. Chem. Soc. Dalton Trans.*, **1990**, 727. ^{35c}Fees, J.; Kaim, W.; Moscherosch, M.; Mathels, W.; Klima, J.; Krejcik, M.; Zalis, S., *Inorg. Chem.*, **1993**, *32*, 166.
- ³⁶Stoeffler, H.D.; Thornton, N.B.; Temkin, S.L.; Schanze, K.S., *J. Am. Chem. Soc.*, **1995**, *117*, 7119.
- ³⁷Turro, C.; Bossman, S.H.; Jenkins, Y.; Barton, J.K.; Turro, N.J., *J. Am. Chem. Soc.*, **1995**, *117*, 9026.

-
- ³⁸Hartshorn, R.M.; Barton, J.K., *J. Am. Chem. Soc.*, **1992**, *114*, 5919.
- ^{39a}Dupureur, C.M.; Barton, J.K., *J. Am. Chem. Soc.*, **1994**, *116*, 10286. ^{39b}Hiort, C.; Lincoln, P.; Norden, B., *J. Am. Chem. Soc.*, **1993**, *115*, 3448. ^{39c}Haq, I.; Lincoln, P.; Suh, D.; Norden, B.; Chowdhry, B.Z.; Chaires, J.B., *J. Am. Chem. Soc.*, **1995**, *117*, 4788.
- ^{39d}Smith, S.R.; Neyhart, G.A.; Kalsbeck, W.A.; Thorp, H.H., *New J. Chem.*, **1994**, *18*, 397.

Chapter 2: Characterization of the Interactions of Dppz Complexes of Ruthenium(II) with Nucleic Acids

2.1. Introduction

Considerable attention has been given to the design of new chemical methods to distinguish and detect nucleic acids with sequence specificity.¹ Our laboratory has focused in part on the development of transition-metal complexes as probes of nucleic acid structure.² We have found that ruthenium complexes serve as very sensitive luminescent reporters of DNA in aqueous solution and may become particularly useful in developing new diagnostics.

It was shown in Chapter 1 that ruthenium polypyridyl complexes, owing to their chemical and spectroscopic properties, are ideally suited for application as sensitive, noncovalent probes for polymer structure. In particular, we will focus on the unusual optical features of ruthenium(II) complexes containing the dipyrrophenazine ligand. Recently, it was reported that dipyrrophenazine (dppz) complexes of ruthenium(II) may serve as "molecular light switches" for DNA.³ The dipyrrophenazine ligand has an extended aromatic surface area which allows for extensive intercalative stacking in DNA; dppz complexes bind avidly to DNA through intercalation (for $[\text{Ru}(\text{bpy})_2\text{dppz}]^{2+}$, $\log K \geq 7$). In aqueous solutions at ambient temperatures the complex shows no photoluminescence but luminesces intensely in the presence of double-stranded DNA. The luminescence enhancement on binding to DNA is $> 10^4$, compared to an enhancement of ~ 20 for the conventional dye ethidium.⁴

In this chapter, we examine the binding interactions of dppz complexes of ruthenium(II) with DNA and RNA so as to identify the scope and versatility of this luminescent reporter in probing nucleic acids. In particular, we explore the photophysical properties of $[\text{Ru}(\text{phen})_2\text{dppz}]^{2+}$ and $[\text{Ru}(\text{bpy})_2\text{dppz}]^{2+}$ (Figure 2.1) upon binding to nucleic acids which differ in sequence and conformation. In addition, features relevant to

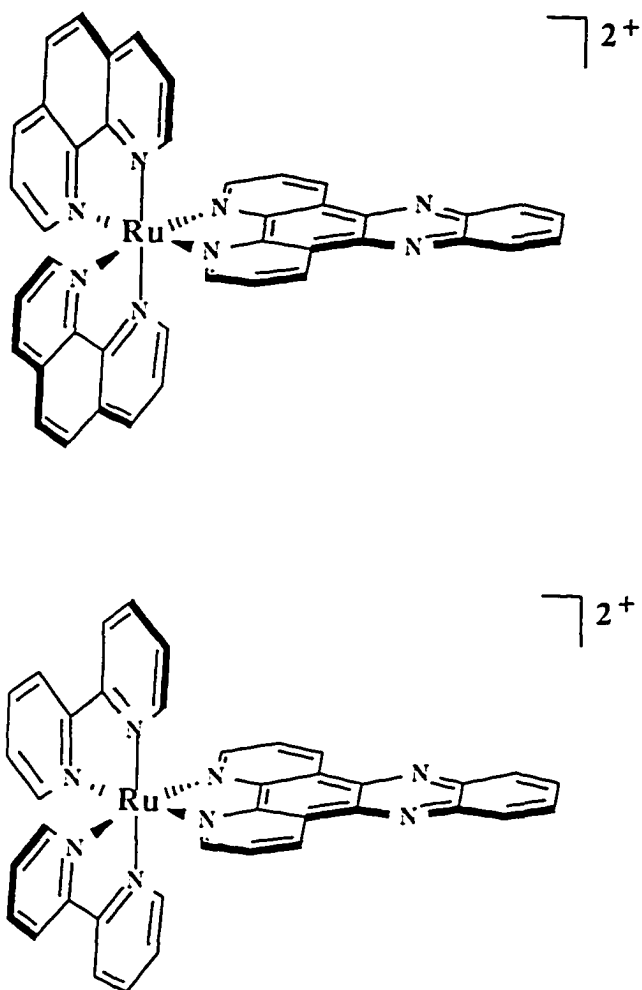


Figure 2.1. Structures of metal complexes [Ru(phen)₂dppz]²⁺ (top) and [Ru(bpy)₂dppz]²⁺ (bottom).

the binding interaction such as the mode of binding and sequence-specificity will also be discussed. We find the luminescent parameters to be remarkably sensitive to the DNA structure at the intercalation site and, more specifically, to how the structure protects the dppz ligand from interactions with solvent. These luminescent probes may provide unique diagnostic markers for conformation.

2.2. Experimental

Buffers and Chemicals. All experiments were conducted in deionized, distilled water containing 50 mM NaCl and 5 mM Tris, pH 7.0. Experiments requiring Z-form DNA were carried out in buffer containing 20 mM NaCl, 4 μ M $[\text{Co}(\text{NH}_3)_6]^{3+}$, and 2 mM Tris, pH 7.0. $\text{RuCl}_3 \cdot 3\text{H}_2\text{O}$ was purchased from Johnson and Matthey/AESAR and $\text{K}_4\text{Fe}(\text{CN})_6$ from Alrich Gold Label; both were used without further purification.

Ruthenium Complexes. Tris(2,2'-bipyridyl)ruthenium(II) dichloride was purchased from Aldrich Chemical Co. and used without further purification. The complex bis(2,2'-bipyridyl)(dipyrido[3,2-*a*:2',3'-*c*]phenazine)ruthenium(II) (hexafluorophosphate), $[\text{Ru}(\text{bpy})_2\text{dppz}](\text{PF}_6)_2$ was prepared as reported previously.⁵ $[\text{Ru}(\text{phen})_2\text{dppz}](\text{PF}_6)_2$ (phen = 1,10-phenanthroline) was synthesized using a similar method.

Nucleic Acids. Polymeric nucleic acids were purchased from Pharmacia as the lyophilized salt. All nucleic acid stock solutions were dialyzed extensively to remove small fragments and to bring them to the appropriate ionic strengths. Yeast tRNA^{Phe} was purchased from Boehringer Mannheim Biochemicals and dissolved in 10 mM Tris buffer, pH 7.5. The Z conformation of DNA was promoted by the addition of $[\text{Co}(\text{NH}_3)_6]^{3+}$ to B-form poly (dG·dC)·poly (dG·dC) and characterized using the negative Cotton effect observed at 290 nm in the circular dichroic spectrum.⁶ Oligonucleotides used in the triple-helix experiments were synthesized using either a Pharmacia gene assembler or an Applied Biosystems DNA synthesizer Model 392 and were purified using reverse-phase HPLC. MgCl_2 (10 μ M) was added to oligonucleotide solutions to stabilize triple-helix

formation.⁷ Formation of the triple-helix was confirmed by melting temperature experiments. Dissociation of the third strand was observed at 50° C; duplex melting occurred at 90° C.

Spectroscopic Measurements. All absorption spectra were measured using either a Varian Cary 219 spectrophotometer or a Hewlett-Packard 8450 diode array spectrophotometer. Circular dichroism measurements were made on a JASCO J-500 spectropolarimeter. Luminescence measurements were made on a SLM 8000C fluorimeter. Samples contained a metal/nucleotide ratio of 0.1 and were thermally equilibrated for 10 minutes in a thermostated sample chamber at 20° C. Luminescence quantum yields were obtained by direct comparison to a 10 μM [Ru(bpy)₃]²⁺ solution irradiated at 440 nm ($\Phi = 0.042$).⁸ Peak integrals were obtained using the SLM software package. Quenching experiments were conducted by adding 5-20 μL aliquots of a 20 mM [Fe(CN)₆]⁴⁻ stock solution to samples containing 10 μM metal and 100 μM nucleotides in the appropriate buffer. Emission lifetimes were measured using a Lambda Physik LPX-200 XeCl excimer pumped dye laser in the Laser Resource Center of the Beckman Institute, as previously described.⁹ Each emission decay trace resulted from an average of 500 laser shots. The decay traces were deconvoluted using a nonlinear least-squares minimization program.

Topoisomerase Assay. The extent of helix unwinding was determined as described previously.¹⁰ Samples were electrophoresed in 0.7% agarose and visualized after incubation for 45 minutes with 5×10^{-4} M [Ru(bpy)₂dppz]²⁺; no destaining was required. The unwinding angles were determined from plots of $-\tau$ (the number of superhelical turns) versus the concentration of metal complex according to¹¹

$$\sigma = -20 r_c (\Phi / 360) = -r_c \Phi / 18$$

where σ is the superhelical density of the plasmid, r_c equals the amount of metal complex ions bound per nucleotide when all of the superhelices are removed, and Φ is the unwinding angle. On the basis of the equilibrium dialysis experiments, added ruthenium

concentrations in this assay could be assumed to be totally bound.

Singlet Oxygen Cleavage of Plasmid DNA Using [Ru(phen)₂dppz]²⁺. The 140 and 180 base pair fragments of pUC18 used in photocleavage experiments were produced by restricting with *Eco* RI and *Pvu* II. Fragments were labeled at their 5' terminus using T4 Polynucleotide Kinase (Boehringer Mannheim Biochemicals) and γ -³²P-ATP (NEN DuPont). Samples were made up with 5 mM Tris, 50 mM NaCl solution buffered at pH 7.0. Enantiomers of [Ru(phen)₂dppz]²⁺ used in photocleavage experiments were obtained according to previously described methods.¹² Deuterated tris buffer was made by dissolving *d*₅-tris (Aldrich) in D₂O and titrating to desired pH using 1 M DCl solution. Irradiations were performed with a 442 nm He-Cd laser (Liconix) for one hour. After irradiation, samples were precipitated, dried, and then washed twice with water, followed by piperidine (1 M) treatment for 30 minutes at 90° C. After removal of piperidine, samples were loaded on an 8% denaturing polyacrylamide gel. Cleavage at 1 μ M ruthenium was quantitated using a phosphorimager (Molecular Dynamics). Normalization was performed by integrating the area under each lane to obtain total cleavage intensity and then dividing the cleavage by the total intensity. Data was also corrected for light damage.

2.3. Results

2.3.1. Unwinding of Supercoiled DNA

The extent of DNA helix unwinding by a noncovalently bound species may be quantitated by examining the change in superhelical density in a plasmid after relaxation of the plasmid in the presence of bound complex with topoisomerase I.^{13, 11a,b} The ability to unwind DNA is consistent with an intercalative mode of binding, an association which results in local distortion of the double helix. This effect is manifested in large topological changes in the plasmid which are observable by agarose gel electrophoresis.

Metal polypyridyl complexes containing dppz as the intercalating ligand unwind

pBR322 DNA with unwinding angles of similar magnitude as avid intercalating agents such as ethidium bromide (26°)^{11a} and $[\text{Ru}(\text{phen})_2\text{phi}]^{2+}$ (26°).¹⁰ Shown in Figure 2.2 is an agarose gel of a topoisomerase unwinding experiment in which topoisomerase I has been used to relax pBR322 samples containing increasing amounts of metal complex. From these titrations, it has been determined that the Δ enantiomer of $[\text{Ru}(\text{phen})_2\text{dppz}]^{2+}$ has a greater unwinding angle than the Λ enantiomer ($25 \pm 5^\circ$ versus $18 \pm 5^\circ$ per bound ruthenium). Differences in unwinding behavior most likely reflect variations in binding to DNA between the two complexes. Intercalation results in local perturbation of the base pairs and the helical backbone. Unwinding as an effect of intercalation will be sensitive to structural details such as the depth of intercalation, interactions of the ancillary ligands with the sugar-phosphate backbone, and the orientation of the intercalating ligand within the major groove. Given the precise nature of the interaction of each of these complexes with DNA, it is not surprising that different unwinding behavior is observed for each enantiomer.

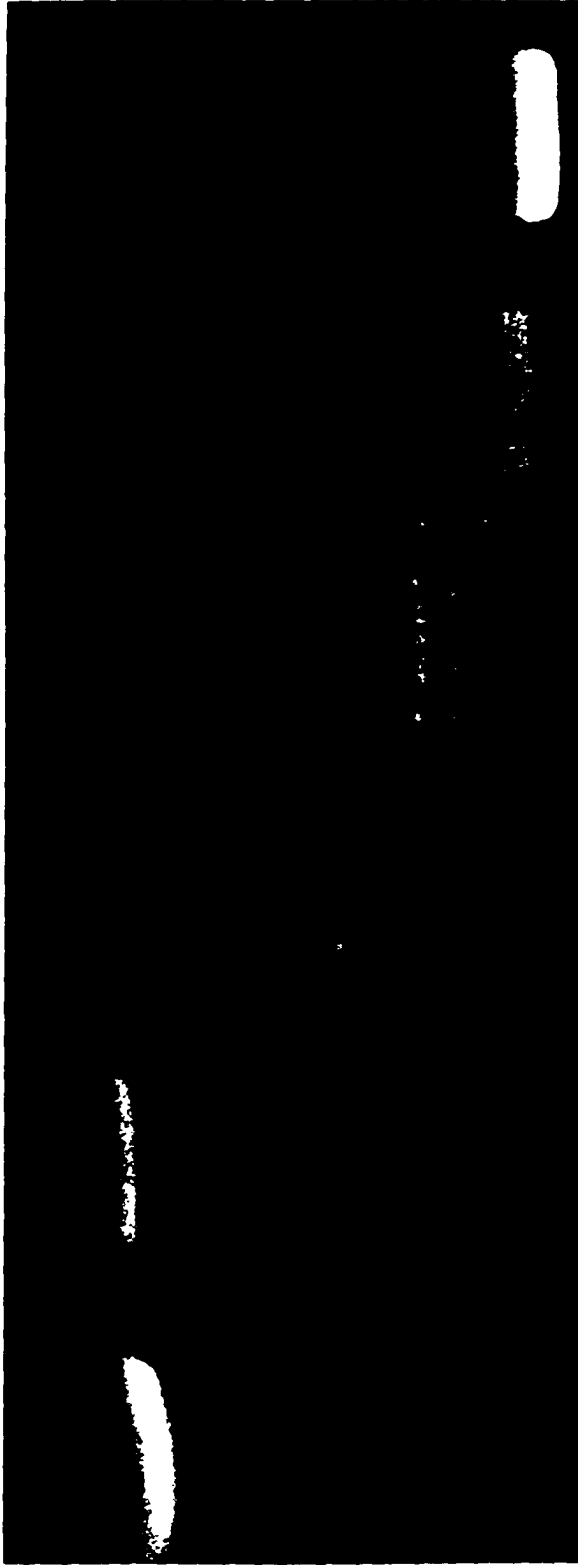
It should be noted that the agarose gel displaying the unwinding of pBR322 has been visualized using $[\text{Ru}(\text{bpy})_2\text{dppz}]^{2+}$ as a luminescent stain. The luminescence enhancement therefore is clearly evident in gels. Some comparison to the commonly used stain ethidium may be made. The emission enhancement of $[\text{Ru}(\text{bpy})_2\text{dppz}]^{2+}$ upon binding to DNA is $\geq 10^4$, compared to an enhancement of ~ 20 for ethidium.⁵ Due to the substantial emission enhancement of the ruthenium complex, no destaining step is required to eliminate background luminescence, which would be advantageous in instances requiring high contrast. The luminescence quantum yield for the ruthenium complex is, however, lower than for ethidium, so that experiments requiring high signal would benefit more from application of ethidium.

2.3.2. Quenching by Water of the Luminescent Excited State

The light switch effect of the dppz complexes upon intercalation has been

Figure 2.2. Agarose gel showing the unwinding of plasmid DNA by $[\text{Ru}(\text{bpy})_2\text{dppz}]^{2+}$ after incubation with topoisomerase I in the presence of increasing amounts of metal complex. Lanes 1-5 show the topoisomer distributions obtained after incubation of plasmid with the enzyme and increasing ruthenium concentrations (3.9 to 8.3 μM). Lane 6 shows DNA without incubation. The gel has been stained with $[\text{Ru}(\text{bpy})_2\text{dppz}]^{2+}$.

1 2 3 4 5 6



attributed to the protection of the phenazine nitrogen atoms from interaction with water in the intercalated form compared to free in aqueous solution. Electrochemical and photophysical measurements of $[\text{Ru}(\text{bpy})_2\text{dppz}]^{2+}$ in both its ground and excited states show that the charge transfer is localized onto the phenazine portion of the ligand.^{5,14} Based upon 1-D and 2-D ^1H -NMR studies of selectively deuterated $[\text{Ru}(\text{phen})_2\text{dppz}]^{2+}$ bound to hexamer oligonucleotide duplex $d(\text{GTCGAC})_2$,^{15a} it is clear that it is the dppz ligand which intercalates and thus would be protected. To establish that the quenching of the ruthenium excited state is indeed the result of interactions with water, we examined the quenching of the excited state of the complex by water in a nonaqueous solvent.

Figure 2.3 shows a Stern-Volmer plot for luminescence quenching of $[\text{Ru}(\text{phen})_2\text{dppz}]^{2+}$ in acetonitrile with increasing concentrations of H_2O and D_2O . Addition of D_2O also quenches the emission of the complex but with a slower rate. The isotope effect, $k_{\text{H}}/k_{\text{D}}$, of 2.1 supports the notion of quenching through vibrational deactivation via a hydrogen bonding pathway.¹⁶ Alternatively, we can consider the quenching mechanism as involving proton complexation and/or transfer to the nitrogens of the reduced dppz ligand resulting from the charge transfer process. The excited state of $[\text{Ru}(\text{phen})_2\text{dppz}]^{2+}$ was quenched in acetonitrile with organic molecules which could serve as proton donors. It was shown that for proton transfer donors in the pK range from 3 to 12, quenching of ruthenium luminescence occurs close to the diffusion controlled limit with rate constants between 4×10^8 and $5 \times 10^9 \text{ M}^{-1}\text{s}^{-1}$.¹⁷

The luminescence quenching can also be followed using time-resolved techniques. Table 2.1 shows the excited-state lifetimes for the dppz complexes in nonaqueous solvent and intercalated into calf thymus DNA. Time-resolved quenching studies of $[\text{Ru}(\text{phen})_2\text{dppz}]^{2+}$ by H_2O and D_2O resulted in a similar $k_{\text{H}}/k_{\text{D}}$ of 2.2. It is noteworthy that the ratio of the luminescence of the intercalated complex in calf thymus DNA relative to $[\text{Ru}(\text{bpy})_3]^{2+}$ (0.94) is comparable to the relative luminescent intensity measured in acetonitrile (0.57). As in a nonaqueous system, the intercalation

Figure 2.3. Stern-Volmer plots for steady-state (top) and time-resolved (bottom) luminescence quenching of 10 μM $[\text{Ru}(\text{phen})_2\text{dppz}]^{2+}$ in acetonitrile by H_2O (circles) and D_2O (triangles).

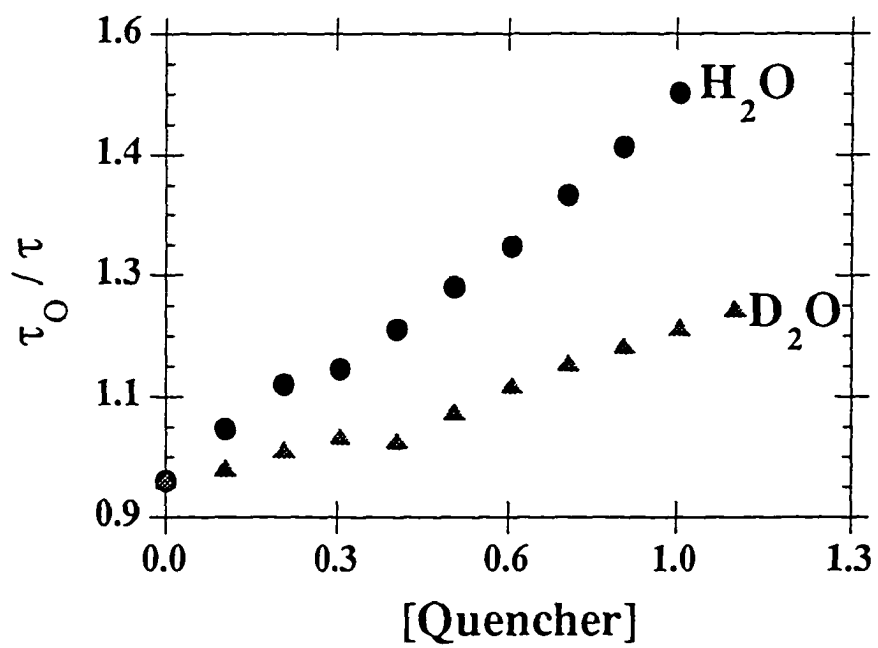
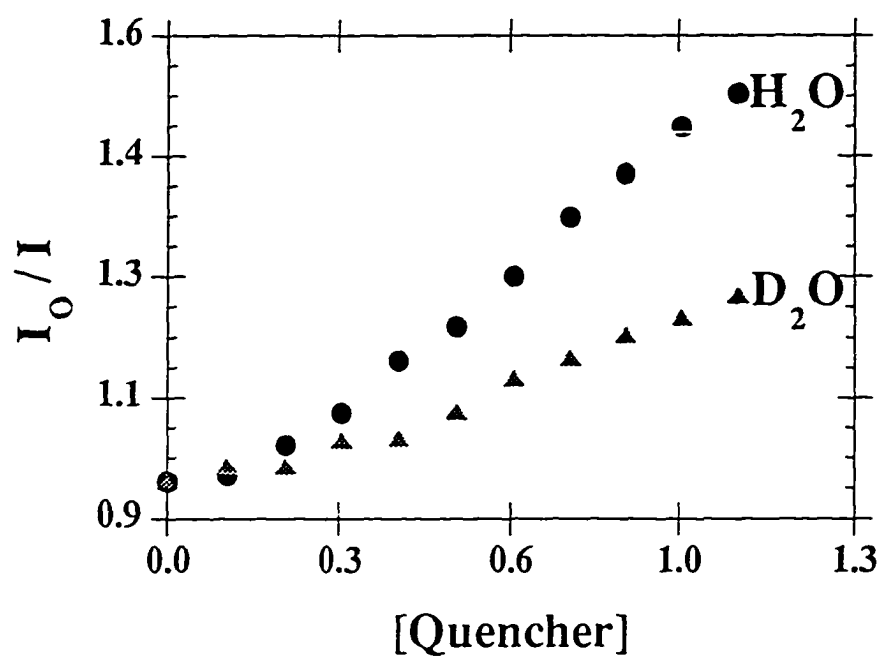


Table 2.1. Emission characteristics of [RuL₂dpppz]²⁺ in non-aqueous solvent and intercalated into calf thymus DNA.^a

Solvent / Nucleic Acid	[Ru(bpy) ₂ dpppz] ²⁺			[Ru(phen) ₂ dpppz] ²⁺				
	τ (ns) ^b	% ^c	λ_{max} (nm) ^b	R.I. ^d	τ (ns) ^b	% ^c	λ_{max} (nm) ^b	R.I. ^d
Acetonitrile	180		622	0.54	180		619	0.57
Calf Thymus DNA	340	20	621	0.16	770	40	617	0.94
	90	80			120	60		

^aAll steady-state measurements conducted at 20° C using 10 μM ruthenium/100 μM nucleotides.

^bError estimated to be $\pm 10\%$ for both steady-state and time-resolved measurements.

^cLifetime ratios calculated from the magnitudes of the pre-exponential factors produced by the fitting program.

^dRelative emission intensities (R.I.) were determined as a ratio of emission relative to a 10 μM [Ru(bpy)₃]²⁺ solution.

environment completely protects the dppz ligand from interactions with water; in addition, as with $[\text{Ru}(\text{phen})_3]^{2+}$, the intercalated complex is also rigidly held in the DNA helix which likely increases its luminescence still further relative to that in nonaqueous solution. These results are consistent with the proposed mechanism for the light switch effect.

2.3.3. Anionic Quenching of Ruthenium Complexes in the Presence of DNA

As shown in Table 2.1, upon intercalation into B-DNA, a biexponential decay in emission is observed for both dppz complexes, indicating the presence of two distinguishable DNA binding modes for each complex. One might consider that the bound enantiomers show decays in emission at different rates. Photophysical studies carried out on the resolved enantiomers of $[\text{Ru}(\text{phen})_2\text{dppz}]^{2+}$ show biexponential decays for *each* enantiomer upon binding to calf thymus DNA, excluding a stereochemical basis for the biphasic kinetics.¹⁸ Interestingly, the decay rate constants and the pre-exponential factors for the Δ -enantiomer are similar to those of the racemate. Approximately 85% of the emission from the racemic mixture is contributed by the Δ -enantiomer; the contribution from the Λ -enantiomer is expected to be negligible compared to the Δ -enantiomer owing to a substantial difference in the emission quantum yields. Preferential emission by the Δ -isomer in the presence of right-handed double-helical DNA is completely consistent with earlier studies conducted on $[\text{Ru}(\text{phen})_3]^{2+}$.^{19,2d}

Biphasic decays in emission have also been observed in luminescence studies of the parent complex, $[\text{Ru}(\text{phen})_3]^{2+}$, bound to calf thymus DNA. The differential kinetics were attributed to two different binding modes: for the intercalative interaction the excited-state lifetime of $[\text{Ru}(\text{phen})_3]^{2+}$ is increased from 0.6 to 2 μs (no difference in emission decay rate has been found between intercalatively bound enantiomers of $[\text{Ru}(\text{phen})_3]^{2+}$), while for the groove-bound interaction, the excited-state lifetime is

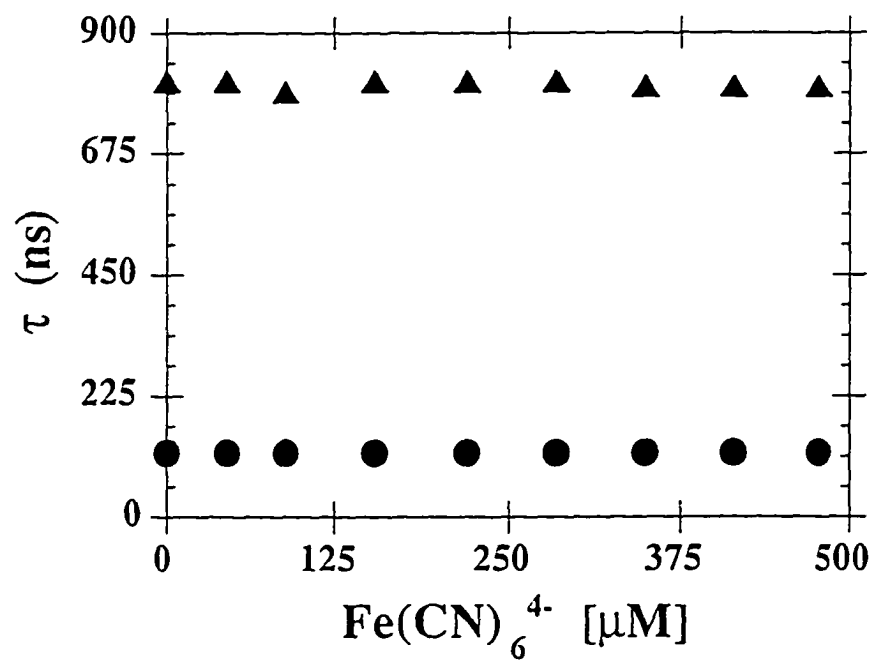
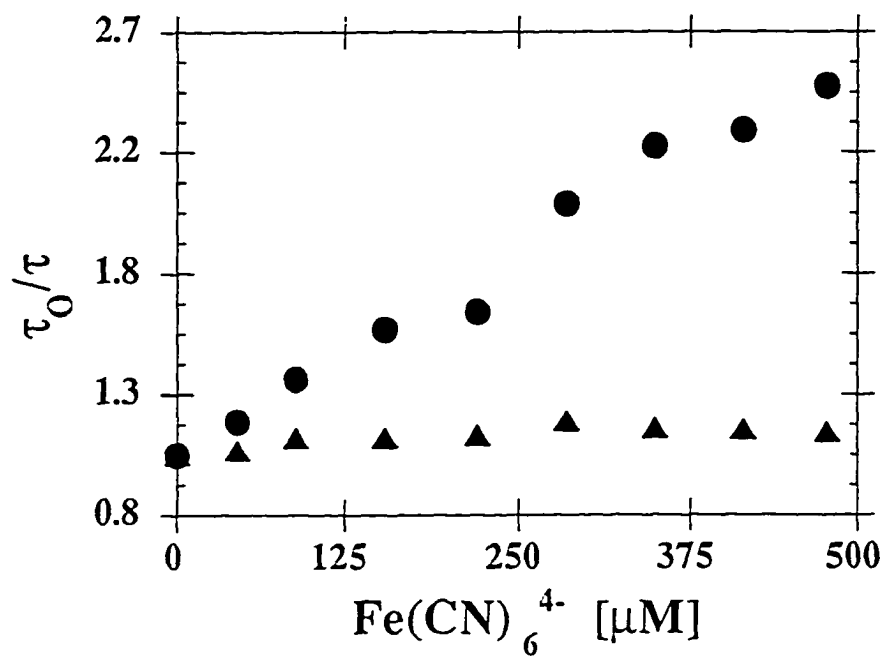
comparable to that of the free form. These two modes were assigned in part through quenching studies using anionic quenchers such as $[\text{Fe}(\text{CN})_6]^{4-}$ which quenches the groove-bound form with an efficiency less than that of free ruthenium (owing to the association of the groove-bound species with the DNA polyanion) but does not quench the closely bound intercalated form.²⁰ Quenching of the excited state using an anionic quencher therefore permits the discrimination between differently bound ruthenium species.

In an effort to characterize the biexponential decay characteristics of the dppz complexes, time-resolved quenching experiments with ferrocyanide were therefore also conducted. Figure 2.4 shows the results for $[\text{Ru}(\text{phen})_2\text{dppz}]^{2+}$ with $[\text{Ru}(\text{phen})_3]^{2+}$ displayed as a comparison. As can be seen in the figure, no quenching by $[\text{Fe}(\text{CN})_6]^{4-}$ is evident, even after the addition of a 50-fold excess of the quencher; an analogous result is apparent with $[\text{Ru}(\text{bpy})_2\text{dppz}]^{2+}$. These results indicate that *both* lifetimes correspond to modes where the complex is embedded in the interior of the helix, inaccessible to the quencher. The results therefore suggest that for these dppz complexes, both binding modes may be intercalative.

As a complement to the ferrocyanide quenching studies, quenching of the ruthenium luminescence can be accomplished using a positively charged species such as $[\text{Ru}(\text{NH}_3)_6]^{3+}$ which associates with the double helix via a combination of both electrostatic and hydrogen bonding interactions. When $[\text{Ru}(\text{NH}_3)_6]^{3+}$ is used to quench the ruthenium luminescence, the two emissive components are quenched with different rates.²¹ The results indicate that the two binding components are tightly associated with the helix in a manner which allows their discrimination by the $[\text{Ru}(\text{NH}_3)_6]^{3+}$ quencher, again supporting the presence of two different intercalative associations with the helix.

The absence of a significant surface bound mode for the dppz complexes is not surprising, given the large increase in binding affinity for the dppz complexes compared to $[\text{Ru}(\text{phen})_3]^{2+}$. What is unusual is our ability to detect using photophysical methods

Figure 2.4. Luminescent quenching of the long-lived component (triangle) and short-lived component (circle) for 10 μM $[\text{Ru}(\text{phen})_3]^{2+}$ (top) and $[\text{Ru}(\text{phen})_2\text{dppz}]^{2+}$ (bottom) in the presence of 100 μM calf thymus DNA by $[\text{Fe}(\text{CN})_6]^{4-}$. The quenching is plotted in Stern-Volmer form for $[\text{Ru}(\text{phen})_3]^{2+}$ and shows the surface-bound form to be quenched, while the intercalatively bound component is more difficult to quench. In the case of $[\text{Ru}(\text{phen})_2\text{dppz}]^{2+}$, the plot shows no variation in luminescence for either component as a function of added quencher, consistent with the assignment of both components as intercalative.



the presence of two different intercalative associations with the helix. In addition to our luminescence results, other photophysical studies on asymmetrically substituted $[\text{Ru}(\text{phen})_2\text{dppz}]^{2+}$ derivatives^{4b} as well as differential quenching experiments using hydrophobic and polar proton transfer quenchers¹⁷ support a model based upon two intercalative binding geometries: (i) a perpendicular mode where the dppz ligand intercalates from the major groove such that the metal-phenazine axis lies along the dyad axis, and (ii) a side-on mode where the metal-phenazine axis lies along the long axis of the base pairs. This model is in full agreement with the previously mentioned ¹H-NMR studies on selectively deuterated $[\text{Ru}(\text{phen})_2\text{dppz}]^{2+}$ bound to d(GTCGAC)₂.(ref) At least two major groove bound orientations were identified based upon the upfield chemical shifts for the dppz ligand and the intermolecular NOEs between the dppz ligand and a bound A5H₈ proton located in the major groove. The chemical shift pattern supports the presence of two distinguishable populations of intercalative binding orientations, one symmetric and one nonsymmetric, and is a result fully consistent with the photophysical data.

2.3.4. Sequence Dependence of the Emission

Summarized in Table 2.2 are the changes in steady-state luminescence and time resolved parameters observed upon binding to AT- versus GC-containing synthetic polymers by $[\text{Ru}(\text{bpy})_2\text{dppz}]^{2+}$ and $[\text{Ru}(\text{phen})_2\text{dppz}]^{2+}$. A difference is clearly evident. The maximum wavelength for emission ranges from 620 nm to 624 nm for AT-sequences and 606 nm to 610 nm for GC-sequences. Results with calf thymus DNA are intermediate (but closer to the AT-rich DNA). It is perhaps not surprising that the emission is sensitive to the base-pair site surrounding the phenazine ligand. This trend is reinforced by the differences in excited state lifetimes of the dppz complexes bound to the polymers which differ in sequence. Complexes bound to AT-sequences display longer excited state lifetimes (~ 300 - 800 ns) compared to GC-sequences (~ 200 - 400 ns).

Table 2.2. Emission characteristics of [RuL₂dpppz]²⁺ upon binding to AT- vs. GC-containing synthetic polymers.^a

Nucleic Acid	[Ru(bpy) ₂ dpppz] ²⁺				[Ru(phen) ₂ dpppz] ²⁺			
	τ (ns) ^b	% c	λ_{\max} (nm) ^b	R.I. ^d	τ (ns) ^b	% c	λ_{\max} (nm) ^b	R.I. ^d
Poly d(GC) ·	220	60	610	0.29	290	60	606	0.61
Poly d(GC)	70	40			70	40		
Poly dG ·	260	30	610	0.29	400	40	607	0.74
Poly dC	70	70			90	60		
Poly d(AT) ·	320	20	624	0.17	740	40	620	0.75
Poly d(AT)	90	80			120	60		
Poly dA ·	340	40	626	0.23	840	60	621	1.39
Poly dT	80	60			110	40		

^aAll steady-state measurements conducted at 20° C using 10 μ M ruthenium/100 μ M nucleotides.

^bError estimated to be \pm 10% for both steady-state and time-resolved measurements.

^cLifetime ratios calculated from the magnitudes of the pre-exponential factors produced by the fitting program.

^dRelative emission intensities (R.I.) were determined as a ratio of emission relative to a 10 μ M [Ru(bpy)₃]²⁺ solution.

Differences extend, however, beyond the base composition of the site. It is interesting that among the different sequences, the longest excited state lifetimes are observed with poly dA·poly dT, which is considered²² to be the structure of greatest stiffness among the synthetic variations.

2.3.5. Cleavage of pUC18 Restriction Fragments By $^1\text{O}_2$ Generated From Photoexcited $[\text{Ru}(\text{phen})_2\text{dppz}]^{2+}$

Luminescence^{2d} and competition dialysis studies²³ performed on the enantiomers of $[\text{Ru}(\text{phen})_3]^{2+}$ indicated slight sequence preferences for the individual enantiomers with the Δ isomer favoring GC rich sequences and the Λ isomer favoring AT rich sequences. The observed enantioselectivity was suggested to be a reflection of the size of the major groove relative to the size of the complex. The increased binding affinity and the extent of luminescence enhancement for dppz complexes of ruthenium(II) preclude employing similar techniques for sequence-selectivity investigations. Unlike $[\text{Ru}(\text{phen})_3]^{2+}$, the luminescence enhancement upon binding to DNA is not directly related to complex affinity but is rather a function of the stacking geometry of the dppz ligand within the helix.

Measurements of site- or sequence-specificities are routinely performed in our laboratory on phenanthrenequinonediimine complexes of rhodium(III); the photochemical properties of these complexes facilitate the direct determination of preferred binding sites.²⁴ In the absence of similar photochemical features, the binding specificity for dppz complexes of ruthenium(II) can not be determined directly; however, the photophysical properties of $[\text{Ru}(\text{phen})_2\text{dppz}]^{2+}$ can be used to generate $^1\text{O}_2$, a reactive species capable of mediating DNA strand scission.

In order to determine the sequence specificity for $[\text{Ru}(\text{phen})_2\text{dppz}]^{2+}$, the strand cleavage patterns produced by singlet-oxygen mediated cleavage of the 5'- ^{32}P labeled 140 and 180 basepair pUC18 fragments (*Eco* RI, *Pvu* II) were examined. Ruthenium

polypyridyl complexes have been shown to photosensitize efficiently the formation of singlet oxygen, a reactive species which can oxidize the DNA bases.²⁵ The rate of base reactions within the DNA strand parallels the oxidation potential of the individual nucleobases with guanine oxidation being the most facile, followed by thymine, cytosine, and adenine. Singlet oxygen cleavage has been used to confirm the specificity of $[\text{Ru}(\text{TMP})_3]^{2+}$ for A-form nucleic acids.^{2b}

In general, from the photocleavage it appears that the complex and its resolved enantiomers are non-specific (Figures 2.5, 2.6, and 2.7). The cleavage promoted by $[\text{Ru}(\text{phen})_2\text{dppz}]^{2+}$ is analyzed alongside the cleavage produced by $[\text{Ru}(\text{phen})_3]^{2+}$ photosensitization of singlet oxygen in order to obtain information about the intrinsic reactivity of the individual guanines in the strand. Based on previous results observed using Λ - $[\text{Ru}(\text{TMP})_3]^{2+}$, a ruthenium complex targeted against the A-conformation, distinct cleavage patterns are expected for sequence- or site-specific binding. Due to the locally high concentrations of singlet oxygen produced by preferentially bound ruthenium molecules, oxidation of other bases in addition to guanine occurs. Since singlet oxygen is a diffusible species, bands of cleavage are obtained with the strongest intensity located at the center of the band, again consistent with locally high concentrations of singlet oxygen. In the absence of any preferential binding, the cleavage patterns are expected to resemble those produced by $[\text{Ru}(\text{phen})_3]^{2+}$, which selectively oxidizes guanines with cleavage intensities dependent upon the intrinsic reactivity of the guanines in the strand. All cleavage patterns observed are similar to that generated by $[\text{Ru}(\text{phen})_3]^{2+}$.

It is evident that more cleavage occurs with Δ ruthenium than with Λ ruthenium. This correlates with the reported luminescence lifetimes for the resolved enantiomers; since it is the excited state of the metal complex that sensitizes singlet oxygen formation, more cleavage is expected from the Δ enantiomer. The increase in cleavage which occurs in the presence of D_2O suggests that the cleavage reaction is mediated by singlet oxygen. As was shown earlier, however, the ruthenium excited state lifetime also increases in the

Figure 2.5. Gel showing singlet oxygen mediated photocleavage of 5'-labeled 140 base pair pUC18 fragment (*Eco* RI, *Pvu* II) by $[\text{Ru}(\text{phen})_2\text{dppz}]^{2+}$. The lanes from left to right on the gel are: A+ G (1) and C+T (2) sequencing lanes, light control (3), light control treated with piperidine (4), dark control (5), 1 μM (6) and 5 μM (7) racemic ruthenium, dark control (8), 1 μM (9) and 5 μM (10) Λ -ruthenium, dark control (11), 1 μM (12) and 5 μM (13) Δ -ruthenium, 5 μM Δ -ruthenium in D_2O (14), and 10 μM $[\text{Ru}(\text{phen})_3]^{2+}$ (15). All samples except for $[\text{Ru}(\text{phen})_3]^{2+}$ were irradiated for one hour. Sample containing $[\text{Ru}(\text{phen})_3]^{2+}$ was irradiated for 20 minutes.

1 2 3 4 5 6 7 8 9 10 11 12 13 14 15

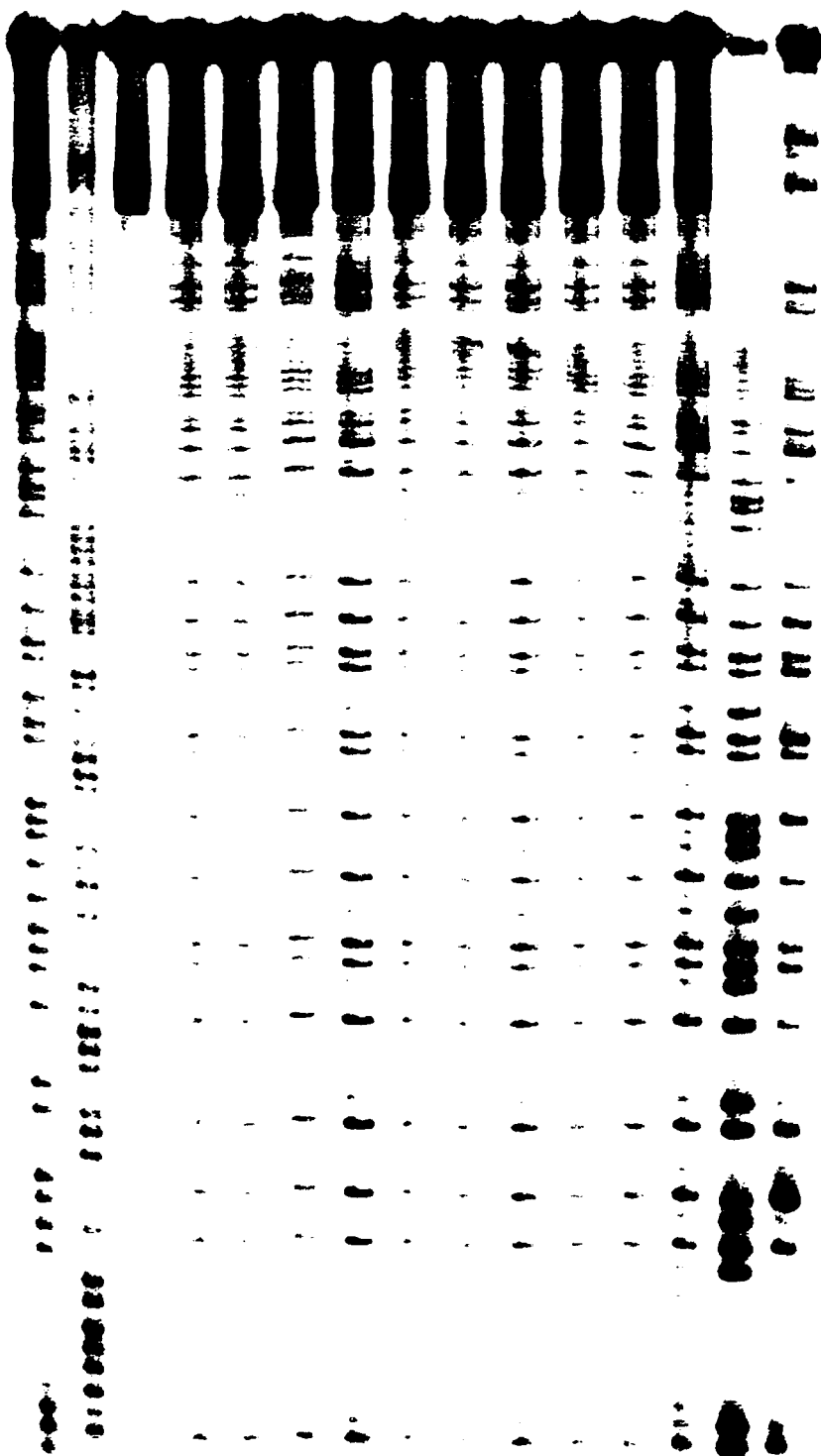


Figure 2.6. Gel showing singlet oxygen mediated photocleavage of 5'-labeled 180 base pair pUC18 fragment (*Eco* RI, *Pvu* II) by $[\text{Ru}(\text{phen})_2\text{dppz}]^{2+}$. Lanes from left to right on gel are: A + G (1) and C + T (2) sequencing reactions, 10 μM $[\text{Ru}(\text{phen})_3]^{2+}$ cleavage (3), light control (4), light control treated with piperidine (5), dark control (6), 0.5 μM (7) and 1 μM (8) racemic ruthenium, dark control (9), 0.5 μM (10) and 1 μM (11) Λ -ruthenium, dark control (12), and 0.5 μM (13) and 1 μM (14) Δ -ruthenium. All samples except for $[\text{Ru}(\text{phen})_3]^{2+}$ were made up on deuterated buffer and irradiated for one hour. The sample containing $[\text{Ru}(\text{phen})_3]^{2+}$ was made up in water and irradiated for 20 minutes.

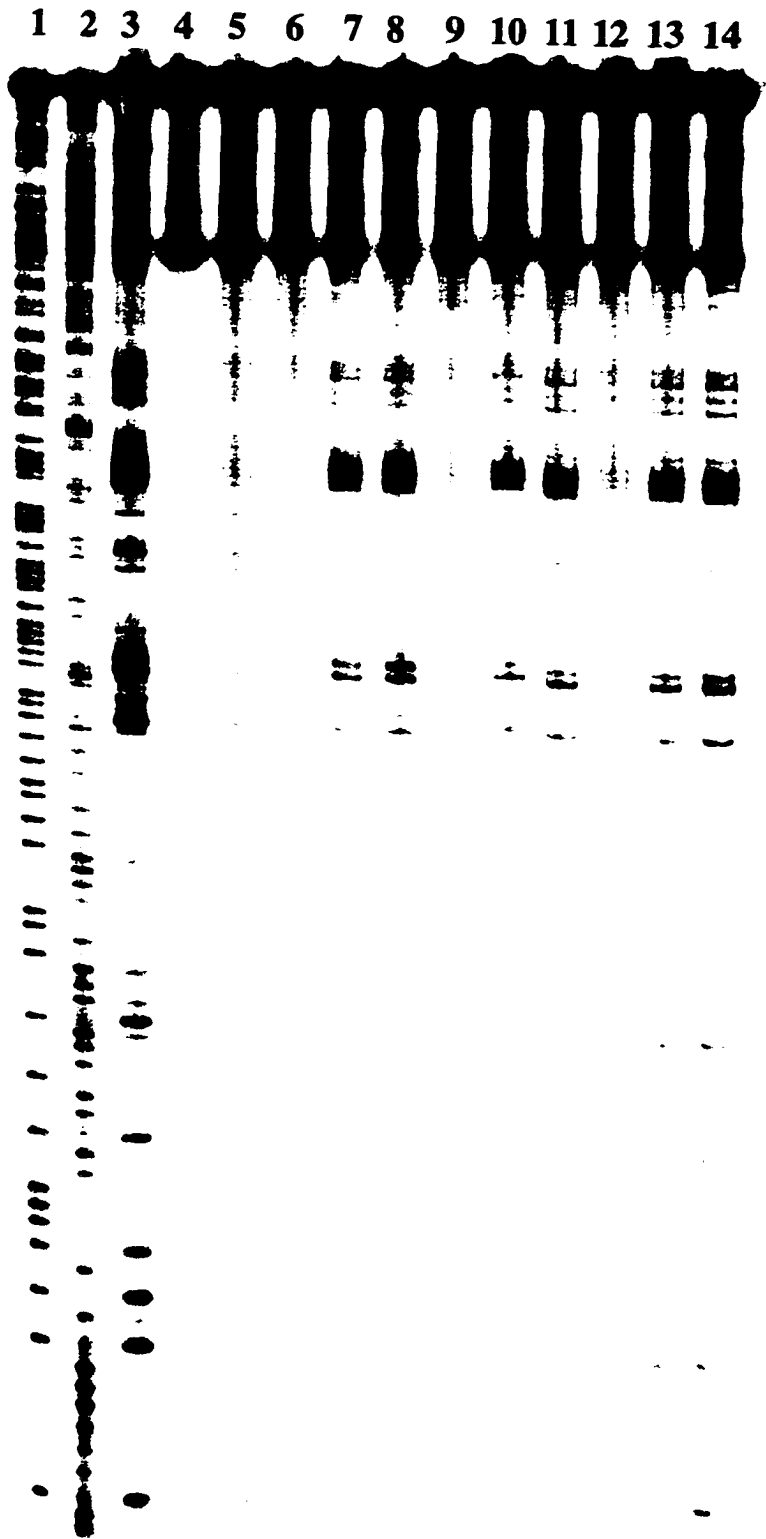
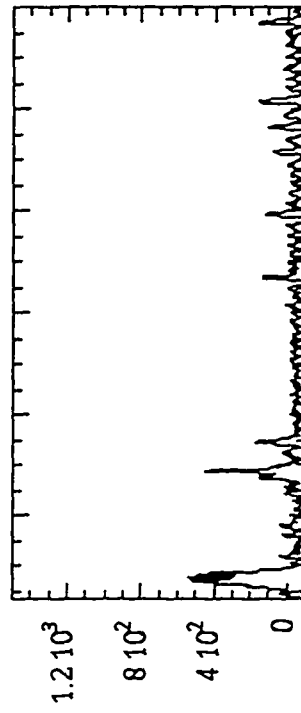
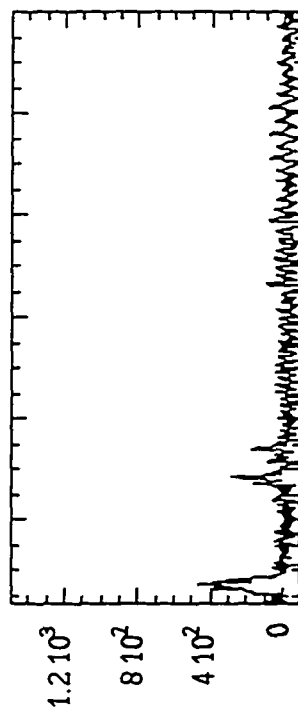
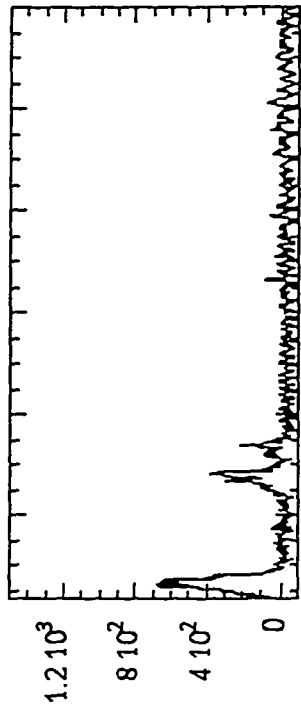
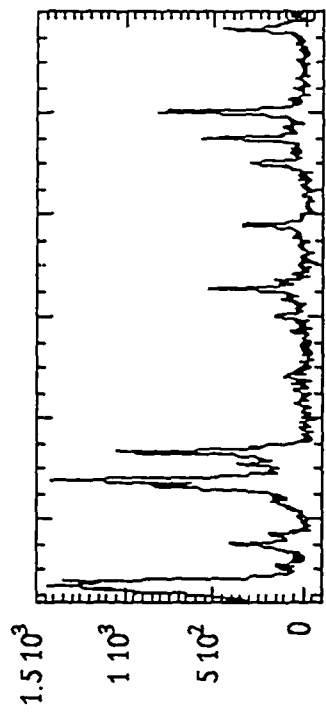


Figure 2.7. Graphs comparing cleavage patterns produced by $[\text{Ru}(\text{phen})_3]^{2+}$ (upper left), racemic $[\text{Ru}(\text{phen})_2\text{dppz}]^{2+}$ (upper right), Λ - $[\text{Ru}(\text{phen})_2\text{dppz}]^{2+}$ (lower left), and Δ - $[\text{Ru}(\text{phen})_2\text{dppz}]^{2+}$ (lower right) after subtraction of the light control and normalization for the cleavage intensity. The cleavage of the 180 base pair pUC18 fragment in the presence of 1 μM metal was used for quantitation. Arbitrary intensity units are measured along the y-axis while the x-axis represents position along the gel lane (left to right corresponds to top of cleavage lane to bottom).



presence of D₂O by two-fold so it is difficult to discern whether the D₂O effect is a result of the increase in singlet oxygen lifetime, ruthenium excited state lifetime, or a combination of both factors.

It is interesting that the mode of binding is not significant in determining cleavage efficiency; dppz complexes have binding constants at least three orders of magnitude larger than [Ru(phen)₃]²⁺ and yet [Ru(phen)₃]²⁺-promoted cleavage is visibly greater. The cleavage efficiency appears to be more a function of the relative excited state lifetimes; the lifetime of the long component of [Ru(phen)₂dppz]²⁺ bound to calf thymus DNA is about 800 ns (20% of the lifetime decay) whereas the lifetime of [Ru(phen)₃]²⁺ is about 2 μs. This is consistent with the results reported comparing the cleavage efficiencies of [Ru(bpy)₂dppz]²⁺ with [Ru(bpy)₃]²⁺.²⁶

2.3.6. Variation in Emission Characteristics with Double Helical Conformation

Table 2.3 shows the variation in steady-state luminescence and time resolved parameters by [Ru(bpy)₂dppz]²⁺ and [Ru(phen)₂dppz]²⁺ as a function of nucleic acid conformation. Both the relative intensity of emission and the rate of decay in emission appear to be quite sensitive to the overall nucleic acid conformation. Highest luminescence is evident with triple-helical DNA, followed by Z- and B-form helices, with lower luminescence evident with the A conformation.

Emission intensity is seen to be lowest for the A-form double helices, poly r(AU)·poly r(AU) and poly rG·poly dC. With [Ru(bpy)₂dppz]²⁺, the emission intensity is ~4% of that observed with its deoxyribose B-form analogue. In A-form helices, the base pairs are pushed back toward the periphery of the double helix, resulting in a very deep and narrow major groove.²⁷ The shape of this cavity hinders the intercalation of tris(phenanthroline) complexes of ruthenium(II)^{2d} and likely also affects the longer dppz ligand in the same manner. It is surprising that intercalation even occurs at all with the A-form, showing the avidity of binding for dppz complexes. Although less pronounced,

Table 2.3. Emission characteristics of $[\text{RuL}_2\text{dpppz}]^{2+}$ upon binding to nucleic acids of varying conformations.^a

Nucleic Acid	$[\text{Ru}(\text{bpy})_2\text{dpppz}]^{2+}$				$[\text{Ru}(\text{phen})_2\text{dpppz}]^{2+}$			
	τ (ns) ^b	% c	λ_{max} (nm) ^b	R.I. ^d	τ (ns)	% c	λ_{max} (nm) ^b	R.I. ^d
Poly d(G-m ⁵ C) · Poly d(G-m ⁵ C)	240	40	606	0.25	360	40	606	0.51
	60	60			90	60		
Z-Poly d(GC) · Poly d(GC)	220	60	608	0.28	270	60	608	0.60
	70	40			70	40		
Calf Thymus DNA Z conditions	330	40	621	0.21	750	40	616	0.80
	80	60			120	60		
Poly r(AU) · Poly r(AU) ^e	400	10	626	0.0057	490	20	620	0.10
	50	90			80	80		
Poly rG · Poly dCe	540	10	620	0.0067	520	30	616	0.04
	70	90			80	70		
100 μM Poly dT · Poly dA · Poly dT ^f	430	70	621	0.60	530	60	621	1.45
	170	30			170	40		
tRNA ^{Phe}	300	30	624	0.06	300	30	620	0.18
	60	70			70	70		

- ^aAll steady-state measurements conducted at 20° C using 10 μM ruthenium/100 μM nucleotides.
- ^bError estimated to be ± 10% for both steady-state and time-resolved measurements.
- ^cLifetime ratios calculated from the magnitudes of the pre-exponential factors produced by the fitting program.
- ^dRelative emission intensities (R.I.) were determined as a ratio of emission relative to a 10 μM [Ru(bpy)₃]²⁺ solution.
- ^eError in time-resolved measurements for A-form polynucleotides more uncertain than 10% given the low overall luminescent intensity.
- ^f10 μM Mg²⁺ was added to stabilize triplex formation.

the differential effect is still clear with $[\text{Ru}(\text{phen})_2\text{dppz}]^{2+}$ (13% relative intensity with poly r(AU)·poly r(AU) compared to poly d(AT)·poly d(AT)). The lowered sensitivity likely reflects how efficiently the ancillary ligands protect the dppz in the groove from access of water (*vide infra*). The overall differences apparent with the A-form compared to B-DNA also support intercalation by these ruthenium complexes from the major groove; other metallointercalators have been shown to bind DNA from the major groove based on x-ray crystallography,²⁸ NMR,²⁹ and also in DNA cleavage experiments.²⁴

Substantial luminescence is apparent on binding to Z-form polymers, consistent with an "intercalative interaction" for the dppz complexes in Z-DNA as well as B-DNA. Earlier studies comparing a range of spectroscopic parameters for ruthenium(II) complexes, notably $[\text{Ru}(\text{phen})_3]^{2+}$ enantiomers, on binding to B- versus Z-DNA have indicated that intercalative binding may occur for metallointercalators with a Z-form helix,⁹ compared to other intercalators such as ethidium³⁰ which promote transitions back to the B form. It must also be noted that since the transition to the Z-form requires the addition of cobalt hexammine, we have included as a control the spectroscopic parameters for calf thymus DNA, still primarily in the B-form, in the presence of cobalt hexammine.

Also included are the luminescent parameters for poly d(G-m⁵C)·poly d(G-m⁵C), which in the B-form shows small but significant decreases in luminescent intensity on binding by the dppz complexes compared to B-form poly d(GC)·poly d(GC). An increase in the percentage of the shorter lifetime component also occurs for both metal complexes. Since the cytidine methyl group protrudes from the major groove, this decrease in intensity is consistent with the perturbed access of the complexes upon intercalation from the major groove. In addition, the protrusion of the methyl group in the groove may impede the "head-on" intercalative interaction, resulting in an increased canted mode of binding.

2.3.7. Binding to a Triple Helix

Table 2.3 includes the luminescent parameters for binding of $[\text{Ru}(\text{bpy})_2\text{dppz}]^{2+}$ and $[\text{Ru}(\text{phen})_2\text{dppz}]^{2+}$ to a triple helical conformation. As may be evident from the Table, the highest luminescent intensities with $[\text{Ru}(\text{bpy})_2\text{dppz}]^{2+}$ and longest excited state lifetimes are observed upon binding to the triple helical conformation. This effect is substantially more pronounced upon binding of the bpy derivative in comparison to $[\text{Ru}(\text{phen})_2\text{dppz}]^{2+}$. The increased lifetime is in part the result of association with the AT sequence. However, in addition, this substantial protection with a triple helix for the dppz ligand from water is understandable given the extended surface area for stacking of a triply bonded array. The triple helix, furthermore, in contrast to an A-form helix, may also provide access for stacking from the major groove.³¹

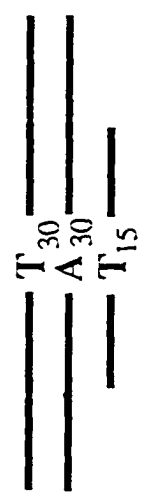
Figure 2.8 schematically illustrates luminescence experiments to test whether intercalative binding by $[\text{Ru}(\text{bpy})_2\text{dppz}]^{2+}$ occurs within the triple helical region or possibly instead at the junction of the triple helical segment with the duplex. It was recently demonstrated that the intercalator ethidium bromide also binds to a triple helix.³² Other planar aromatic chromophores such as ellipticine³³ and acridine³⁴ have been reported to intercalate exclusively at the triplex-duplex junction, rather than within the triple helix itself, indicating the presence of an altered conformation at the junction which creates a strong binding site for these planar, aromatic chromophores. We therefore compared luminescence intensity for $[\text{Ru}(\text{bpy})_2\text{dppz}]^{2+}$ in the presence of $d(\text{A})_{30} \cdot d(\text{T})_{30}$ to which was added either one equivalent of $d(\text{T})_{15}$, two equivalents of $d(\text{T})_{15}$, or one equivalent of $d(\text{T})_{30}$. Upon triple helix formation with only one equivalent of $d(\text{T})_{15}$, two junctions would be present and at most 50% of the steps on the oligomer complex would represent intercalation sites. With $d(\text{T})_{30}$, essentially all sites would be triple helical and lacking in junctions with a duplex. With the addition of two equivalents of $d(\text{T})_{15}$, statistically both the number of triple helical steps and the number of junctions would be intermediate between the two extremes. The greatest luminescence is clearly evident with

Figure 2.8. Schematic diagram of the relative luminescence of $[\text{Ru}(\text{bpy})_2\text{dppz}]^{2+}$ bound to different oligomers. The luminescent intensity correlates with the percentage of triple helix in these oligomeric mixtures, rather than with the number of junctions bordering triple-helical regions, and indicates the greatest luminescence of the ruthenium complex upon intercalation into the triple-helical regions.

Relative Luminescent Intensity

Junctions

% Triple



50

2

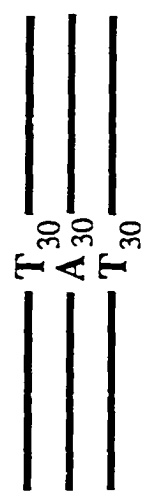
0.31



50-100

1-2

0.39



100

0

0.62

$d(T)_{30} \cdot d(A)_{30} \cdot d(T)_{30}$ which demonstrates that it is the triple helical sites rather than the junctions that contribute to the luminescence. A similar but again less pronounced effect is evident with $[Ru(phen)_2dppz]^{2+}$.

2.3.8. Binding to tRNA^{Phe}

As may be seen in Table 3, binding to a folded RNA such as tRNA^{Phe} yields greater luminescence than is observed with a double helical A-form polymer such as poly r(AU)-poly r(AU). This observation suggests that the dppz complexes bind to alternate sites on the folded tRNA. To test this notion, a competitive binding experiment was conducted using $[Rh(phen)_2phi]^{3+}$, which has been shown to bind specifically to sites of tertiary interaction on tRNA^{Phe}.³⁵ Figure 2.9 shows this competition experiment. With added rhodium complex, which itself does not luminesce, the luminescence of the bound $[Ru(bpy)_2dppz]^{2+}$ is seen to decrease, but only to approximately 30% of its original value. This result would suggest that at least one but not all sites of binding by the dppz complex on tRNA^{Phe} overlap with the tertiary sites targeted by $Rh(phen)_2phi^{3+}$. This result is furthermore consistent with the observation, described above, of enhanced luminescence upon association with triple helical DNA sites.

2.4. Discussion

2.4.1. Mode of Binding to DNA for Dppz Complexes of Ruthenium(II)

The unwinding results indicate (i) unwinding of the DNA helix and (ii) a luminescent change on binding to DNA. Previous studies showed (iii) retention of polarization in emission on excitation with polarized light⁹ and (iv) an increase in binding affinity for the dppz complex due to its extended aromatic framework compared to that for $[Ru(phen)_3]^{2+}$ ($\log K \sim 4$).^{2d} In addition, NMR experiments performed on $[Ru(phen)_2dppz]^{2+}$ and selectively deuterated $[Ru(phen)_2dppz]^{2+}$ with the hexamer oligonucleotide duplex $d(GTCGAC)_2$ show (v) significantly greater upfield shifts of the

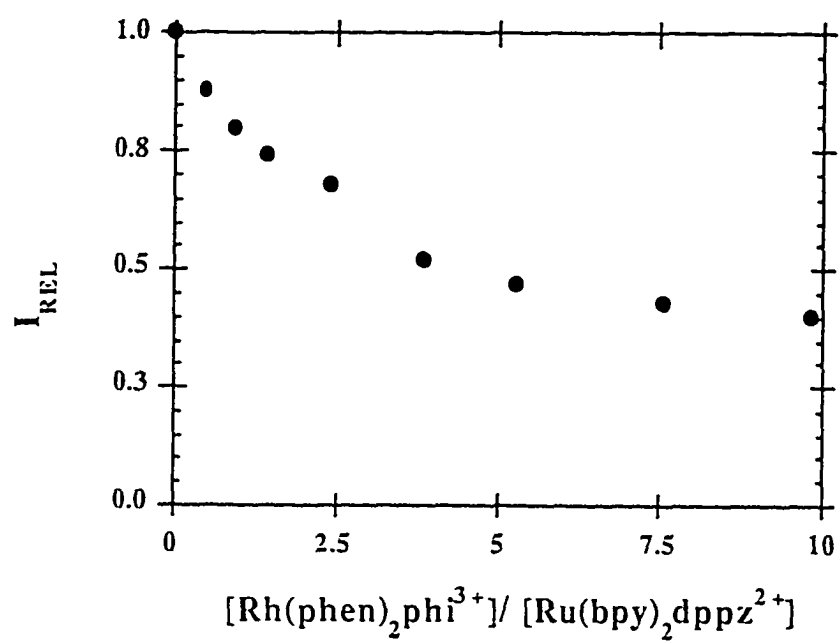


Figure 2.9. Plot showing the relative luminescence of $[\text{Ru}(\text{bpy})_2\text{dppz}]^{2+}$ ($10 \mu\text{M}$) bound to tRNA^{Phe} ($720 \mu\text{M}$ nucleotides) as a function of increasing concentrations of $[\text{Rh}(\text{phen})_2\text{phi}]^{3+}$.

dppz protons relative to the ancillary phenanthroline resonances, confirming the exclusive interaction of the dppz ligand with the base stack and (vi) NOE crosspeaks between the dppz ligand and a bound A5H₈ resonance located in the major groove.^{15a,b} The luminescence and unwinding studies collectively support the assignment of binding of the complex to double-helical DNA through intercalation³⁶ while the NMR evidence clearly identifies the major groove approach of the intercalative interaction.

2.4.2. Sequence-specificity of [Ru(phen)₂dppz]²⁺

The sequence-specificity of [Ru(phen)₂dppz]²⁺ and its enantiomers was examined using ¹O₂-mediated cleavage of pUC18 restriction fragments. According to the cleavage results, no preferential binding is observed for [Ru(phen)₂dppz]²⁺. The apparent dependence of this method on the excited state lifetime of the complex and the reaction preference for oxidation at guanines limits the scope of sequence analysis using this technique. The apparent lack of sequence-specificity displayed by [Ru(phen)₂dppz]²⁺ in the cleavage gels, however, is not surprising given the extended shape of the dppz intercalator. Detailed studies on the recognition characteristics of [Rh(phen)₂phi]³⁺ binding to DNA have shown a preference for sites along the double helix where the major groove is open.²⁴ In order to optimize stacking with the bases, [Rh(phen)₂phi]³⁺ probably has to intercalate more deeply into the major groove relative to the ruthenium complex due to the phi intercalator being short and wide. This requirement is an interaction which results in steric clashes of the ancillary phenanthroline ligands with the phosphate backbone and forms the basis of its specificity for open major grooves. The longer length of the dppz ligand compared to phi allows the ruthenium complex to be accommodated by a greater number of sites.

2.4.3. Comparison of Luminescent Parameters for [Ru(phen)₂dppz]²⁺ and [Ru(bpy)₂dppz]²⁺

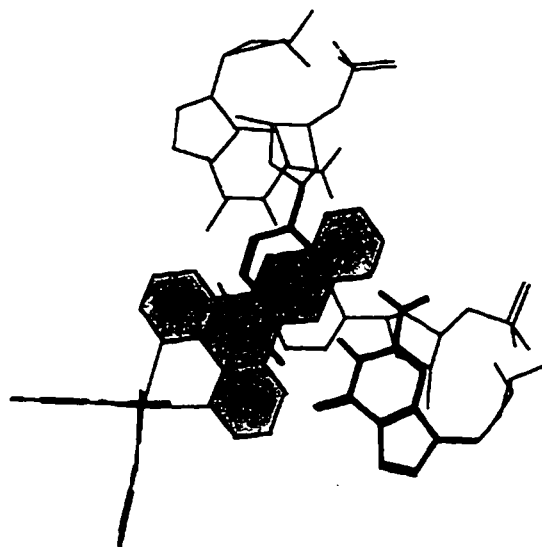
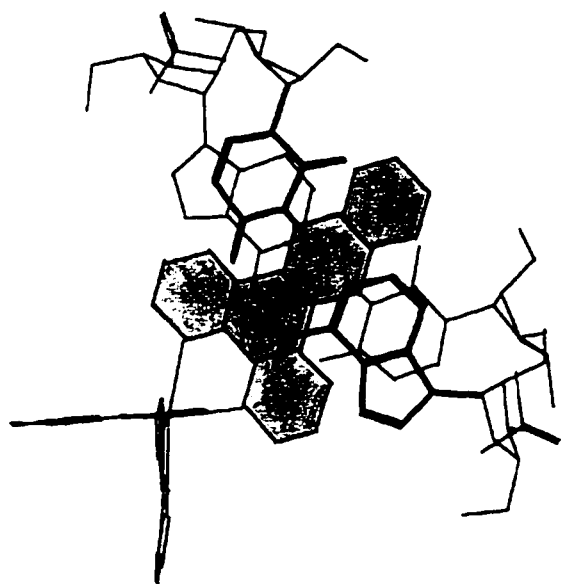
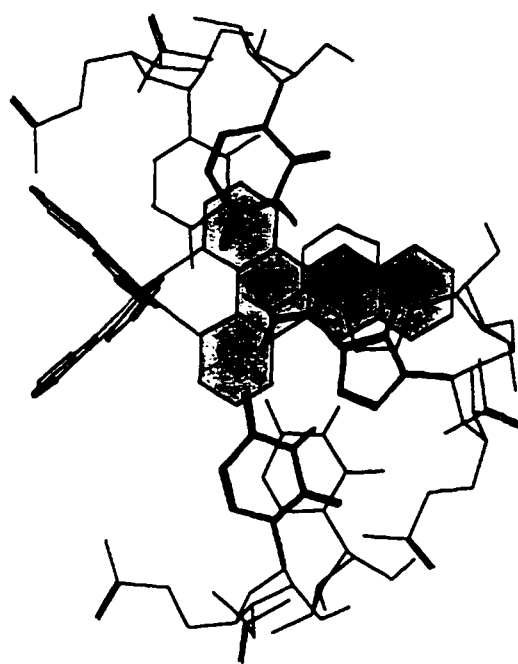
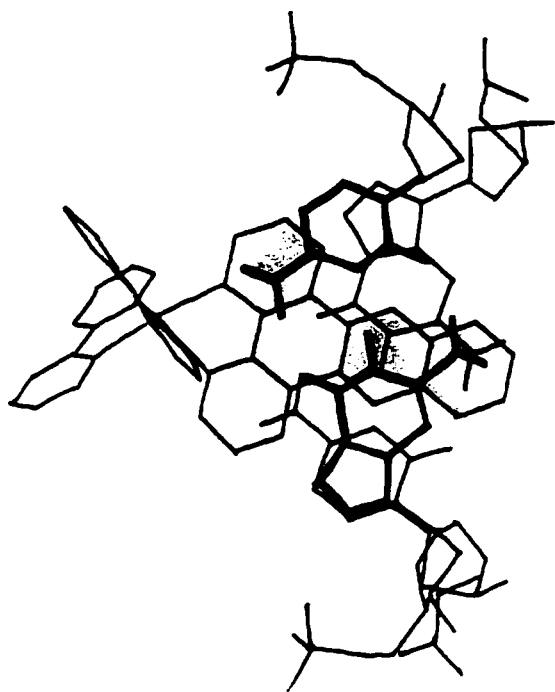
The relative luminescence intensity and excited state lifetime with each polynucleotide are consistently seen to be greater for $[\text{Ru}(\text{phen})_2\text{dppz}]^{2+}$ than for $[\text{Ru}(\text{bpy})_2\text{dppz}]^{2+}$. In fact it is the value of the long lifetime component that is found to vary substantially between the complexes, whereas the short lifetimes are always similar in magnitude. The difference in these parameters therefore depends sensitively upon the ancillary ligands. The ancillary phenanthrolines are larger than the bipyridines, certainly yielding a greater aromatic surface and increased hydrophobicity. The increased size and hydrophobicity of the phenanthroline ligand must affect the ability of the ligands to shield the dppz ligand from water, thereby preserving the emission resulting from the MLCT excited state. Bipyridines also shield the dppz ligand from water but not to the same extent. Because the ancillary bipyridines are not as efficient in shielding as are the phenanthrolines, the luminescence of the bpy derivative becomes a more sensitive source of discrimination between sites and conformations.

The fact that substantial differences between complexes are seen in the longer lived excited state component and not the short lifetime component also supports our assignments of perpendicular and side-on models for intercalation. In the side-on model, because the ancillary ligands are canted toward one side of the groove, they should both be equally ineffective at protecting the exposed phenazine nitrogen from water. Consequently, there is only a slight variation in the short lifetimes for the two complexes. For the perpendicular mode, which corresponds to the longer lived excited state component, differences in extents of water protection, owing to shielding by the different size ancillary ligands, would be expected.

2.4.4. Correlation of Conformational Luminescence Parameters with Water Protection

Figure 2.10 shows a model to illustrate how the different conformations may fix the overlap between the base pairs (or triples) and the intercalated complex. Since

Figure 2.10. Models, looking down the helix axis, which illustrate possible intercalation by the dppz complex into the major groove of the A-, B-, and Z- forms as well as into a triple-helical (figures are displayed clockwise, starting with the A-form in the lower left corner) conformation to show the varying degrees of overlap of the base pairs (or triples) in the different nucleic acid conformations with the intercalated dppz complex. With the B-, Z-, and triple-helical conformations, more protection of the phenazine ring by the bases stacked above and below may be evident. The B-form structure was generated using crystal structure data from a dinucleotide intercalation site (Wang et al., 1978). Intercalation sites for the other conformations were constructed by building a dinucleotide using known helical parameters (Saenger, 1984) and rotating the top base pair or triple in the opposite direction (of helix winding) by 10° around the helix axis (26° unwinding angle for the intercalator). Graphics were generated using MACROMODEL. These models illustrate how stacking of the dppz complex into the different conformations might provide different levels of protection of the phenazine nitrogen atoms from water. The greatest extent of protection and most substantive overlap is clearly with the triple-helical array.



structural information is available only for intercalation into a B-form site, for the purposes of considering luminescence parameters with various conformations, we have assumed an analogous intercalation and we have unwound the base pair (triple) sites by 10° from its starting conformation (in the opposite sense for the Z-site) so as to accommodate an intercalator. One can see the appropriate matching of surface areas for the dppz ligand, in either side-on or perpendicular modes, with a B-conformation. In the case of the A-conformation, with access from the major groove, poor overlap of the phenazine ligand with the helix is found. This correlates with the low relative luminescent intensities found with the A-conformation. In contrast, extensive overlap of the dppz ligand is evident with a triple helical arrangement, since now the extended surface area of the base triple completely surrounds the intercalating ligand; with the triple helix, the highest level of luminescence is observed. The luminescence data, therefore, viewed in the context of these overlap models, point to a basic correlation of relative luminescence and excited state lifetime with how well the given conformation serves to protect the phenazine ligands from water accessibility.

2.5. Conclusions

$[\text{Ru}(\text{bpy})_2\text{dppz}]^{2+}$ and $[\text{Ru}(\text{phen})_2\text{dppz}]^{2+}$ have been shown to be extremely sensitive luminescent probes of nucleic acids, since the complexes, which show no emission in aqueous solution, luminesce intensely upon intercalation in duplex DNA. This "molecular light switch" effect is seen to depend upon the protection of the phenazine ligand from water that occurs with intercalation of the complex into the helix. The level of water protection and hence luminescent properties of the complexes are sensitive to the nucleic acid conformation. Indeed the highest level of emission is observed upon binding to triple helical DNA, where substantial overlap and stacking between the dppz ligand and base triple likely occurs. The variations in luminescence properties also indicate aspects of the binding orientations of the dppz complexes on the

helix. The luminescence data are consistent with two intercalative binding modes: one, in which the metal-phenazine axis lies along the DNA dyad axis, and another, in which the metal-phenazine axis is perpendicular to the DNA dyad axis. These intercalative interactions have been shown, furthermore, to arise in the major groove of DNA. The dipyridophenazine complexes of ruthenium(II) therefore represent novel reporters of nucleic acid sites and structures, and hence may be valuable in the design of new diagnostic and imaging agents.

References

- ^{1a}Pyle, A.M.; Barton, J.K., *Prog. Inorg. Chem.*, **1990**, *38*, 413. ^{1b}Dervan, P.B., *Science*, **1986**, *232*, 464. ^{1c}Hecht, S.M., *Acc. Chem. Res.*, **1986**, *19*, 383. ^{1d}Tullius, T.D., *Nature*, **1988**, *332*, 663.
- ^{2a}Chow, C.S.; Barton, J.K., *Methods Enzymol.*, **1992**, *212*, 219. ^{2b}Mei, H.Y.; Barton, J.K., *J. Am. Chem. Soc.*, **1986**, *108*, 7414. ^{2c}Kirshenbaum, M.R.; Tribolet, R.; Barton, J.K., *Nucleic Acids Res.*, **1988**, *16*, 7943. ^{2d}Barton, J.K.; Goldberg, J.M.; Kumar, C.V.; Turro, N.J., *J. Am. Chem. Soc.*, **1986**, *108*, 2081.
- ^{3a}Friedman, A.E.; Chambron, J.-C.; Sauvage, J.-P.; Turro, N. J.; Barton, J.K., *J. Am. Chem. Soc.*, **1990**, *112*, 4960. ^{3b}Hartshorn, R.M.; Barton, J.K., *J. Am. Chem. Soc.*, **1992**, *114*, 5919.
- ⁴Le Pecq, J.-B.; Paoletti, C., *Anal. Biochem.*, **1986**, *17*, 100.
- ⁵Amouyal, E.; Homsy, A.; Chambron, J.C.; Sauvage, J.P., *J. Chem. Soc. Dalton Trans.*, **1990**, 1841.
- ⁶Pohl, F. M.; Jovin, T. M., *J. Mol. Biol.*, **1972**, *67*, 375.
- ⁷Plum, G.E.; Park, Y.; Singleton, S.F.; Dervan, P.B.; Breslauer, K. J., *Proc. Natl. Acad. Sci. U.S.A.*, **1990**, *87*, 9436.
- ⁸Van Houten, J.; Watts, R.J., *J. Am. Chem. Soc.*, **1975**, *97*, 3843.
- ⁹Friedman, A.E.; Kumar, C.V.; Turro, N.J.; Barton, J.K., *Nucleic Acids Res.*, **1991**, *19*, 2595.
- ¹⁰Pyle, A.M.; Rehmann, J.P.; Meshoyrer, R.; Kumar, C.V.; Turro, N.J.; Barton, J.K., *J. Am. Chem. Soc.*, **1989**, *111*, 3051.
- ^{11a}Keller, W., *Proc. Natl. Acad. Sci. U.S.A.*, **1975**, *72*, 4876. ^{11b}Waring, M., *J. Mol. Biol.*, **1970**, *54*, 247.
- ¹²Yoshikawa, Y.; Yamasaki, K., *Coord. Chem. Rev.*, **1982**, *28*, 205.
- ¹³Kelley, J.M.; Tossi, A.B.; McConnell, D.J.; OhUigin, C., *Nucleic Acids Res.*, **1985**, *13*,

6017.

¹⁴Chambron, J.-C.; Sauvage, J.-P.; Amouyal, E.; Koffi, P., *New J. Chem.*, **1985**, *9*, 527.

^{15a}Dupureur, C.M.; Barton, J.K., *J. Am. Chem. Soc.*, **1994**, *116*, 10286. ^{15b}Dupurer, C.M.; Barton, J.K., unpublished results.

¹⁶Lin, S.; Struve, W.S., *Photochem. Photobiol.*, **1991**, *54*, 361.

¹⁷Turro, C.; Bossman, S.H.; Jenkins, Y.; Barton, J.K.; Turro, N.J., *J. Am. Chem. Soc.*, **1995**, *117*, 9026.

¹⁸Hjort, C.; Lincoln, P.; Norden, B., *J. Am. Chem. Soc.*, **1993**, *115*, 3448.

¹⁹Barton, J.K.; Danishefsky, A.T.; Goldberg, J.M., *J. Am. Chem. Soc.*, **1984**, *106*, 2172.

²⁰Kumar, C.V.; Barton, J.K.; Turro, N.J., *J. Am. Chem. Soc.*, **1985**, *107*, 5518.

²¹Murphy, C.J.; Arkin, M.R.; Ghatlia, N.D.; Bossman, S.; Turro, N.J.; Barton, J.K., *Proc. Natl. Acad. Sci., U.S.A.*, **1994**, *91*, 5315.

²²Kennard, O.; Hunter, W.H., *Q. Rev. Biophys.*, **1989**, *22*, 327.

²³Satyanarayana, S.; Dabrowiak, J.C.; Chaires, J.B., *Biochemistry*, **1993**, *32*, 2573.

²⁴Sitlani, A.; Long, E.C.; Pyle, A.M.; Barton, J.K., *J. Am. Chem. Soc.*, **1992**, *114*, 2303.

²⁵Paillous, N.; Vicendo, P., *J. Photochem. Photobiol. B: Biol.*, **1993**, *20*, 203.

²⁶Sentagne, C.; Chambron, J.-C.; Sauvage, J.-P.; Paillous, N., *J. Photochem. Photobiol. B: Biol.*, **1994**, *26*, 165.

²⁷Saenger, W. (1981) in *Principles of Nucleic Acid Structure* (Cantor, C.R., Ed.) pp 220-241, Springer-Verlag, New York.

²⁸Wang, A.H.J.; Nathans, J.; van der Marel, G.; van Boom, J.H.; Rich, A., *Nature*, **1978**, *276*, 471.

^{29a}David, S.S.; Barton, J.K., *J. Am. Chem. Soc.*, **1993**, *115*, 2984. ^{29b}Hudson, B.P.;

Dupureur, C.M.; Barton, J.K., *J. Am. Chem. Soc.*, **1995**, *117*, 9379. ^{29c}Collins, J.G.;

Shields, T.P.; Barton, J.K., *J. Am. Chem. Soc.*, **1994**, *116*, 9840.

³⁰Terrance Walker, G.; Stone, M.P.; Krugh, T.R., *Biochemistry*, **1985**, *24*, 7462.

-
- ³¹Chow, C.S.; Behlen, L.S.; Uhlenbeck, O.C.; Barton, J.K., *Biochemistry*, **1992**, *31*, 972.
- ^{32a}Mergny, J.L.; Collier, D.; Rougee, M.; Montenay-Garestier, T.; Helene, C., *Nucleic Acids Res.*, **1991**, *19*, 1521. ^{32b}Scaria, P.V.; Shafer, R.H., *J. Biol. Chem.*, **1991**, *266*, 5417.
- ³³Perroualt, L.; Asseline, U.; Rivalle, C.; Thuong, N.T.; Bisagni, C.; Giovannangeli, C.; Le Doan, T.; Helene, C., *Nature*, **1990**, *344*, 358.
- ³⁴Collier, D.A.; Mergny, J.; Thuong, N.; Helene, C., *Nucleic Acids Res.*, **1991**, *19*, 4219.
- ³⁵Chow, C.S.; Barton, J.K.; *J. Am. Chem. Soc.*, **1990**, *112*, 2839.
- ³⁶Long, E.C.; Barton, J.K., *Acc. Chem. Res.*, **1990**, *23*, 271.

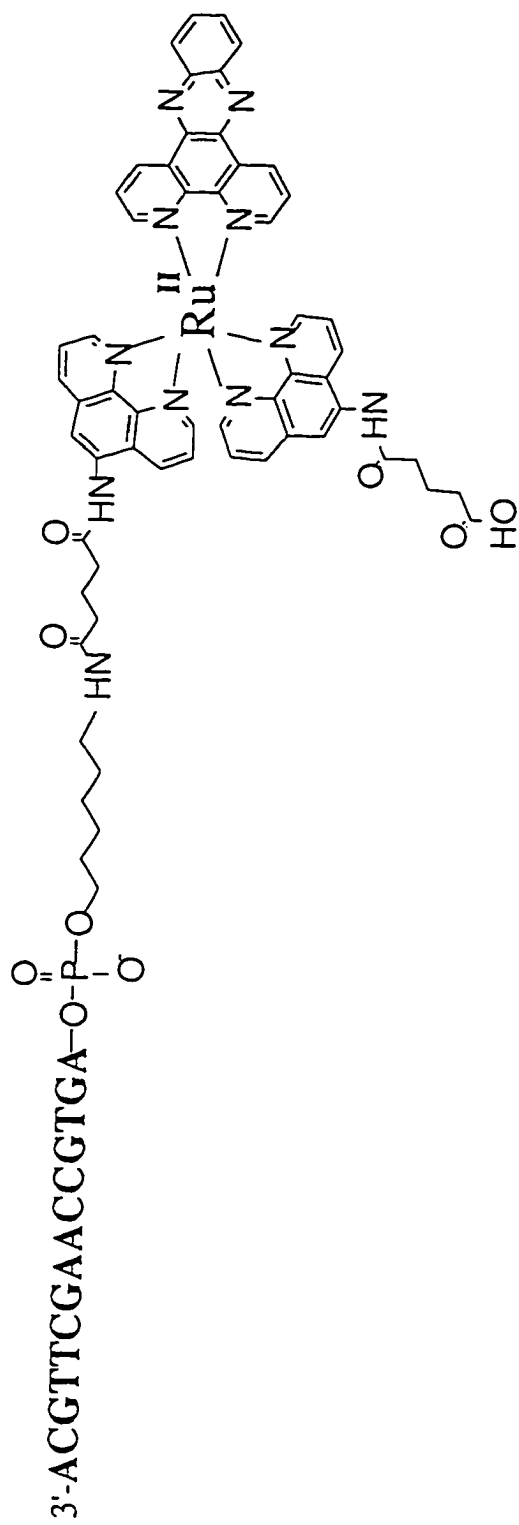
Chapter 3: Synthesis and Characterization of Ruthenium-Oligonucleotide Conjugates

3.1. Introduction

The search for novel diagnostics for DNA detection has generated interest in the potential applications of polypyridyl complexes of ruthenium(II).¹ These complexes are ideally suited as probes for nucleic acids due to their structural and spectroscopic properties. In addition to being water-soluble, coordinatively-saturated, and inert to substitution, ruthenium complexes also possess a well-characterized metal-to-ligand charge transfer (MLCT) transition which gives rise to long-lived emission when these complexes are excited with visible light. One emphasis in our laboratory has been in the development of polypyridyl complexes of ruthenium(II) as novel spectroscopic reporters of nucleic acids.² Recently, we reported that ruthenium complexes containing the dipyrrophenazine ligand may serve as "molecular light switches" for DNA.³ These complexes, which bind DNA avidly through intercalation, show no luminescence in aqueous solution. Upon intercalation into the helix and the concomitant protection of the phenazine ring from quenching by interaction with water, intense luminescence is apparent.

This chapter describes in detail the synthesis and characterization of oligonucleotides covalently modified at their 5' terminus by a dipyrrophenazine complex of ruthenium(II), $[\text{Ru}(\text{phen})_2\text{dppz}]^{2+}$. Figure 3.1 illustrates the structure of a representative metalated oligonucleotide. Two strategies for the assembly of these conjugates have been developed: one method is based upon modification of oligonucleotides still bound to the solid support whereas the second route is performed in solution with the fully purified oligonucleotide. The two synthetic methodologies will be compared and their advantages and limitations discussed. Strategies for the functionalization of oligonucleotides with bathophenanthroline complexes of ruthenium(II) in solution have also been reported by Bannwarth and coworkers.^{1a} In addition to

Figure 3.1. Representative ruthenated oligonucleotide. The oligonucleotide can be attached to $[\text{Ru}(\text{phen}')_2\text{dppz}]^{2+}$ through a variety of different linkers. Illustrated here is a hexamethylene linker connected to the oligonucleotide via a phosphodiester bond.



describing the synthetic routes developed, novel enzymatic methods for extending the length of metalated oligonucleotides will be presented. These unusual probes are being constructed to examine both the sequence specific detection of DNA and photoinduced electron transfer mediated by the DNA double helix.⁴

3.2. Experimental

Materials and Methods. $\text{RuCl}_3 \cdot 3\text{H}_2\text{O}$ was purchased from Johnson & Mathey/AESAR. Purified $[\text{Ru}(\text{phen}')_2\text{dppz}]\text{Cl}_2$ for the coupling reactions was provided by Michelle Arkin and Dr. Sabine Coates. Anhydrous solvents used were obtained from Fluka. Automated DNA synthesis was performed on an Applied Biosystems Inc. 392 DNA synthesizer using reagents purchased either from ABI or Glen Research. Oligonucleotides were purified using reverse-phase high performance liquid chromatography (either a Waters 600E system equipped with a Waters 484 tunable detector or a Hewlett-Packard 1050 HPLC system). High temperature HPLC was carried out on a Hewlett-Packard 1090 HPLC system. Ultraviolet-visible spectra were recorded on a Hewlett-Packard 8452 diode array or a Cary 219 spectrophotometer. FAB-MS were obtained at the Southern California Mass Spectrometry Facility at the University of California, Riverside. ESI-MS were taken by either Dr. Amy Harms in the laboratory of Professor Richard Smith at Batelle Institute, Pacific Northwest Laboratories, or Dr. Larry Heimark at Schering-Plough. MALDI-TOF was performed at the Protein Peptide Micro Analytical Facility at Caltech.

Synthesis and Purification of bis(5-amidoglutaryl-1,10-phenanthroline) (dipyridophenazine)ruthenium(II)(hexafluorophosphate), $[\text{Ru}(\text{phen}')_2\text{dppz}](\text{PF}_6)_2$. The functionalized ligand, phen', was prepared using a previously described method.⁵ $[\text{Ru}(\text{phen}')_2\text{dppz}](\text{PF}_6)_2$ was synthesized according to the method used for the preparation of $[\text{Ru}(\text{bpy})_2\text{dppz}](\text{BF}_4)_2$.⁶ The crude product mixture can be partially purified by column chromatography (basic alumina), washing with an 80/20 mixture of

acetonitrile/water, and product eluted using a 70/20/10 mixture of acetonitrile/water/acetic acid. The three isomers can be separated by reverse-phase HPLC (isocratic elution, 75% 50 mM ammonium acetate or tetraethylammonium acetate/25% acetonitrile).

¹H-NMR and FAB-MS Characterization of the Three Isomers of [Ru(phen')₂dppz]²⁺. Fractions are identified in order of elution from a C₁₈ reverse-phase column. Peaks in the aliphatic region were not used for characterization due to solvent interference. Resonances corresponding to the two outer sets of methylene protons in the linker could be identified. The innermost set of methylene protons were mostly likely obscured by the large residual solvent peak.

First fraction -- ¹H-NMR shifts in ppm (d₃-CD₃CN): 9.63 (dd, 1H), 8.98 (broad s, 1H), 8.71 (dd, 1H), 8.62 (s, 1H), 8.52 (dd, 1H), 8.47 (quart., 1H), 8.20 (dd, 1H), 8.13 (quart., 1H), 8.10 (dd, 1H), 7.93 (dd, 1H), 7.76 (dd, 1H), 7.65 (dd, 1H), 7.57 (dd, 1H). FAB-MS, M⁺ = 1002.

Second fraction -- ¹H-NMR shifts in ppm (d₃-CD₃CN): 9.61 (dd, 1H), 9.64 (dd, 1H), 8.89 (broad s, 2H), 8.70 (d, 2H), 8.62 (s, 1H), 8.61 (s, 1H), 8.53 (d, 2H), 8.47 (quart., 2H), 8.21 (d, 1H), 8.13 (quart., 2H), 8.08 (multiplet, 3H), 8.05 (d, 1H), 7.93 (d, 1H), 7.77 (multiplet, 2H), 7.67 (multiplet, 2H), 7.58 (multiplet, 2H). FAB-MS, M⁺ = 1002.

Third fraction -- ¹H-NMR shifts in ppm (d₃-CD₃CN): 9.63 (dd, 1H), 8.94 (broad s, 1H), 8.70 (d, 1H), 8.63 (s, 1H), 8.53 (d, 1H), 8.46 (quart., 1H), 8.13 (quart., 1H), 8.09 (multiplet, 2H), 8.05 (dd, 1H), 7.76 (dd, 1H), 7.65 (dd, 1H), 7.59 (dd, 1H). FAB-MS, M⁺ = 1002.

Modification of Oligonucleotides at the 5' Terminus with a Primary Amine.

Oligonucleotides can be modified at their 5' terminus with a primary amine by both automated and manual methods. Amine linkers of different lengths containing a phosphodiester linkage to the oligonucleotide are commercially available. The hexamethylene phosphodiester linkage (Aminolink2) used in solution phase synthesis was

purchased from Applied Biosystems, Inc. A method for manually attaching aminoalkyl linkers to oligonucleotides via a carbamate linkage has also been described.⁷ Briefly, after removal of the 5' trityl protecting group, the 5' hydroxyl terminus can be activated with a solution of carbonyldiimidazole (Aldrich) in dioxane. Following removal of excess reagent, the activated oligonucleotide is condensed with a diaminoalkane (Aldrich), resulting in a carbamate linkage stable to the conditions required for cleavage and deprotection of the oligonucleotide.

Solution Phase Synthesis of Ruthenated Oligonucleotide Using DCC/HOBT as Activating Agents. Dicyclohexylcarbodiimide (DCC, Aldrich) and 1-hydroxybenzotriazole (HOBT, Aldrich) were added to $[\text{Ru}(\text{phen}')_2\text{dppz}](\text{PF}_6)_2$ (C_1 isomer, 1 mg) in 1:1 DMF/dioxane. Complete activation as determined by HPLC analysis occurred after 24 hours at 37° C. Amino-linked oligonucleotide (770 nm) was then added as a suspension followed by LiOH to ensure deprotonation of the amine. The solution was covered and put in a 37° C shaker. Reaction was monitored by HPLC. After four days, the reaction was quenched with water, filtered, and the product isolated by reverse-phase HPLC.

Solution Phase Synthesis of Ruthenated Oligonucleotide Using EDC as Activating Agent. Equimolar amounts of HPLC-purified amino-modified oligonucleotide (100 nm) and unmodified complement were annealed in 5 mM phosphate, 50 mM NaCl, pH 7.0 buffer (concentration about 100 μM duplex). A solution of $[\text{Ru}(\text{phen}')_2\text{dppz}](\text{PF}_6)_2$ (from 1 to 2 mgs) in about 20 μL DMF was added to DNA solution. Tube was vortexed and centrifuged to ensure complete solubility of metal complex. The counterion of the complex can be changed to chloride prior to reaction using anion-exchange chromatography. The chloride salt of the complex has a higher solubility in aqueous solution. 5 μmoles of dimethylaminopropylethylenedicarbodiimide (EDC, Fluka) taken from a concentrated stock solution in phosphate buffer was added to ruthenium/DNA solution. Tube was vortexed and centrifuged. Reaction was run overnight in a covered container at room temperature. Excess ruthenium was removed from the reaction using FPLC chromatography

(Pharmacia, MonoQ column). Sodium chloride used in eluting ruthenated oligonucleotide from the FPLC column was removed using Sep-pak C₈ cartridges (Millipore). Ruthenated duplex was purified using reverse-phase HPLC and then subsequent removal of the complementary strand was accomplished using either gel electrophoresis or high temperature HPLC. Ruthenated-oligonucleotide can be isolated from the gel matrix by soaking gel pieces in tris-borate buffer overnight at 37° C. Alternatively, in place of the complementary DNA strand, a complementary mixed DNA/RNA strand can be used. The mixed strand was prepared by using the RNA coupling cycle on an ABI DNA synthesizer. After cleavage of the strand from the solid support using methanolic ammonia, the protecting groups were cleaved using a 1 M solution of tetrabutylammonium fluoride in THF (Aldrich), and the strand desalted using oligonucleotide purification cartridges from ABI. The crude DNA/RNA mixed strand was used directly, without further purification, in the coupling reaction. The coupling reactions were performed as described above except that prior to HPLC purification, reactions were dried down and resuspended in concentrated ammonium hydroxide (2 hours at 55° C) to cleave strand containing RNA nucleotides.

Solid Phase Synthesis of Ruthenated Oligonucleotide Using DSC as Activating Agent. Approximately two milligrams of [Ru(phen')₂dppz](PF₆)₂ (either second or third fraction) along with excess disuccinimidylcarbonate (DSC, Fluka) was dried under vacuum. One ml of 1:1 dry DMF/dioxane was added and the solution degassed. Solution was stirred for three days under argon at room temperature. LiOH was dried under vacuum. One ml of dry DMA was added to LiOH and solution degassed. Solution was stirred at room temperature under argon for at least eight hours. Carbamate-derivatized DNA resin (2.5 μm high loading CPG from Glen Research) was transferred to a dried flask. LiOH solution was added to the DNA resin (about 10 equivalents LiOH to DNA ends). An equivalent volume of dry dioxane was added to mixture and solution degassed. Resin was stirred under argon overnight at room temperature. Activated metal

solution was added to the resin via cannula. Flask was stirred, covered and under argon, at ~ 55 °C for approximately four days. Resin was filtered and washed with DMF until the filtrate ran clear. Resin was then dried using diethyl ether. Ruthenated oligonucleotide was cleaved and deprotected using concentrated NH_4OH at 55 °C for at least six hours. After removal of the NH_4OH , ruthenated oligonucleotide was purified by reverse-phase HPLC.

HPLC Purification of Ruthenated-Oligonucleotides. Ruthenated oligonucleotides were purified by reverse-phase HPLC (Dynamax 250 x 10 mm 300 Å C_{18} column) using 100 mM ammonium acetate or triethylammonium acetate/acetonitrile gradients. EDC reactions were purified using 250 x 5 mm Rainin Microsorb 300 Å C_{18} reverse phase columns. High temperature HPLC runs utilized 20 mM ammonium acetate/acetonitrile gradients. The order of elution was free oligonucleotide (10-15% acetonitrile), followed by ruthenated oligonucleotide (20-35% acetonitrile generally), and then ruthenium complex. The relative mobilities of ruthenated oligonucleotides on reverse phase columns are strongly dictated by the oligonucleotide portion of the conjugate. The absorbance was monitored simultaneously at 260 nm and 440 nm. Peaks eluting between the oligonucleotide and ruthenium which appeared to have an enhancement in 260 nm absorbance relative to the free ruthenium complex were collected. HPLC fractions were lyophilized dry, desalted using either a Millipore sep-pak C_8 cartridge or an Amicon centricon-3 centrifuge filter, and then stored in 5 mM tris base, 50 mM NaCl, pH 7.0 buffer.

Phosphate Analysis. Phosphate analysis was performed according to previously described methods.⁸ Calibration curves were constructed using phosphate solutions of known concentrations for quantitation purposes. Phosphate analysis was used in conjunction with uv-visible spectroscopy to determine sample concentrations.

Snake Venom Phosphodiesterase/Alkaline Phosphatase Assay. Reactions for base digestion assay contained samples (0.25 nm to 1 nm strand), 10 μL 10X alkaline phosphatase buffer, 10 μL 1 M MgCl_2 , 3 μL snake venom phosphodiesterase (Sigma), 3

μL alkaline phosphatase (Boehringer Mannheim Biochemicals), and water to make up 100 μL total volume. Covered samples were incubated for two hours up to overnight at 37° C. Samples were filtered through cellulose acetate and then analyzed using reverse-phase HPLC (Rainin Microsorb 250 x 5 mm 100 Å C₁₈ column, gradient of 250 mM ammonium acetate or triethylammonium acetate/acetonitrile). Cellulose acetate was used for filtration rather than nylon due to greater metal absorption by nylon membrane filters. For quantitation, peak integrals were compared to calibration curves constructed from known concentrations of nucleoside standards (Sigma).

Primer Extension of Ruthenated Oligonucleotide. The primer extension reaction mixture contained 1 pm ruthenium-labeled or unmodified template, 20 pm primer, 50 μM dNTPs (except for dGTP), 1 μL α -³²P-dGTP, 6-7 U Sequenase (USB Biochemicals), water, and 10X buffer to make up 15 μL . The extension reaction was run for one hour at 37° C and terminated using 15 μL TE. Samples were extracted twice using phenol/chloroform/isoamyl alcohol. A small aliquot of each sample was diluted with an equal volume of 1x sequencing gel dye and loaded on a 20% denaturing polyacrylamide gel.

Ligation of Ruthenated Oligonucleotide to a 5'-Phosphorylated Strand.

Oligonucleotides for ligation were phosphorylated at the 5' terminus using automated methods. T4 DNA ligase was purchased from New England Biolabs. Reaction mixtures contained 20 mM Tris·HCl (pH 7.6), 5 mM MgCl₂, 5 mM DTT, 50 $\mu\text{g}/\text{ml}$ of BSA, 0.25 mM dATP, and 1.5 U enzyme. Samples were annealed and subsequently cooled to 0° C before addition of the enzyme. The ligation reaction was run for four hours at room temperature and then quenched by the addition of 50 mM EDTA. After heat denaturation of the enzyme at 60° C for 30 minutes, the enzyme was extracted using phenol/chloroform/isoamyl alcohol. For preparatory scale reactions, the entire reaction mixture can be directly injected onto a reverse-phase HPLC column. The highly charged nature of the enzyme results in elution close to the void volume.

Representative Metal-Oligonucleotide Conjugates. Ru-NH(CH₂)₆NHCO₂-TCTAAGCCATCCGCT-3' was synthesized using the solid phase method with DSC activation (C₁ isomer). Product was analyzed by enzymatic digestion and ESI-MS. Calculated mass for neutral molecule is 5613 D. Observed mass is 5607 D.

Ru-NH(CH₂)₆NHCO₂AGAAGGCCTGGT-3' was synthesized using the solid phase method with DSC activation (C₁ isomer and late eluting metal fraction). Product was analyzed by enzymatic digestion and ESI-MS. Calculated mass for neutral molecule is 4835 D. Observed mass is 4830 D.

Ru-NH(CH₂)₉NHCO₂AGTGCGAAG-3' was synthesized using both the solid phase method with DSC activation (C₁ isomer) and the solution phase method with EDC as coupling reagent (C₁ isomer and late eluting metal fraction). Product from both syntheses gave analogous ESI-MS spectra. Calculated mass for neutral molecule is 3954 D. Observed mass is 3954 D.

Ru-NH(CH₂)₉NHCO₂AGTGCGAAGGCCTGGAACGT-3' was synthesized by ligation of Ru-NH(CH₂)₉NHCO₂AGTGCGAAG-3' to 5'-pGCCTGGAACGT-3' using T4 DNA ligase and the complementary 20mer strand as the template. Product was purified by high temperature HPLC. Yield for ligation is estimated to be at least 50%. Product was characterized by MALDI-TOF. Calculated mass for neutral molecule is 7374 D. Observed mass is 7376 D.

Ru-NH(CH₂)₉NHCO₂AGTCTTATATAAAATATCGT-3' was synthesized using the solution phase method with EDC activation (early eluting metal fraction). Product was analyzed by MALDI-TOF mass spectrometry. Calculated mass for neutral molecule is 7281 D. Observed mass is 7284 D.

Ru-NH(CH₂)₉NHCO₂AGTGCGAAGGCC-3' was synthesized using the solid phase method with DSC activation (C₁ isomer). Product was analyzed by ESI-MS. Calculated mass for neutral molecule is 4862 D. Observed mass is 4862 D.

Ru-NH(CH₂)₉NHCO₂AGTGCGAAGGCCTGGAACGT-3' was synthesized

using the solid phase method with DSC activation (C_1 isomer). Product was analyzed by ESI-MS. Calculated mass for neutral molecule is 7356 D. Observed mass is 7354 D with some lower molecular weight fragments. The signal to noise ratio in the obtained spectrum was very low.

Ru-NH(CH₂)₉NHCO₂AGTGTATATAAACGT-3' was synthesized using the solution phase method with EDC as coupling reagent (late eluting metal fraction). The synthesis was performed with both DNA and mixed DNA/RNA complements. Product was analyzed by quantitative phosphate analysis, base analysis and ESI-MS. Sample was submitted to two different facilities for ESI-MS. One measurement yielded a mass of 5782 D which is close to the calculated mass of 5783 D. The other measurement resulted in a lower mass of 5544 D so it is clear that fragmentation to give a single species with a lower mass than the parent molecule can occur.

Ru-NH(CH₂)₉NHCO₂AGTGCATATATAAAGTACGT-3' was synthesized using the solution phase method with EDC as a coupling reagent (both early eluting and late eluting metal fractions). The synthesis was performed with both DNA and mixed DNA/RNA complements. Product was analyzed by quantitative phosphate analysis and base analysis.

Ru-NH(CH₂)₉NHCO₂AGTCATGTGGCCTAGTCCGT-3' was synthesized using the solution phase method with EDC as a coupling reagent (late eluting metal fraction). The synthesis was performed with both DNA and mixed DNA/RNA complements. Product was analyzed by quantitative phosphate analysis, base analysis, and ESI-MS. Calculated mass for neutral molecule is 7289 D. Observed mass is 7289 D.

Ru-NH(CH₂)₉NHCO₂AGTCTAGGCCTATCGT-3' was synthesized using the solution phase method with EDC as a coupling reagent (early eluting metal fraction and C_1 isomer). The synthesis was performed with a DNA complement. Product was analyzed by quantitative phosphate analysis, base analysis, ESI-MS, and MALDI-TOF. Calculated mass for neutral molecule is 6041 D. Observed mass is 6038 D.

Ru-NH(CH₂)₉NHCO₂AGTCTGTAAACATCGT-3' was synthesized using the solution phase method with EDC as a coupling reagent (C₁ isomer). The synthesis was performed with a DNA complement. Product was analyzed by quantitative phosphate analysis, base analysis, ESI-MS, and MALDI-TOF. Calculated mass for neutral molecule is 6040 D. Observed mass is 6037 D.

Ru-NH(CH₂)₆OPO₂AGTGCCAAGCTTGCA-3' was synthesized using the solution phase method with DCC and HOBT as the coupling reagents (C₁ isomer). Product was analyzed by phosphate analysis.

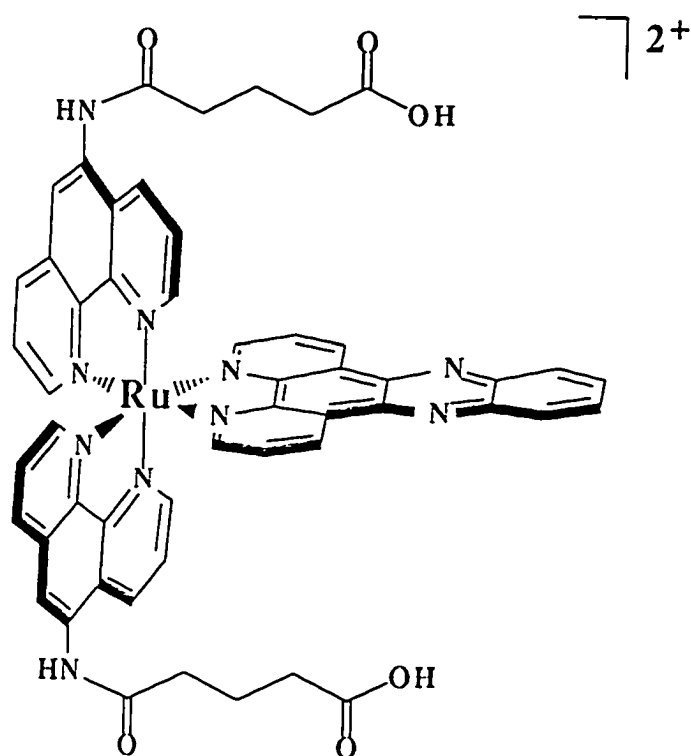
3.3. Results and Discussion

3.3.1. Synthesis of the Functionalized Ruthenium Complex, [Ru(phen')₂dppz]²⁺

Figure 3.2 shows the structure of [Ru(phen')₂dppz]²⁺, a ruthenium complex containing a functionalized phenanthroline ligand available for further derivatization. The synthesis of the metal complex is illustrated in Scheme 3.1. Due to substitution at the 5 position of the phenanthroline ligand, it is possible to obtain three products, all of which vary in the displacement of the phen' ligand about the metal center; two products are of C₂ symmetry and one product has C₁ symmetry, which should result in a statistical product distribution of 1:2:1. A reverse-phase HPLC trace of the reaction mixture shows that indeed, we observe three main peaks in a 1:2:1 ratio. The three isomers can be separated using reverse-phase HPLC under isocratic elution conditions, concentrated in vacuo, and then isolated by precipitation with 10% aqueous ammonium hexafluorophosphate.

¹H-NMR has been used to determine the degree of symmetry for each fraction. The first and third fractions have been assigned as complexes with C₂ symmetry while the second fraction has been identified as the C₁ isomer. The symmetry of the complex can be identified by comparison of the chemical shift patterns observed in the ¹H-NMR spectrum for each isomer (Figure 3.3). The spectrum for the second fraction is much more complicated than the spectra produced by the first and third fractions, indicating lower

Figure 3.2. Structure of functionalized ruthenium complex, $[\text{Ru}(\text{phen}')_2\text{dppz}]^{2+}$.



Scheme 3.1. Synthesis of $[\text{Ru}(\text{phen}')_2\text{dppz}]^{2+}$ and the products which can be obtained. Isomers vary only in the displacement of the functionalized phenanthroline around the metal center.

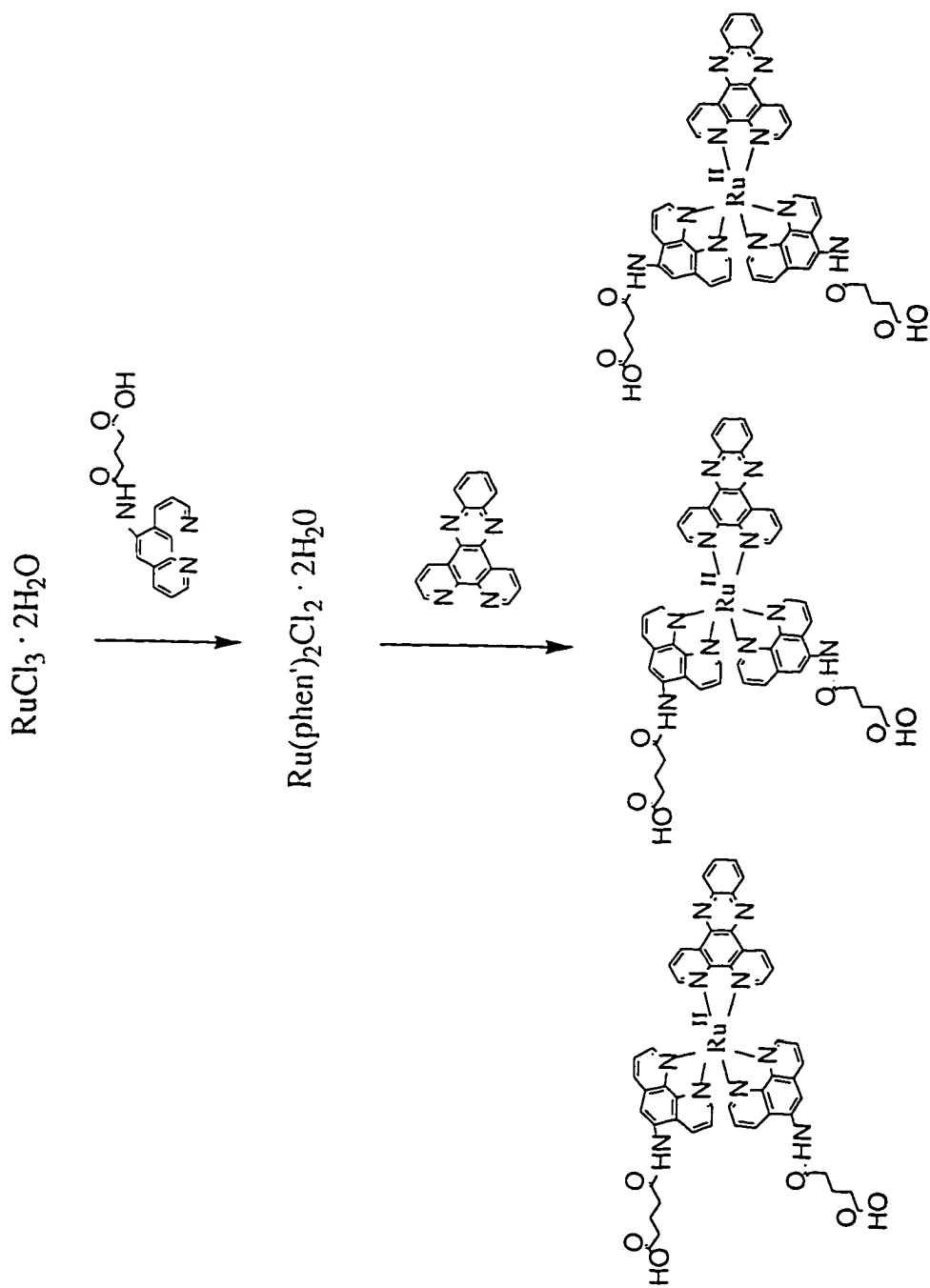
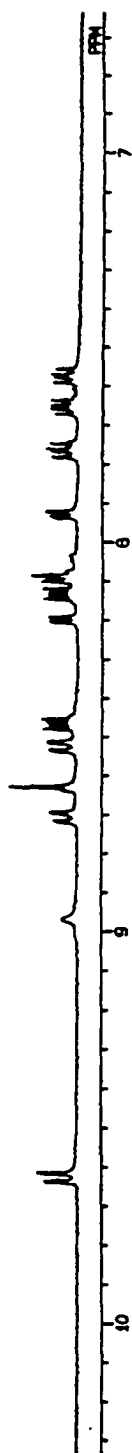
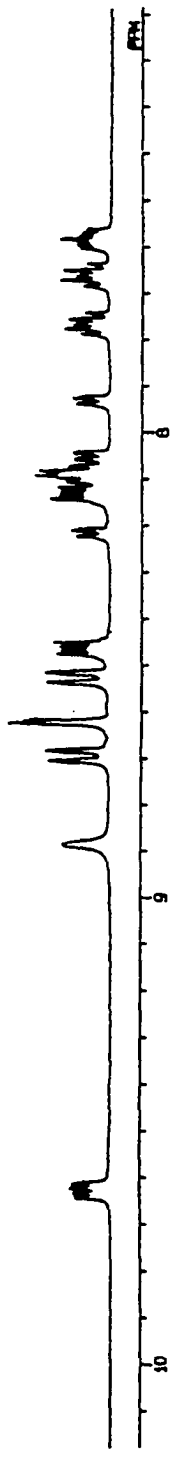


Figure 3.3. $^1\text{H-NMR}$ spectra of the aromatic region of the three isomers of $[\text{Ru}(\text{phen}')_2\text{dppz}]^{2+}$.

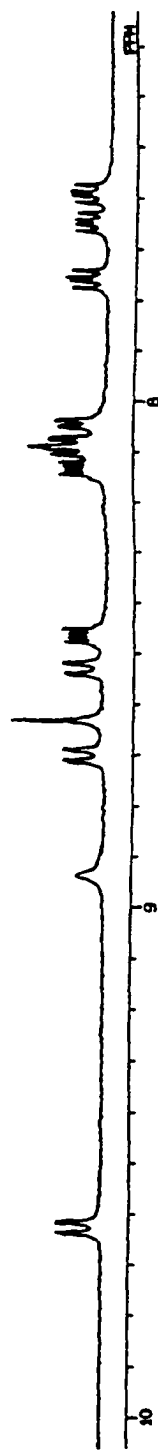
Fraction 1



Fraction 2



Fraction 3



complex symmetry. This difference in spectrum complexity is most clearly illustrated by examination of the shift pattern produced by the resonance corresponding to the proton at the 6 position of the phenanthroline ring, adjacent to the 5-amino substitution (chemical shift around 8.6 ppm for each isomer). If the two ancillary phenanthrolines are symmetrically displaced around the ruthenium center, then the 6-position proton shows up as one singlet due to the C_2 symmetry of the complex. If the metal complex does not possess a C_2 axis of symmetry, then the same proton on the two ancillary phenanthrolines will be in slightly different environments, resulting in two singlets with almost identical chemical shifts. The symmetry assignments made by $^1\text{H-NMR}$ are consistent with predicted product distributions and the ratios observed by HPLC.

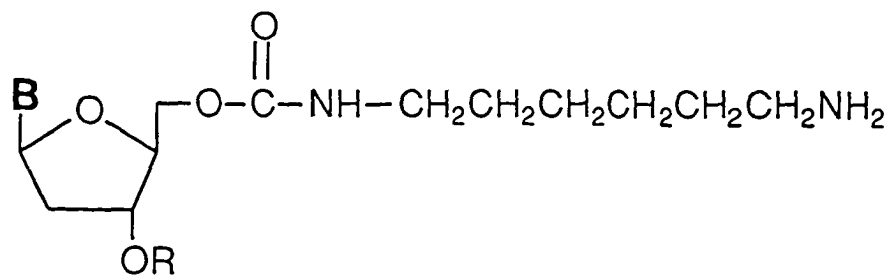
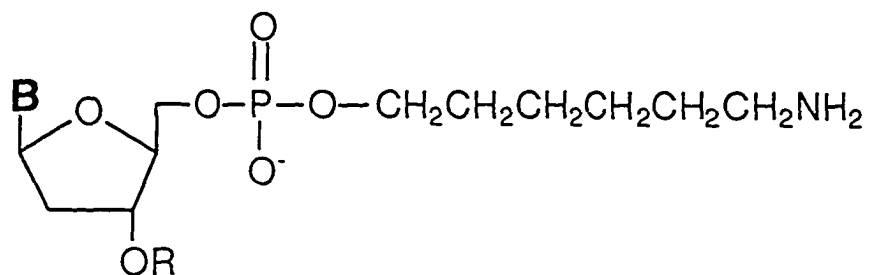
In the absence of a crystal structure, it is not possible to assign further the C_2 symmetric isomers. Complex symmetry is an important consideration in the coupling reaction due to the presence of *nvo* available arms for modification. Coupling to either arm of a C_2 symmetric complex results in products related by an axis of rotation. Coupling of the C_1 isomer produces, in the simplest case, at least two different products. If the diastereomers from coupling of the individual enantiomers are resolved, then at least four products with similar retention times can be observed in the HPLC, in addition to any side reactions the other functionalized phenanthroline may undergo. By using a symmetric starting material, reaction purification and product analysis is greatly simplified.

3.3.2. Synthetic Strategies

Synthesis of Oligonucleotides Modified at the 5' Terminus With a Primary Amine.

Figure 3.4 shows the two different linkages which have been used in our laboratory to functionalize the DNA for further modification. The two linkers differ in the chemical connection to the oligonucleotide. Linkers containing the phosphodiester connection are commercially available, with a variable number of methylene groups, and can be attached to the 5' terminus using automated methods. The primary drawback of the commercial

Figure 3.4. Structures of the two linkers utilized in the different coupling reactions. The aminoalkyl phosphodiester is shown on top and the aminoalkyl carbamate is shown on the bottom.

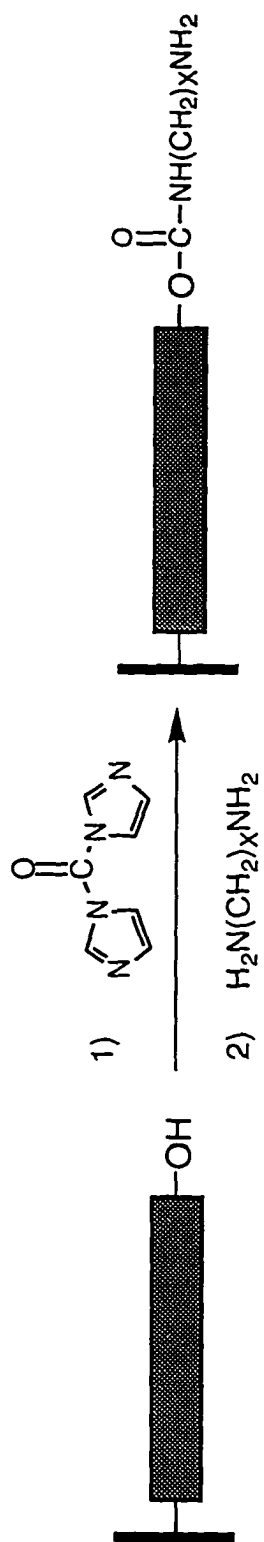


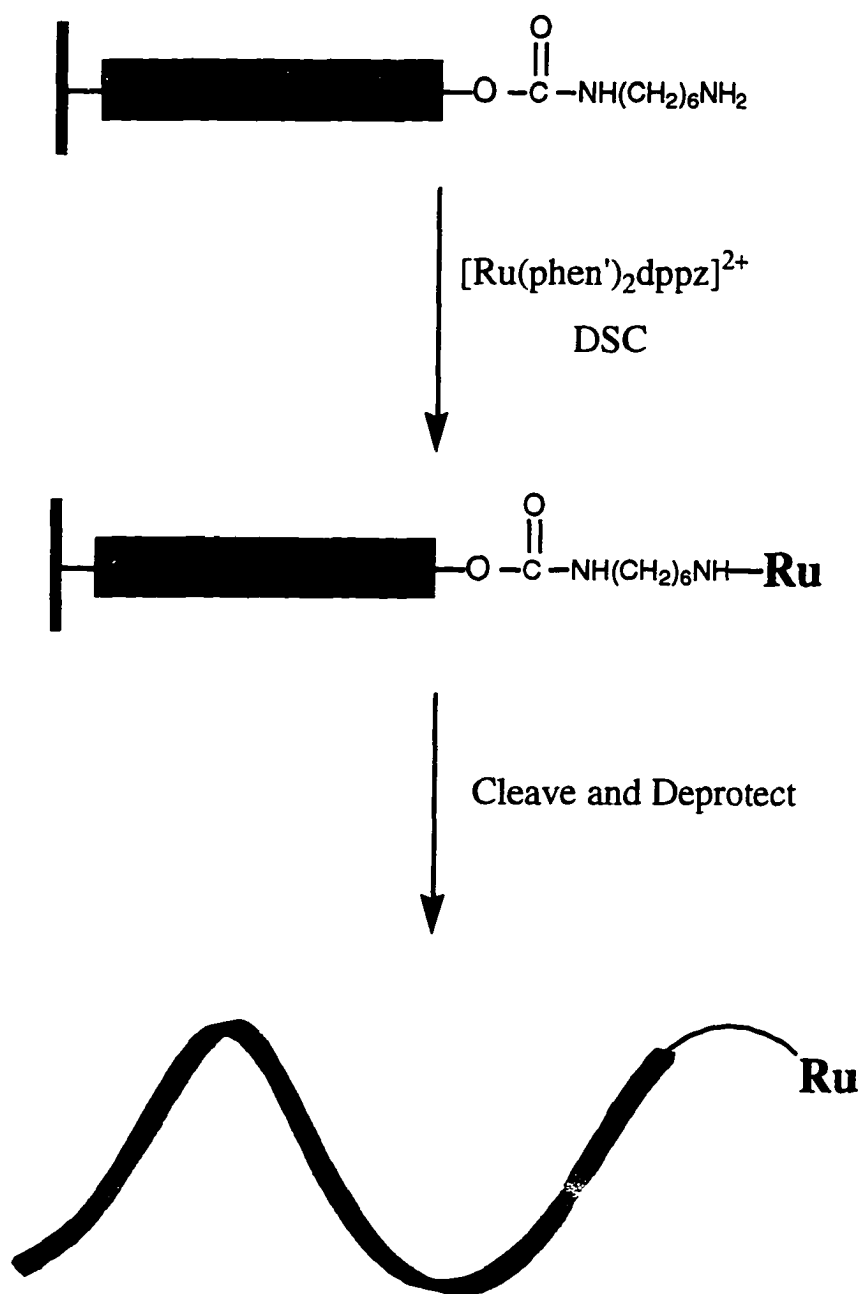
reagent is that the amine functionality is blocked by a base labile protecting group which can not be removed without concomitant cleavage of the oligonucleotide from the resin or deprotection of the phosphate backbone. This impedes a strategy based upon coupling to the oligonucleotide still bound to the support. Alternatively, oligonucleotides can be derivatized with a primary amine using a manual approach illustrated in Scheme 3.2 which results in a carbamate linkage to the oligonucleotide. This synthesis results in 1) a higher yield of modified oligonucleotide (> 90%), and 2) a much cleaner reaction due to the higher efficiency of functionalization compared to automated methods. These conditions allow the subsequent coupling of the ruthenium complex to be accomplished on the resin with the oligonucleotide protecting groups still intact. In addition, the carbamate linkage is more amenable to modification; the linker length is varied simply by changing the diaminoalkane starting material. Linkers containing oxygen or nitrogen heteroatoms along the aliphatic chain can also be incorporated using the manual approach.⁹

Coupling of the Ruthenium Complex to 5'-Aminoalkylated Oligonucleotide. Two strategies have been developed in our laboratory for the synthesis of metal-oligonucleotide conjugates: (i) a solid phase method and (ii) a solution phase method. In solid phase coupling (Scheme 3.3), an activated ester of the ruthenium complex is added to oligonucleotide still attached to the solid support. Following the coupling reaction, the metal-oligonucleotide is cleaved and deprotected from the resin in the same manner as the free oligonucleotide. The fully deblocked and HPLC purified oligonucleotide is added either to metal complex activated *in situ* or metal complex activated prior to the coupling reaction in the solution phase synthesis (Scheme 3.4).

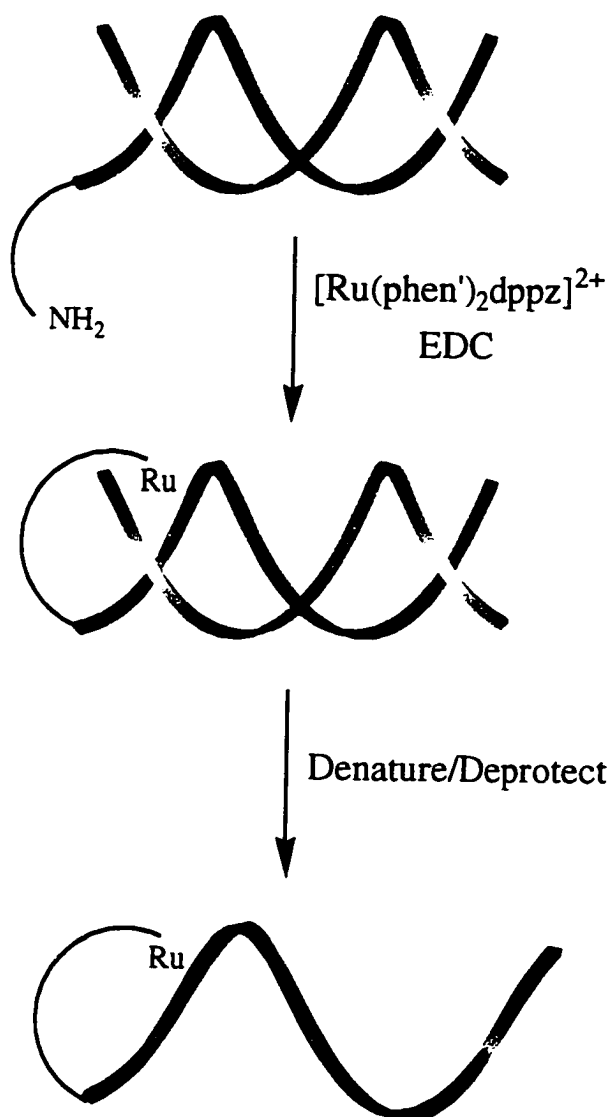
Comparison of Coupling Methods. The conjugation of organic moieties to DNA is routinely reported, with many different methods available for functionalization at either terminus or off of the bases.¹⁰ Covalent modification of oligonucleotides by metal complexes does not appear to be as readily accomplished. Several inherent features of the reaction exist which make it difficult to use previously established methods. One of the

Scheme 3.2. Functionalization of the support-bound oligonucleotide using carbonyldiimidazole and a diaminoalkane. Note how readily the linker length can be varied by substitution of the diaminoalkane.



Scheme 3.3. Assembly of ruthenium modified oligonucleotide on the solid support.

Scheme 3.4. Solution phase synthesis of ruthenated oligonucleotide using EDC.



biggest problems posed by commonly used solution phase procedures is solvent incompatibility; the standard activation of a carboxylic acid toward nucleophilic addition to form a peptide bond involves the intermediate formation of an active ester of the ruthenium complex. Coupling reagents used in the formation of amide bonds often require anhydrous conditions. DNA, even in its partially deblocked state, is insoluble in organic solvents. Unfortunately, the water essential for DNA solubility rapidly hydrolyzes the activated ester before the desired reaction occurs, regenerating the starting material. Originally, this incompatibility was overcome by using a mixed-phase system. Oligonucleotides modified with $[\text{Ru}(\text{phen})_2\text{phen}']^{2+}$, $[\text{Rh}(\text{phen})_2\text{phen}']^{3+}$, $[\text{Rh}(\phi)_2\text{phen}']^{3+}$ ($\phi = 9,10\text{-phenanthrenequinonediimine}$) and $[\text{Ru}(\text{phen}')_2\text{dppz}]^{2+}$ were first synthesized by addition of the activated metal complex to a suspension of the aminoalkylated oligonucleotide.¹¹

In solution, both circular dichroism and uv-visible measurements suggest that single-stranded DNA interacts with the metal complex. As a result, although the reaction components may be in contact, the reactive groups may still be separated. Additionally, the carboxylic acid functionality on the phen' ligand is able to react intramolecularly with the amide nitrogen, thus forming the kinetically and thermodynamically favored cyclic product.⁵ These factors combined with the low intrinsic reactivity of the metal complex account for the low reproducibility of the first solution-phase method pursued.

Water soluble carbodiimides such as EDC can be used in aqueous solvents as condensing agents to form amide bonds. With fully deprotected DNA, modification at bases containing exocyclic amines has been reported.¹² Selective modification of fully deblocked DNA in aqueous conditions has been successfully achieved by protecting the amine functionalities via hydrogen bonding with the complementary strand.¹³ Additionally, the hybridized duplex may serve as a scaffold to position the ruthenium complex for subsequent coupling, kinetically facilitating the reaction by preorganization of the components. This is consistent with the observed reaction times for the two different

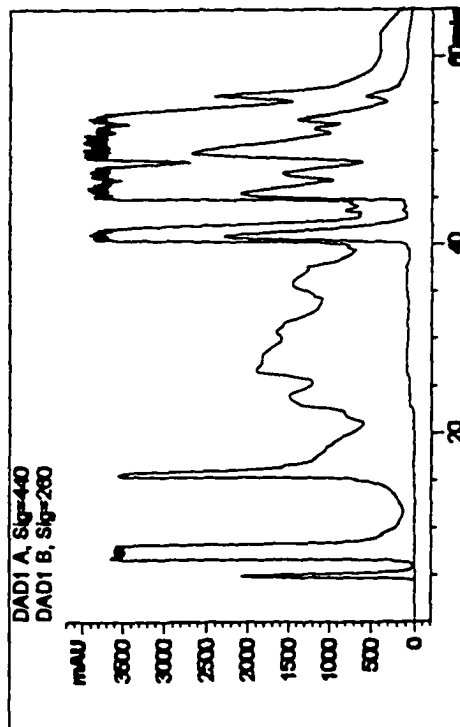
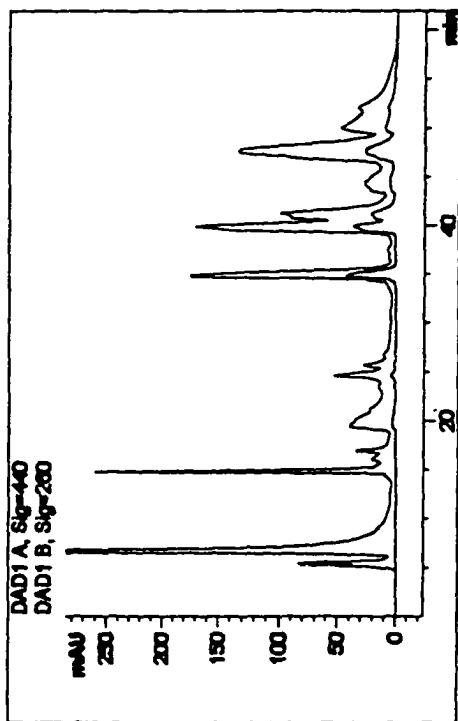
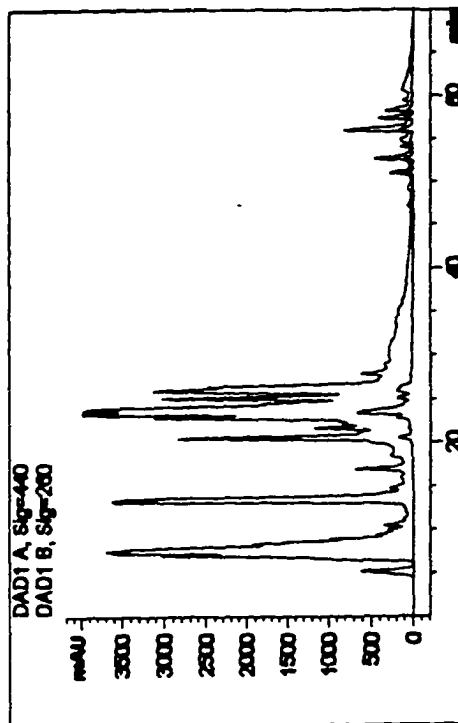
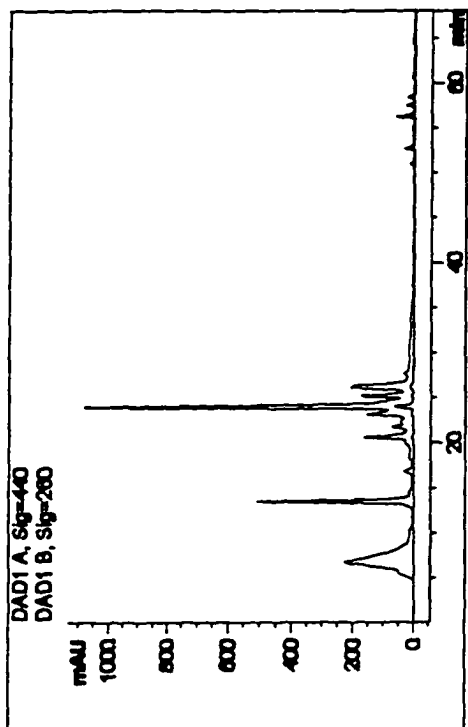
methods; although solution phase coupling takes longer to set up due to the necessary purifications of aminoalkylated oligonucleotide and complement, the reaction is complete after overnight incubation at room temperature compared to the several days required for complex activation and subsequent reaction for solid phase coupling. After completion of the reaction, the contaminating complementary strand can be removed by denaturing gel electrophoresis or high temperature HPLC. A complementary strand containing a mixture of DNA and RNA has also been used with success. Here cleavage of the complementary strand is effected by the addition of base.

Prior to the initial HPLC purification of solution phase reactions, the unreacted $[\text{Ru}(\text{phen})_2\text{dppz}]^{2+}$ must be removed from the reaction mixture using anion-exchange FPLC chromatography. Otherwise, metalated duplexes interact with the excess ruthenium complex adsorbed onto the reverse-phase column material, resulting in smearing of the product along the column. This blobbing effect is illustrated in Figure 3.5. Analytical scale traces of both non-FPLC and FPLC-purified material yield sharp, clearly distinct peaks. Injection of the entire reaction mixture, however, results in large increases in the peak widths for non-FPLC purified material, leading to difficulties in purification and isolation of reproducible peaks at high temperature. In contrast, removal of unreacted starting metal complex yields a preparatory scale HPLC trace analogous to the analytical chromatogram.

For $[\text{Ru}(\text{phen})_2\text{dppz}]^{2+}$, thus far the main advantages of using solution phase over solid phase methodology are reproducibility and reaction yield (20 to 80% versus 1%). Performing the reaction on fully protected, support-bound oligonucleotide, however, ensures specific modification of the primary amine functionality. Less time for reaction preparation and product isolation is required for the solid phase reaction and, for unknown reasons, sample analysis by ESI-MS appears to be more facile for conjugates constructed using the solid phase technique.

A minor drawback of the solid phase strategy is the inconvenience of monitoring the reactions; aliquots of resin have to be removed and deprotected prior to HPLC analysis.

Figure 3.5. Analytical (top) and preparatory (bottom) HPLC chromatograms of Ru-NH(CH₂)₉NHCO₂AGTCTAGGCCTATCGT-3' reaction mixture. Prior to HPLC purification, the reaction shown on the right was filtered using anion-exchange FPLC chromatography to remove the unreacted metal complex. Each chromatogram displays a 260 nm trace (top line) and a 440 nm trace (bottom line).



Adsorption of the metal complex to the solid support is also a concern due to potential inhibition of cleavage of the modified oligonucleotide from the resin. A decrease in yield due to incomplete recovery of material has been observed for rhodium-peptide conjugates synthesized on the solid support.⁵ This problem appears to be partially alleviated by using controlled pore glass resin rather than polystyrene-based supports.

A variety of activating groups have been examined for both the solid phase synthesis and the mixed phase solution synthesis. The mixed phase synthesis has only been accomplished using the DCC/HOBT pair. In the solid phase procedure, successful construction has been observed repeatedly using DSC and has been observed once using the DCC/HOAT (1-hydroxyazabenzotriazole) couple. For complexes containing the functionalized phen', the reaction is not always reproducible. A reproducible, high yielding, solid phase synthesis has been developed in our laboratory for covalently attaching rhodium complexes containing a functionalized bipyridine ligand⁵ to oligonucleotides.¹⁴ The functionalized bipyridine analogue of $[\text{Ru}(\text{phen}')_2\text{dppz}]^{2+}$ does not appear to work as well as the rhodium synthesis, but work is underway to improve the yield of the reaction. It is desirable to have high yielding syntheses based upon both methods in order to construct doubly labeled oligonucleotides.

Solid phase coupling of the ruthenium complex to oligonucleotides derivatized with hexamethylenecarbamate linkers often resulted in HPLC traces with multiple peaks in the region where metal-oligonucleotide normally elutes (results not shown). Distinct peaks isolated from the mixture and submitted for ESI-MS analysis gave virtually identical results, indicating that although the retention times were different, the chemical compositions were analogous. The individual fractions were not characterized by CD spectroscopy so diastereomer formation and resolution is a possibility. Part of the basis for the complicated mixture was the use of the C₁ isomer which was the metal fraction that appeared to work most reproducibly. No interconversion was observed among peaks at room temperature. By heating the individual fractions, it was discovered that some of the

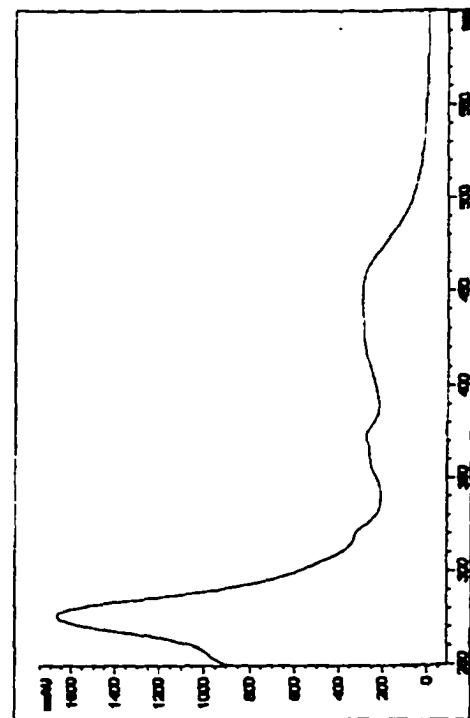
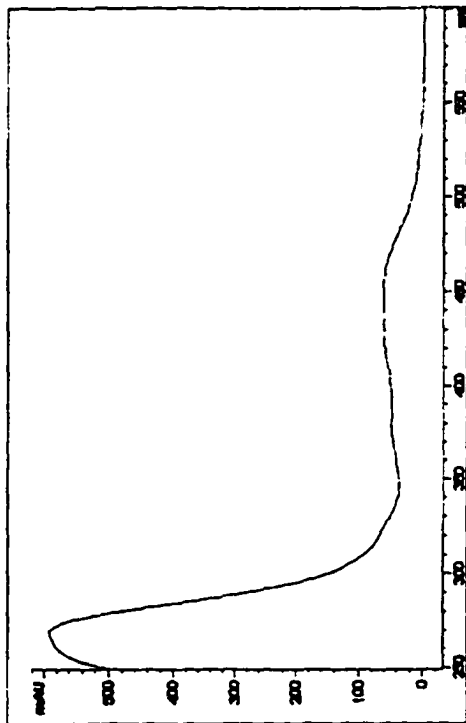
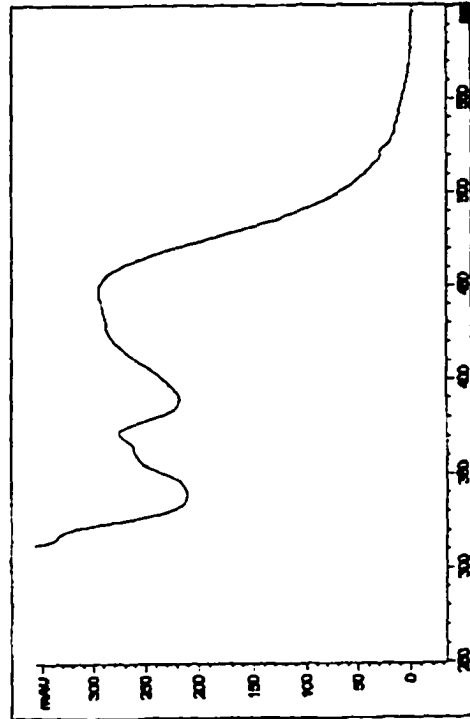
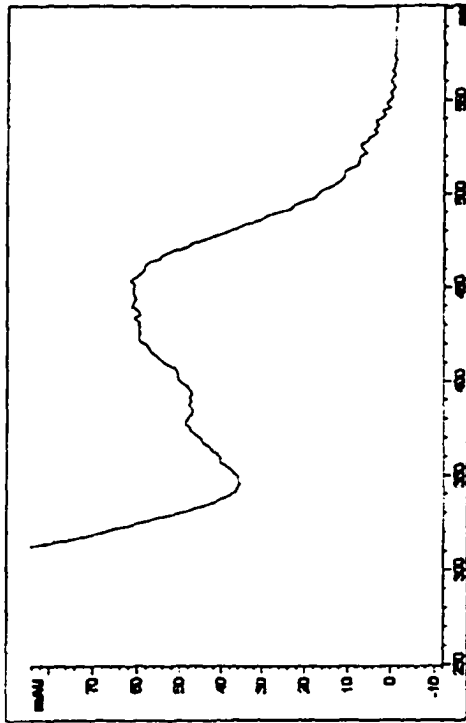
peaks corresponded to conformers. A change in peak distribution did not occur but rather conversion to one peak which appeared to be the thermodynamic conformer. This complexity of product formation has been shown to be partially alleviated by using a symmetric isomer for coupling. Alternatively, using $[\text{Ru}(\text{phen})(\text{phen}')\text{dppz}]^{2+}$ as a starting material may also aid in product purification and characterization.

3.3.3. Characterization of Oligonucleotides Appended at the 5' Terminus With $[\text{Ru}(\text{phen}')_2\text{dppz}]^{2+}$

Electronic Spectroscopy. Figure 3.7 shows the uv-visible spectrum for $\text{Ru-NH}(\text{CH}_2)_6\text{NHCO}_2\text{AGAAGGCCTGGT-3'}$. The conjugates can be characterized by an increase in the absorption at 260 nm, consistent with addition of the oligonucleotide strand. This increase is not directly additive; comparison of the calculated extinction coefficient ($\sim 298,000 \text{ M}^{-1}\text{cm}^{-1}$ ¹⁵), the extinction coefficient for the noncovalent analogue ($\sim 260,000 \text{ M}^{-1}\text{cm}^{-1}$), and ruthenated oligonucleotide ($\sim 195,000 \text{ M}^{-1}\text{cm}^{-1}$) reveals significant hypochromicity at 260 nm (35% for ruthenated 12mer). Depending upon the interaction between the metal complex and the oligonucleotide, extensive hypochromicity in the dppz intraligand transition is sometimes observed (up to 30% at 372 nm). This hypochromicity also extends into the MLCT transition, which is often used in calculation of sample concentrations. Due to the variability in hypochromicity observed for each individual conjugate (up to 15% at 440 nm), concentrations determined from uv-vis absorption spectra were often verified by phosphate analysis.

Phosphate Analysis. Information about the stoichiometry of coupling can be gained via phosphate analysis. Since there are two functionalized phenanthrolines per ruthenium molecule, the possibility of coupling to both arms always exists. Phosphate analysis is a colorimetric assay in which the formation of a molybdenum-oxo complex is used to ascertain the phosphate concentration of a sample. Phosphate analysis of all ruthenated conjugates synthesized thus far reveals a 1:1 stoichiometry of strand to

Figure 3.6. Absorption spectra of Ru-NH(CH₂)₆NHCO₂AGAAGGCCTGGT-3' (top) and free ruthenium complex (bottom). Note the increase in absorption at 260 nm consistent with the addition of oligonucleotide and the hypochromicity in the dppz intraligand transition at 372 nm.



ruthenium complex in every case. The strand concentration as calculated from phosphate analysis is used in conjunction with the metal concentration measured from the MLCT absorption in determining final sample concentrations.

Enzymatic Digest. Digestion of ruthenated oligonucleotide with the enzymes snake venom phosphodiesterase and alkaline phosphatase reveals valuable information about the bases which comprise the oligonucleotide strand. Comparison of the different nucleoside areas allows confirmation of the base content within the strand. In addition, comparison of sample retention times with those of nucleoside standards can be used to determine whether the bases have been modified. Even slight modifications of the bases result in changes in mobility on a reverse phase HPLC column and are alterations reflected in the observed base ratios. Here, the carbamate linker is used advantageously over the phosphodiester linker. Due to the carbamate linkage, the connection between the 5' terminal base and the linker is not severed by the phosphodiesterase. As shown in Figure 3.7, quantitation of the nucleoside pattern resulting from the enzymatic digestion of Ru-NH(CH₂)₉NHCO₂-AGTCTAGGCCTATCGT-3' gives a deoxyadenosine concentration which is lower than the calculated amount. This decrease is consistent with the loss of the 5' terminal base. At high acetonitrile concentrations, a peak which absorbs in the visible region is occasionally observed. This peak most likely corresponds to the 5' terminal base which is still attached to the ruthenium complex via the carbamate linker.

Mass Spectrometry. The ruthenated oligonucleotides have also been characterized successfully using both electrospray ionization (ESI) and matrix-assisted laser desorption ionization (MALDI) mass spectrometry. This procedure establishes that the ruthenium complex and the oligonucleotide are covalently bound. Shown in Figures 3.8 and 3.9 are representative examples of spectra obtained using the two different ionization methods. As is evident from the figure, ionization of ruthenated oligonucleotides using either technique does not result in extensive fragmentation of samples.

Figure 3.7. HPLC trace of Ru-NH(CH₂)₉NHCO₂AGTCTAGGCCTATCGT-3' (top) and unmodified oligonucleotide (bottom) after incubation with snake venom phosphodiesterase and alkaline phosphatase. The decrease in deoxyadenosine content is consistent with the loss of the 5' terminal base. The chromatogram for the unmodified oligonucleotide shows only the 260 nm trace while both the 260 nm and 440 nm chromatograms are displayed for the ruthenated oligonucleotide. In the enzymatic digest of the metalated strand, a peak with the characteristic Ru(II) dppz absorbance elutes at higher acetonitrile concentrations.

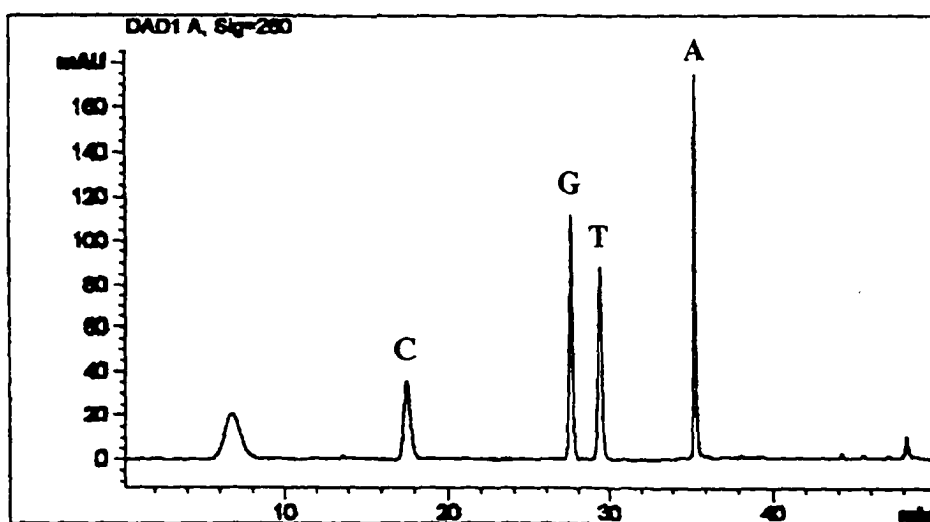
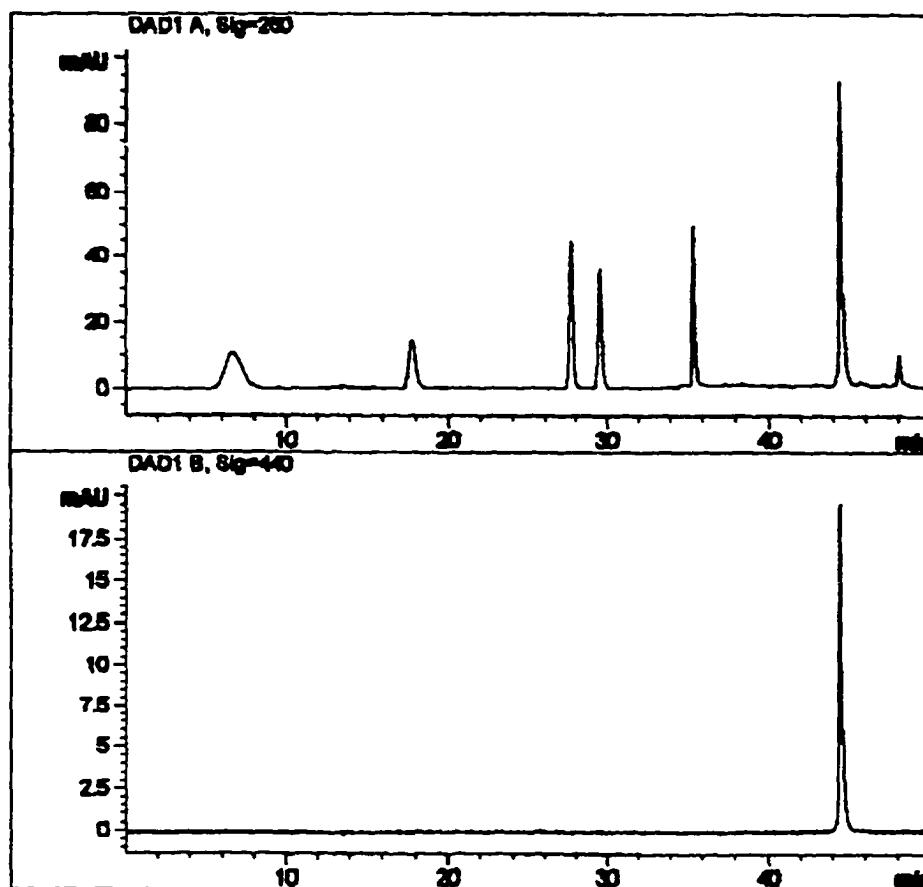


Figure 3.8. ESI-MS of Ru-NH(CH₂)₉NHCO₂AGTGTATATAAACGT-3'. Shown on the top is the raw data. The distribution of peaks in the spectrum correspond to differently charged ions resulting from the ionization process. The low molecular weight species seen at the left most likely correspond to nucleotide fragments produced from the ionization process. Shown on the bottom is the computer reconstructed spectrum.

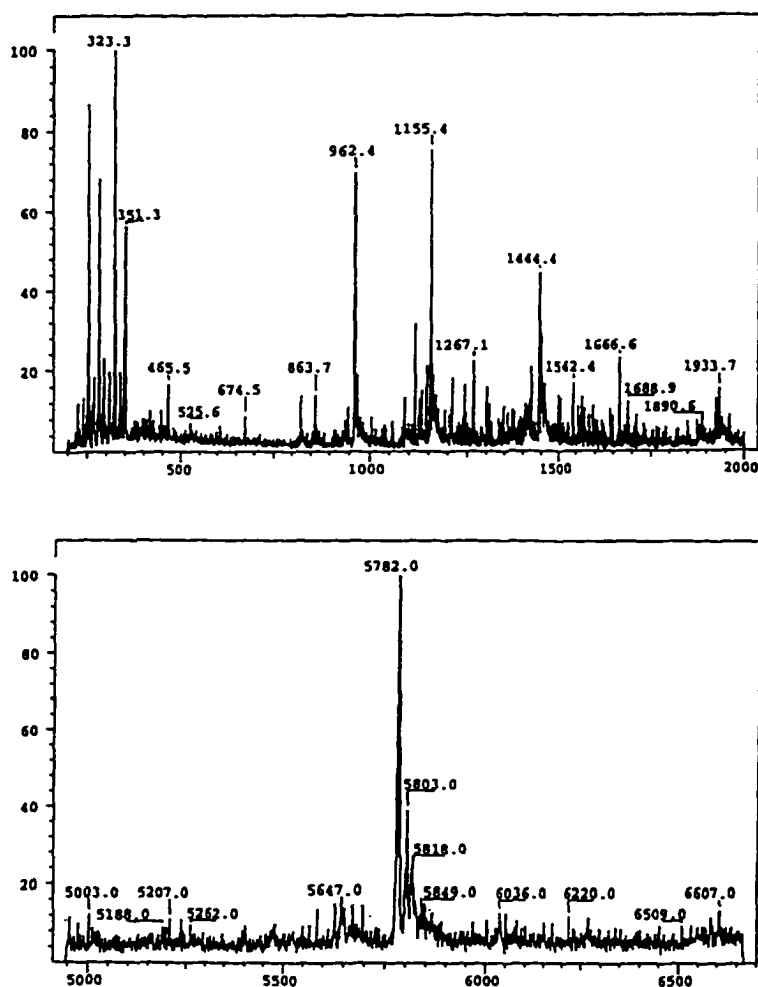
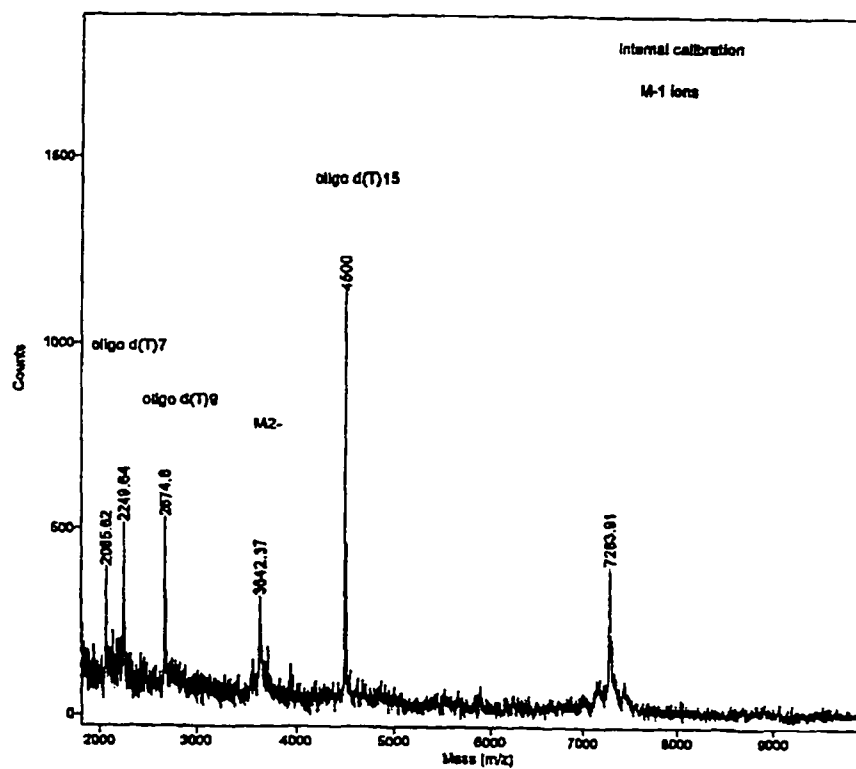


Figure 3.9. MALDI-TOF of Ru-NH(CH₂)₉NHCO₂AGTCTTATATAAAAATATCGT-3'.

The additional peaks correspond to oligonucleotide markers used for internal calibration.



Some fragmentation, along with a lower signal to noise ratio, of samples synthesized using the EDC solution phase method has been observed by both ESI-MS and MALDI-TOF. Frequently, peaks consistent with loss of bases have been observed for both techniques. In addition, for solution phase samples, low molecular weight species have been observed which may correspond to nucleotide fragments, as shown in Figure 3.8. It is difficult to discern whether the quality of the spectrum is due to impurities already present in the sample or due to fragmentation from the ionization process itself. In order to aid sample desorption in ESI-MS for samples synthesized using EDC, it is necessary to add additives to the sample such as imidazole, triethylamine, or piperidine to reduce desorption problems associated with sodium. It has previously been observed that upon heating in the presence of piperidine and salt, cleavage of the DNA backbone can be effected.¹⁶ Most likely, the EDC synthesized samples have more salt associated with them than samples synthesized on the solid phase, thereby causing fragmentation of the strand upon desorption. That different mass species (other than the main ion) are observed for the same sample using each technique is consistent with either preferential desorption of different molecules by the two different techniques or contributions to fragmentation by the different ionization processes.

Due to the ionization process, peaks corresponding to species of different charge states are observed in the ESI-MS whereas the singly charged ion predominates in the MALDI-TOF MS with a tiny fraction of the doubly charged ion present. Because the results of differently charged species in ESI-MS can be averaged, the molecular mass obtained by ESI-MS is more accurate than that obtained using MALDI-TOF. Less sample is required for MALDI-TOF analysis than for commercial ESI-MS instrumentation. A major concern in the analysis of oligonucleotides by mass spectrometry is the presence of salt associated with the strands which reduces the sensitivity. MALDI appears to be less sensitive to the presence of sodium in the samples than ESI.

3.3.4. Generation of Longer Ruthenated Oligonucleotides

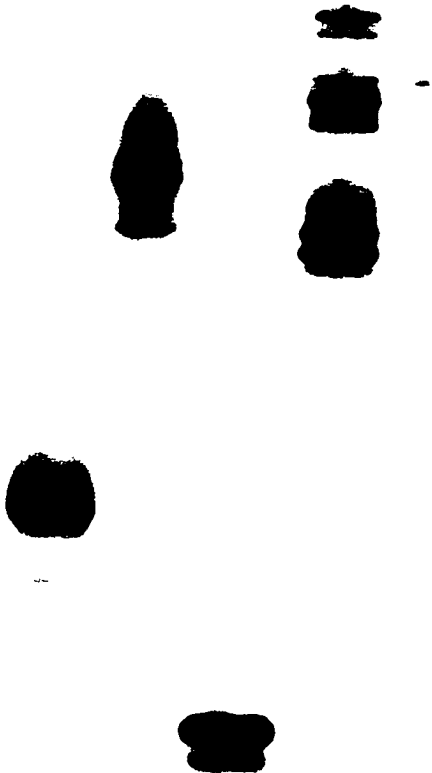
The chemical synthesis of oligonucleotides covalently modified by metal complexes is practical only for oligonucleotide sequences up to about 30 bases long. This limitation is due both to the coupling efficiency of the synthesis and to the higher loading of the resin which results in steric crowding within the pore as the oligonucleotide strands become longer, therefore decreasing coupling efficiency. Two enzyme-based methods have been investigated for extending the length of metalated conjugates: 1) primer extension where a complementary oligonucleotide of a desired length serves as a template for elongation of a ruthenated primer by a DNA polymerase and 2) ligation where a DNA ligase is used to form a phosphodiester bond between the 3' hydroxyl terminus of a ruthenated strand and the 5' phosphate terminus of the strand to be attached. One consideration in using ruthenated oligonucleotides in the presence of enzymes is the possibility that the ruthenium complex may interfere with enzyme activity. Ru-T₁₀ has been successfully modified at the 3' end with α -³²P-ddATP using terminal deoxynucleotidyl transferase without a significant loss in enzyme efficiency.

Primer Extension. Figure 3.10 shows the successful extension of Ru-NH(CH₂)₆NHCO₂AGAAGGCCTGGT-3' by Sequenase, a genetically engineered DNA polymerase. The presence of the ruthenium has a remarkable effect upon the migration of the oligonucleotide through the gel matrix. As the oligonucleotide length is increased, the difference between ruthenium-modified and unmodified oligonucleotide becomes less pronounced. Further characterization of the product was not performed so it is unknown whether complete extension of the primer was achieved. It may be possible to generate longer length probes in quantity by using a thermostable DNA polymerase such as Taq and amplifying in a linear fashion using PCR methodology.

Ligation Using T4 DNA Ligase. In addition to primer extension, another enzyme-based method for synthesizing metalated oligonucleotides of longer length is ligation using T4 DNA ligase. Ligation is the preferred method of elongation due to the greater

Figure 3.10. Extension of both Ru-NH(CH₂)₆NHCO₂AGAAGGCCTGGT-3' and unmodified oligonucleotide using Sequenase. The template is 30 nucleotides in length. The lanes in the figure contain from left to right: (1) 3' labeled ruthenated primer, (2) ruthenium reaction lane, (3) 3' labeled unmodified primer, (4) unmodified primer reaction lane, and (5) template control (no primer).

1 2 3 4 5



simplicity of the reaction catalyzed by the enzyme as compared to primer extension. In the Sequenase reaction, the enzyme is required to perform the sequential addition of nucleotides to a primer whereas in ligation, the enzyme needs to catalyze only one reaction, an ATP-dependent ligation of a 5'-phosphate to a 3'-hydroxyl. In addition, separation of the different components occurs more readily in the ligation reaction. The template in primer extension has to be as long as the desired strand whereas the template in ligation has only to be long enough to properly position the phosphorylated strand for covalent attachment to the 3' terminus of the ruthenium-modified strand.

Figure 3.11 shows the successful ligation of Ru-NH(CH₂)₆NHCO₂AGA-AGGCCTGGT-3' to a 5' phosphorylated oligonucleotide to generate a 35 nucleotide oligomer modified by a ruthenium complex. In this reaction, the template was 18 nucleotides in length to facilitate correct hybridization. The two sets of lanes shown in the gel correspond to unmodified 12mer oligonucleotide and ruthenated 12mer oligonucleotide. A retardation of the band containing radioactivity is observed in the reaction lane which does not occur in either control lane. This is consistent with the appearance of a longer piece of DNA whose formation is dependent upon both the ruthenium modified strand and the template strand. As determined from the gel, the ligation efficiency appears to be high.

The ruthenated oligonucleotide Ru-NH(CH₂)₉NHCO₂AGTGCGAAGGCC-TGGAACGT-3' was constructed via ligation of Ru-NH(CH₂)₉NHCO₂AGTGCGAAG-3' to 5' phosphorylated GCCTGGAACGT-3' on a scale large enough to obtain purified sample for analysis by mass spectrometry. The yield of the reaction was estimated to be at least 50%. The successful elongation of the oligonucleotide was confirmed by MALDI-TOF mass spectrometry of the HPLC purified sample.

3.4. Conclusion

Different synthetic strategies for appending ruthenium polypyridyl complexes to

Figure 3.11. Ligation of Ru-NH(CH₂)₆NHCO₂AGAAGGCCTGGT-3' to the 5' phosphorylated oligonucleotide CATTGGGCGCGAGCTGACATGT labeled with ³²P-ddATP at its 3' terminus. Gel lanes from left to right: (1) ligase reaction, (2) reaction without ruthenated strand, (3) reaction without template, and (4) phosphorylated oligonucleotide standard.

1 2 3 4



the 5' terminus of oligonucleotides have been described; one method is based on functionalization of the oligonucleotide still attached to the solid support and the other is performed in solution using the cleaved, fully deprotected oligonucleotide. These metal-oligonucleotide conjugates have been characterized by a variety of methods which can be used to examine both the metal and the oligonucleotide portions of the conjugate. They are recognized as substrates by DNA modification enzymes such as Sequenase and T4 DNA ligase, allowing the preparation of longer metalated oligonucleotides than is feasible through chemical synthesis. The establishment of synthetic methods for the preparation of oligonucleotides modified at the 5' terminus by $[\text{Ru}(\text{phen})_2\text{dppz}]^{2+}$ facilitates the investigation of these conjugates as novel luminescent probes for the detection of DNA.

References

- ^{1a}Bannwarth, W.; Schmidt, D.; Stallard, R.I.; Hornung, C.; Knorr, R.; Muller, F., *Helv. Chim. Acta*, **1988**, *71*, 2085. ^{1b}Bannwarth, W.; Schmidt, D., *Tet. Letters*, **1989**, *30*, 1513.
- ^{1c}Tessler, J.; Cruickshank, K.A.; Schanze, K.S.; Netzel, T.L., *J. Am. Chem. Soc.*, **1989**, *111*, 7221. ^{1d}Kenten, J.H.; Gudibande, S.; Link, J.; Willey, J.J.; Curfman, B.; Major, E.O.; Massey, R.J., *Clin. Chem.*, **1992**, *38*, 873.
- ^{2a}Chow, C.S.; Barton, J.K., *J. Am. Chem. Soc.*, **1990**, *112*, 2839. ^{2b}Mei, H.Y.; Barton, J.K., *J. Am. Chem. Soc.*, **1986**, *108*, 7414. ^{2c}Kirshenbaum, M.R.; Tribolet, R.; Barton, J.K., *Nucleic Acids Res.*, **1988**, *16*, 7943.
- ^{3a}Friedman, A.E.; Chambron, J.-C.; Sauvage, J.-P.; Turro, N.J.; Barton, J.K., *J. Am. Chem. Soc.*, **1990**, *112*, 4960. ^{3b}Hartshorn, R.M.; Barton, J.K., *J. Am. Chem. Soc.*, **1992**, *114*, 5919.
- ⁴Murphy, C.J.; Arkin, M.A.; Jenkins, Y.; Ghatlia, N.D.; Bossman, S.H.; Turro, N.J.; Barton, J.K., *Science*, **1993**, *262*, 1025.
- ⁵Sardesai, N.Y.; Lin, S.C.; Zimmerman, K.; Barton, J.K., *Bioconj. Chem.*, **1995**, *6*, 302.
- ⁶Amouyal, E.; Homsy, A.; Chambron, J.-C.; Sauvage, J.-P., *J. Chem. Soc. Dalton Trans.*, **1990**, 1841.
- ⁷Wachter, L.; Jablonski, J.; Ramachandran, K.L., *Nucleic Acids Res.*, **1986**, *14*, 7985.
- ⁸Lindberg, O.; Ernsten, L. in *Methods of Biochemical Analysis*; Glick, D. (Ed.); Interscience: New York; Vol. 3, 1954.
- ⁹Bigey, P.; Pratviel, G.; Meunier, B., *Nucleic Acids Res.*, **1995**, *23*, 3894.
- ¹⁰Goodchild, J., *Bioconj. Che.*, **1990**, *1*, 165.
- ¹¹Murphy, C.J.; Jenkins, Y.; Arkin, M.A., unpublished results.
- ¹²Ghosh, S.S.; Musso, G.F., *Nucleic Acids Res.*, **1987**, *15*, 5353.
- ¹³Meade, T.J.; Kayyem, J.F., *Angew. Chem.*, **1995**, *34*, 352-354.
- ¹⁴Holmlin, R.E., unpublished results.

¹⁵based upon summation of the 260 nm extinction coefficients of the metal complex and the oligonucleotide strand

¹⁶Jenkins, Y., unpublished results.

Chapter 4: Biochemical and Photophysical Characterization of Oligonucleotide Duplexes Covalently Modified By $[\text{Ru}(\text{phen}')_2\text{dppz}]^{2+}$

4.1. Introduction

$[\text{Ru}(\text{phen})_2\text{dppz}]^{2+}$ and its derivatives have been reported as novel spectroscopic reporters for nucleic acids.¹ They possess a characteristic light switch feature which makes them unique among the ruthenium polypyridyl complexes developed in this laboratory for DNA detection. In aqueous solutions, quenching of the luminescence occurs due to interactions with the solvent; intercalative binding into double-helical DNA protects these complexes from solvent, resulting in bright photoluminescence. Additionally, the emission properties of dipyrrophenazine complexes of ruthenium(II) are extremely sensitive to both the nucleic acid sequence and conformation.²

Chapter 3 detailed synthetic methods and characterization techniques developed for construction of oligonucleotides covalently modified at the 5' terminus with transition metal complexes. In this chapter, the biochemical and photophysical characterization of oligonucleotide duplexes containing a ruthenated strand will be described. The biochemical analysis is based upon the well-studied physical properties of DNA while the photophysical characterization utilizes the luminescence properties of the ruthenium complex. The effects of subtle variations in the structure of the ruthenated oligonucleotide such as oligonucleotide length, linker length and orientation, and the base sequence at the 5' terminus will be discussed as well as the effects of varying the conditions used for the luminescence measurements. The luminescence properties of one metalated oligonucleotide, $\text{Ru-NH}(\text{CH}_2)_6\text{OPO}_2\text{AGTGCCAAGCTTGCA-3'}$, will be described in detail with a focus on applications in hybridization technology.

4.2. Experimental

Materials and Methods. Automated DNA synthesis was performed on an Applied Biosystems, Inc., 392 DNA synthesizer using reagents purchased from Glen Research. Oligonucleotides were purified using reverse-phase high performance liquid chromatography (either a Waters 600E system equipped with a Waters 484 tunable detector or a Hewlett-Packard 1050 HPLC system). High temperature HPLC was carried out on a Hewlett-Packard 1090 HPLC system. Ultraviolet-visible spectra were recorded on a Hewlett-Packard 8452 diode array or Cary 219 spectrophotometer. Thermal denaturation profiles were obtained with a Hewlett-Packard 8452 diode array spectrophotometer equipped with a Peltier temperature controller. The synthesis and characterization of all ruthenated oligonucleotides discussed in this chapter is detailed in Chapter 3. Oligonucleotides covalently modified at the 5' end with $[\text{Rh}(\text{phi})_2\text{bpy}]^{3+}$ (phi = 9,10-phenanthrenequinonediimine, bpy = 4-butyric acid 4'-methylbipyridine) were provided by R. Erik Holmlin.

3'-³²P Labeling of 5'-Ruthenium Modified Oligonucleotides. Oligonucleotides ruthenated at the 5' terminus were radioactively labeled at the 3' end using α -³²P-ddATP (NEN-DuPont) and terminal deoxynucleotidyl transferase (Boehringer Mannheim Biochemicals). Labeling reactions were performed for only 30 minutes at 37° C to reduce the occurrence of exonuclease activity. Solutions were loaded onto NENSORB C₁₈ columns (DuPont) to remove enzyme and excess α -³²P-ddATP and to desalt samples. Radioactively labeled conjugates were purified using denaturing polyacrylamide gel electrophoresis (10%). Samples were isolated from gel pieces using electroelution (Schleicher and Schuel) and desalted again using NENSORB columns. Labeling efficiency of ruthenated oligonucleotides by terminal deoxynucleotidyl transferase appears to be approximately 25-50% that of the unmodified oligonucleotide.

Nondenaturing Polyacrylamide Gel Electrophoresis. Samples analyzed by PAGE were annealed by heating to 95° C and then slowly cooling to room temperature. After

addition of dye, samples were loaded onto a 20% nondenaturing polyacrylamide gel. Gels were run overnight at room temperature (75 V) to prevent duplex denaturation caused by excessive warming of the gel. Gels were visualized using a phosphorimager (Molecular Dynamics).

Luminescence Measurements. Luminescence measurements were performed as described in Chapter 2 except that samples for steady-state luminescence were thermally equilibrated for 5 minutes in a thermostated sample chamber at 25° C.

4.3. Results and Discussion

4.3.1. Examination of the Structural Integrity of Ruthenated Duplexes

Electrophoretic Mobility Shift Assays. The hybridization of oligonucleotide strands modified by a ruthenium complex at the 5' terminus can be studied using non-denaturing gel electrophoresis to determine whether covalent modification causes drastic structural perturbations of the oligonucleotide portion of the conjugate. Duplex formation by both ruthenated 5'-AGTCTGTAAACATCGT-3' and unmodified oligonucleotide to radioactively labeled complementary strand is demonstrated in Figure 4.1. Addition of either oligonucleotide causes retardation of the radioactive strand, consistent with duplex formation. Interestingly, addition of the ruthenium modified strand results in increased retardation of the duplex compared to the unmodified duplex, consistent with covalent attachment of the ruthenium complex. This increase in retardation is likely due to both a charge and a size effect; the positive charge of ruthenium complex and the added physical bulk of the complex contribute to the migratory properties of the modified oligonucleotide in the gel matrix. That such a dramatic effect is observed upon attachment of one ruthenium complex is remarkable.

Figure 4.1. Hybridization of Ru-NH(CH₂)₉NHCO₂AGTCTGTTAACATCGT-3' to its 5' ³²P-labeled complement. Gel lanes contain (1) 5' ³²P-labeled complementary strand by itself, (2) unmodified duplex, (3) ruthenated duplex, and (4) ruthenated duplex. Both ruthenium samples analyzed were isolated from the same reaction mixture and are believed to be positional isomers based upon their HPLC retention times. Note the decrease in mobility for the duplexes containing ruthenium modified strand compared to the unmodified duplex.

1 2 3 4



Duplex formation by an oligonucleotide bearing a metal complex at the 5' terminus to a complementary oligonucleotide also bearing a 5' terminal metal complex can also be examined using gel electrophoresis. The 3' terminus of a ruthenated oligonucleotide can be labeled using terminal deoxynucleotidyl transferase and α - ^{32}P -ddATP although with a labeling efficiency only 25-50% that of the unmodified oligonucleotide. Ruthenated duplex containing radioactively labeled ruthenium strand has the same mobility properties as ruthenated duplex containing radioactively labeled complementary strand (Figure 4.2). Addition of complement modified by $[\text{Rh}(\phi)_2\text{bpy}]^{3+}$ results in further retardation relative to duplex containing only one intercalator. Diastereomers produced by coupling of the rhodium complex to oligonucleotides can often be resolved by reverse-phase HPLC. Interestingly, the rhodium diastereomers retard the duplex to different extents, with greater retardation observed for Δ isomer and less retardation observed for the Λ isomer (Figure 4.2). This indicates structural variations between the duplexes produced upon hybridization of the diastereomers to the complementary strand, rather than simply retardation caused by charge or size properties. Again, that such an effect is produced by covalent modification of one complex is remarkable. The differential mobilities observed for the two diastereomers also suggest that the appended rhodium complexes interact with the duplex within the gel by intercalation.

Figure 4.3 shows the hybridization gel for the conjugate $\text{Ru-NH}(\text{CH}_2)_9\text{NHCO}_2\text{-AGTCTAGGCCTATCGT-3'}$. Addition of ruthenated strand to its 5' ^{32}P -labeled complement and addition of rhodium labeled strand to 3' ^{32}P -labeled ruthenated complement both result in retardation of the radioactively labeled strand, consistent with duplex formation. In the lane containing only ^{32}P -labeled ruthenated strand, smearing of the radioactive band along with a distinct band which is slightly retarded compared to the proper ruthenated duplex is observed. The self-association clearly evident for the ruthenated strand does not occur with the unmodified complement (lane 1). This behavior is most likely promoted by the self-complementarity of the central eight base pairs and is

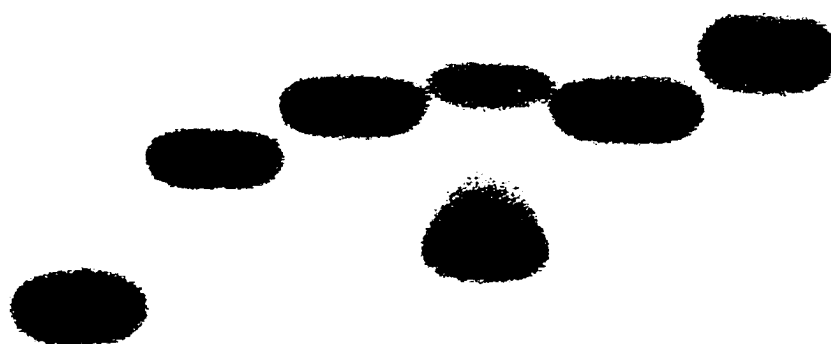
Figure 4.2. Hybridization of Ru-NH(CH₂)₉NHCO₂AGTGTATATAAACGT-3' to both unmodified complement and rhodium modified complement. The gel lanes are as follows: (1) 5' ³²P-labeled complementary strand, (2) unmodified duplex, (3) ruthenated duplex, (4) 3' ³²P-labeled ruthenium modified strand, (5) ruthenated duplex, (6) doubly metalated duplex (rhodium fraction 1), (7) doubly metalated duplex (rhodium fraction 2). The two fractions correspond to diastereomers of the rhodium modified oligonucleotide. Lanes 1-3 contain 5' ³²P-labeled complementary strand and lanes 4-7 contain 3' ³²P-labeled ruthenium modified strand. In duplex lanes containing 3' ³²P-labeled ruthenated strand, not all of the ruthenium modified oligonucleotide is fully bound. Formation of the duplex results in a decrease in the mobility of the ³²P-labeled strand. Modification of one strand of the duplex by the ruthenium complex produces a greater decrease in gel mobility while the doubly metalated duplex is retarded the furthest. Note the dramatic difference in mobility produced by the diastereomers of the rhodium modified oligonucleotide.

1 2 3 4 5 6 7



Figure 4.3. Hybridization of Ru-NH(CH₂)₉NHCO₂AGTCTAGGCCTATCGT-3' to both unmodified complement and rhodium modified complement. The gel lanes are as follows: (1) 5' ³²P-labeled complementary strand, (2) unmodified duplex, (3) ruthenated duplex, (4) 3' ³²P-labeled ruthenium modified strand, (5) ruthenated duplex, and (6) doubly metalated duplex. Lanes 1-3 contain 5' ³²P-labeled complementary strand and lanes 4-6 contain 3' ³²P-labeled ruthenium modified strand. Note the retardation of the radioactively labeled strand in the lane containing only the ³²P-tagged ruthenated single strand.

1 2 3 4 5 6

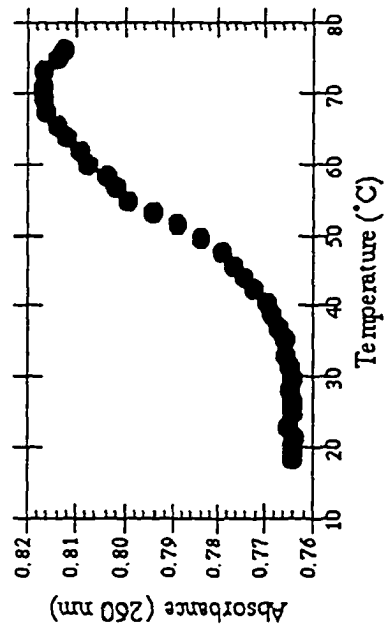
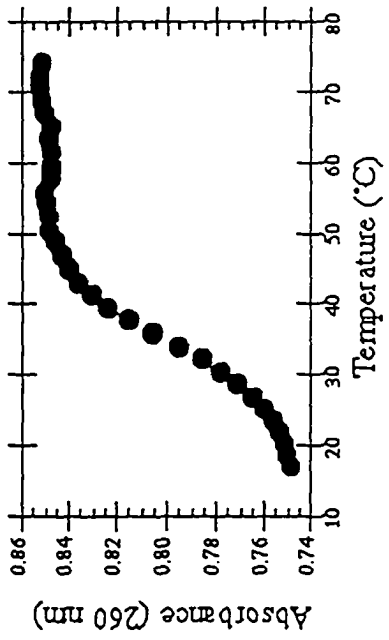
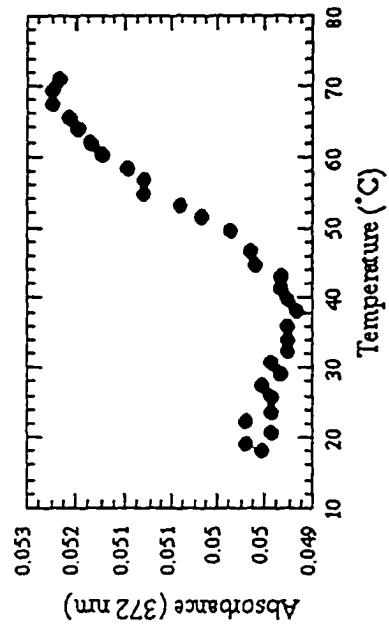
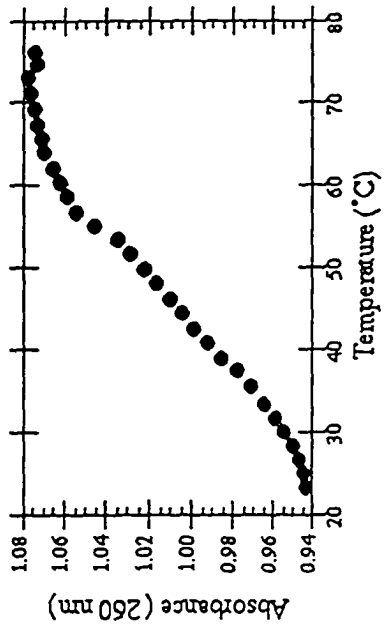


further enhanced by the presence of the ruthenium intercalators which are known to preferentially stabilize the duplex form (*vide infra*).

Thermal Denaturation Studies. Oligonucleotide modifications that destabilize duplex formation can be analyzed via thermal denaturation profiles of the duplex. Significant perturbations of duplex integrity will depress the thermal stability of the duplex, which can be measured by recording the change in absorption with increasing temperature. Intercalators have been found to increase the thermal stability of oligonucleotide duplexes, often raising the melting temperature by as much as 10° C.³ Figure 4.4 shows the changes in the absorbance at 260 nm with increasing temperature for unmodified duplex, an equimolar solution of duplex + noncovalent [Ru(phen)₂dppz]²⁺, and an equimolar solution of duplex covalently modified by ruthenium. The similarity of the melting curves for duplex + ruthenium and ruthenated duplex indicates the absence of drastic structural changes caused by conjugation of the ruthenium complex to the oligonucleotide. In both samples, at least a 10° C stabilization in the duplex T_m is observed upon either covalent modification or noncovalent addition of ruthenium intercalator. Also noteworthy is the shape of the melting temperature profile; the profile for noncovalent ruthenium + duplex is extremely broad whereas the metalated duplex has a much sharper transition. The shape of the melting profile observed for the noncovalently bound oligomer is consistent with random distribution of rutheniums along the duplex which affords stabilization along the entire length of the duplex. With the covalently bound oligomer, binding is localized to one end of the duplex, resulting in localized stabilization and a sharper transition.

Comparison of the melting data obtained from monitoring the absorption recovery at 260 nm to that obtained from monitoring at 372 nm yields an interesting result. Upon intercalation, extensive hypochromicity is often observed in the 372 nm transition where the maximum of the dppz-centered absorption band occurs. If one end of the helix is preferentially stabilized by ruthenium intercalation, then localized melting of the duplex at the terminus opposite the covalently attached ruthenium complex might be expected. In

Figure 4.4. Thermal denaturation profiles recorded at 260 nm for 2 μ M unmodified nine-mer oligonucleotide duplex (upper left), 2 μ M unmodified duplex + 2 μ M $[\text{Ru}(\text{phen})_2\text{dppz}]^{2+}$ (upper right), 2 μ M metalated duplex (Ru-NH(CH₂)₉NHCO₂AGTGCGAAG-3') monitored at 260 nm (lower left) and ruthenated duplex monitored at 372 nm (lower right) in 5 mM phosphate, 50 mM NaCl, pH 7.2 buffer. The difference in profiles of ruthenium-containing samples reflects the binding behavior of the ruthenium complex to the oligonucleotide duplex.



this case, recovery of the absorbance at 260 nm may be initiated at an earlier temperature than the absorbance recovery at 372 nm, which is observed in the data obtained. In the 260 nm melting profile, the absorbance starts to increase at around 35° C whereas in the plot displaying the 372 nm absorbance changes, the absorbance does not increase until a temperature of at least 44° C.

The hyperchromicity observed for the transition from the helical to the random coil state is relatively low for the covalently modified duplex (7%) compared to the 20-30% hypochromicity usually observed upon duplex melting. It is, however, comparable to the hyperchromicity observed for the unmodified duplex by itself (12%). Given the various contributions of both the metal complex and the oligonucleotide to the absorbance at 260 nm and that covalent attachment of an oligonucleotide to the ruthenium complex results in extensive hypochromicity in the 260 nm transition (~35% for ruthenated 12mer), it is not clear what the extent of absorbance recovery would be upon complete denaturation. In the denaturation profile obtained at 372 nm, only about 7% hyperchromicity is observed but the final absorbance is consistent with the ruthenium concentration. Despite the low hyperchromicity, the extent of stabilization provided by the ruthenium complex agrees with NMR melting data of oligonucleotide duplexes in the presence of $[\text{Ru}(\text{phen})_2\text{dppz}]^{2+4}$ and is in general consistent with the amount of duplex stabilization expected for a complex which binds via intercalation. Due to instrumental limitations, this method of analysis is restricted to modified oligonucleotides smaller than 15 bases in length unless agents such as formamide or urea are added to depress the melting temperature.

Comparative Luminescence Titrations. The luminescence properties of the ruthenium complex can be exploited in the characterization of oligonucleotide duplexes containing a strand covalently modified by $[\text{Ru}(\text{phen}')_2\text{dppz}]^{2+}$. The binding behavior of free $[\text{Ru}(\text{phen})_2\text{dppz}]^{2+}$ to the unmodified duplex as determined by the luminescence can be compared to the luminescence observed on binding of free ruthenium to the ruthenated duplex. This allows us to examine the structural integrity of the oligonucleotide portion of

the conjugate by determining whether covalent modification by ruthenium at one terminus adversely affects the ability of the strand to hybridize properly to complement.

The comparative luminescence titrations for the ruthenium modified sequence 5'-AGTGTATATAAACGT-3' are shown in Figure 4.5. Titration of free $[\text{Ru}(\text{phen})_2\text{dppz}]^{2+}$ into a solution containing unmetalated duplex results in a linear increase in the luminescence until the emission saturates between four and five equivalents of ruthenium(II) per duplex. This is consistent with random binding of ruthenium to the duplex and an average binding site of between three to four base pairs.⁵ The analogous experiment performed on the metalated duplex results in a titration curve which almost parallels the results obtained with unmodified duplex. The similarity in the results obtained from the two experiments demonstrates that no significant structural perturbation occurs upon covalent modification of the oligonucleotide strand.

Linear luminescence increases upon addition of $[\text{Ru}(\text{phen})_2\text{dppz}]^{2+}$ that reflect random binding of ruthenium complexes to the oligonucleotide duplex are not always observed, however. Figure 4.6 shows comparative luminescence titrations for both unmodified and modified duplexes of the sequence 5'-AGTCTAGGCCTATCGT-3'. The profiles of each titration clearly suggest preferential association of $[\text{Ru}(\text{phen})_2\text{dppz}]^{2+}$ with this duplex. Even if the luminescence enhancements associated with binding to different sites are significantly different, random binding will produce an average intensity increase per bound ruthenium molecule, thereby resulting in a linear binding curve. Provided that the luminescence quantum yields and the binding affinities for the various sites are significantly different, if preferential binding occurs, then initial addition of ruthenium complex to specific sites on the duplex would result in an incremental intensity change per bound ruthenium. After these sites are saturated, then subsequent metal additions produce a different incremental intensity change per bound ruthenium. If preferential binding occurs to a site where the luminescence quantum yield is low, then the binding curve will appear sigmoidal, as exhibited here. From photophysical studies of $[\text{Ru}(\text{phen})_2\text{dppz}]^{2+}$

Figure 4.5. Luminescence titrations of free $[\text{Ru}(\text{phen})_2\text{dppz}]^{2+}$ into 1 μM oligonucleotide duplex containing $\text{Ru-NH}(\text{CH}_2)_9\text{NHCO}_2\text{AGTGTATATAAACGT-3'}$ (top) and 1 μM unmodified oligonucleotide duplex (bottom). The luminescence intensity for both duplexes saturates at a *total* ruthenium concentration between four to five ruthenium complexes per 15 base pair duplex. The luminescence intensity is reported relative to a 10 μM solution of $[\text{Ru}(\text{bpy})_3]^{2+}$.

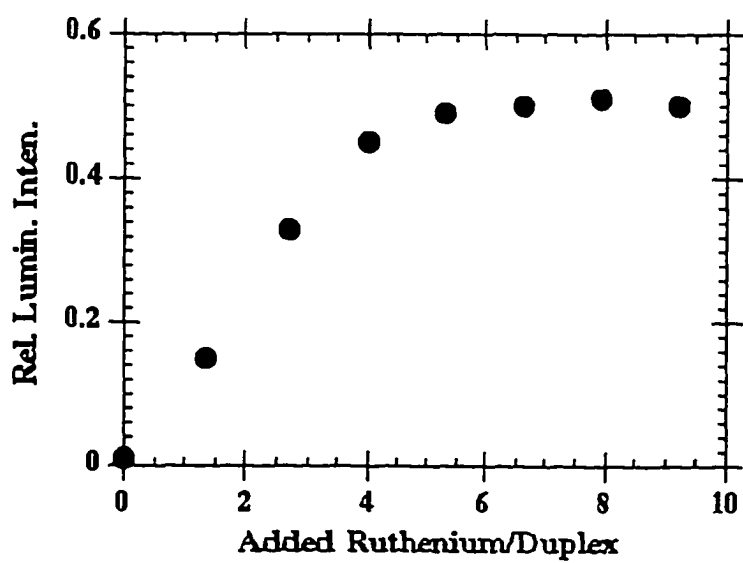
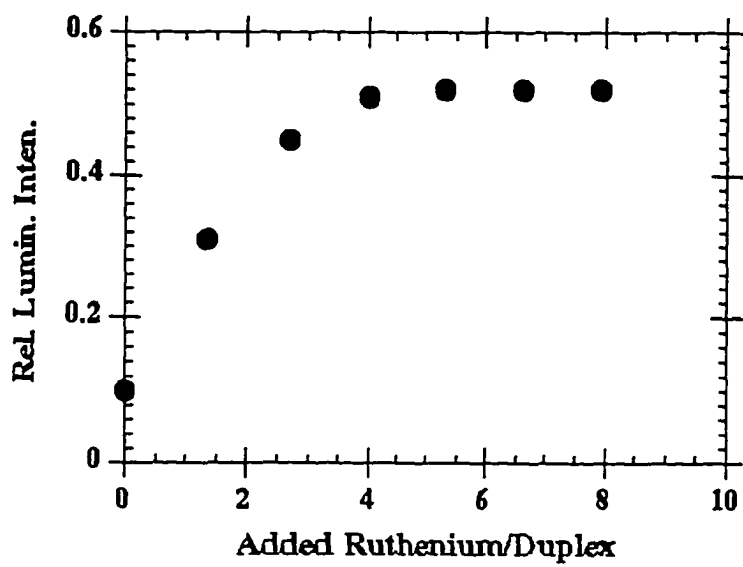
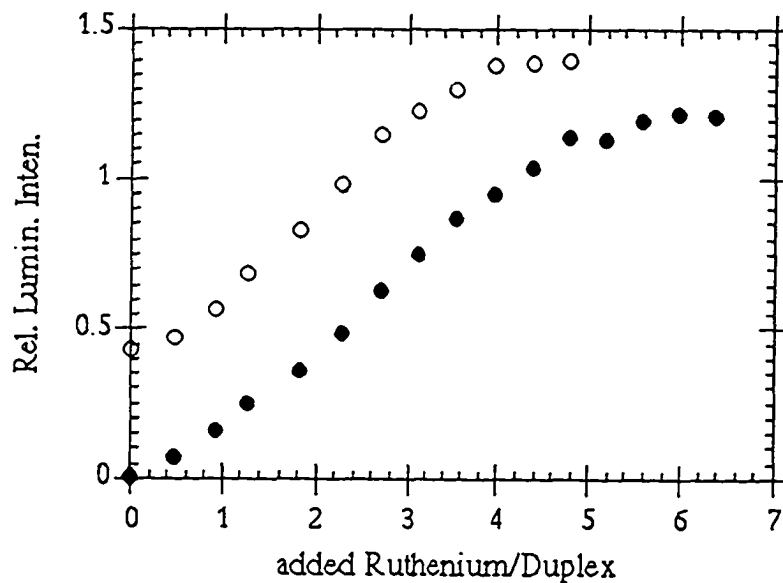


Figure 4.6. Comparative luminescence titrations of free $[\text{Ru}(\text{phen})_2\text{dppz}]^{2+}$ into $5\ \mu\text{M}$ oligonucleotide duplex containing $\text{Ru-NH}(\text{CH}_2)_9\text{NHCO}_2\text{AGTCTAGGCCTATCGT-3'}$ (open circles) and unmodified duplex (closed circles). Some sequence-specificity is apparent from the binding profiles for each duplex. The luminescence is reported relative to a $10\ \mu\text{M}$ solution of $[\text{Ru}(\text{bpy})_3]^{2+}$.



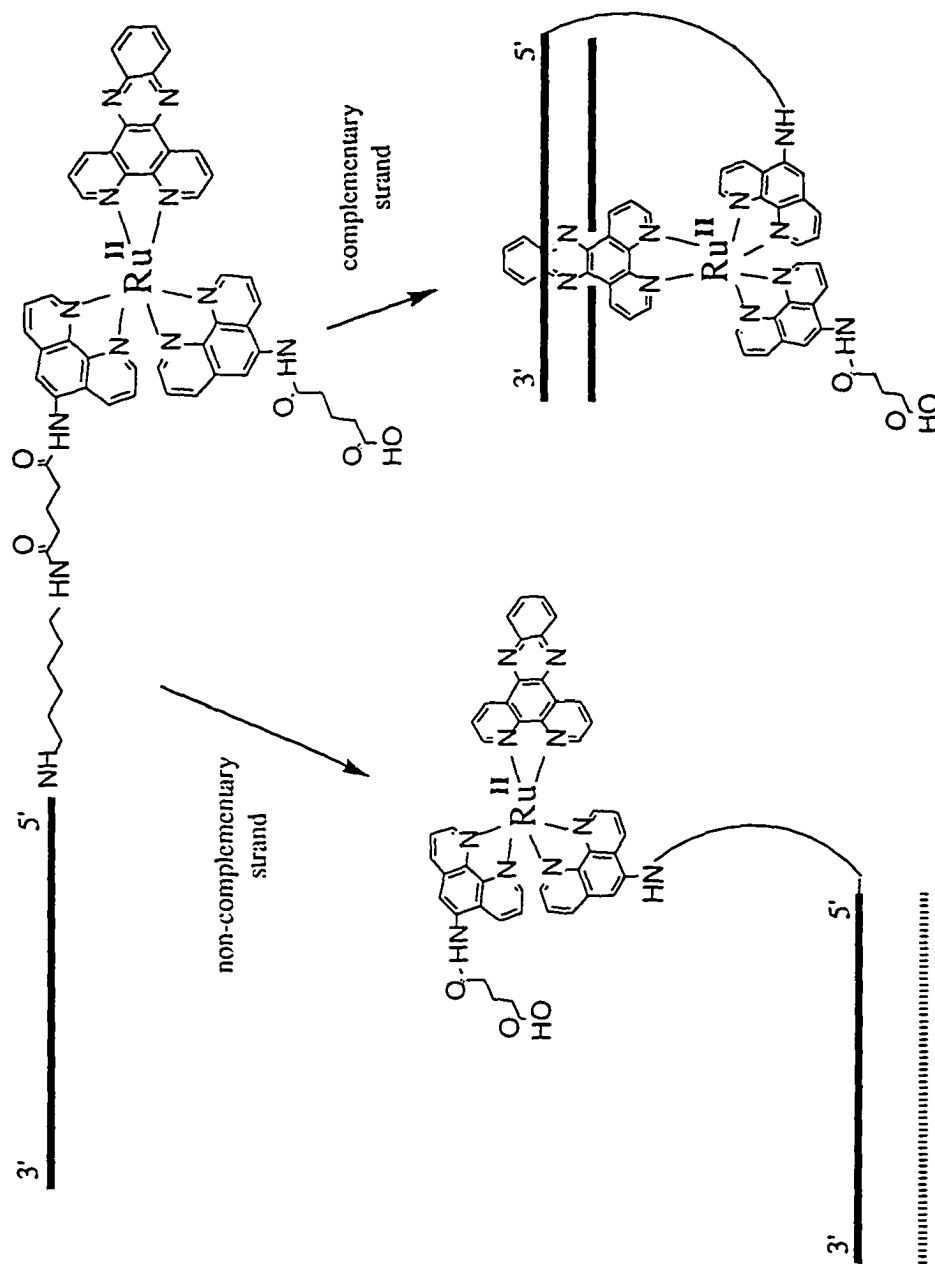
noncovalently bound to oligomers of various sequences, it is clear that variations in sequence influence the emission properties of the intercalated metal complex.² This type of binding profile has also been observed for duplexes 5'-AGTCATGTGGCCTAGTCCGT-3' and 5'-AGTGCGAAGGCCTGG-AACGT-3', and may be characteristic of sequences containing a central GGCC.

Titration of free $[\text{Ru}(\text{phen})_2\text{dppz}]^{2+}$ into the ruthenium-modified duplex results in a binding curve analogous to that of the unmodified duplex except 1) the concentration at which the luminescence saturates is shifted by about 5 μM due to the presence of the covalently bound metal, and 2) the relative luminescence intensity at the saturation point is higher for the ruthenated oligonucleotide. Again, preferential binding by the added noncovalent ruthenium complex is apparent; at low noncovalent ruthenium concentrations, the amount of luminescence increase is less per ruthenium than at higher noncovalent ruthenium concentrations. Due to the initial luminescence contribution of the covalently bound ruthenium (compare 5 μM covalently bound to 5 μM noncovalently bound), the luminescence at saturation is higher for the metalated duplex. Although the titration curves for this sequence do not support random binding of noncovalently added ruthenium complex, the similarity in the results obtained for unmodified and modified duplex demonstrates analogous binding behavior of free ruthenium complex to both duplexes and is evidence that drastic structural perturbations of the oligonucleotide duplex do not occur as a result of covalent attachment of ruthenium complex at the 5' terminus.

4.3.2. Luminescence Characterization of Ruthenated Oligonucleotides

By tethering an oligonucleotide to the ruthenium complex, it may be possible to utilize the light switch effect of $[\text{Ru}(\text{phen})_2\text{dppz}]^{2+}$ for the targeting of single-stranded DNAs (Scheme 4.1). If the single-stranded metal complex were added to a noncomplementary sequence, complex intercalation could not occur due to the absence of

Scheme 4.1.



duplex formation, therefore resulting in little luminescence enhancement. Addition of the single-stranded metal complex to its complementary sequence and subsequent duplex formation, however, would enable intercalation by the metal complex, resulting in significant luminescence enhancement and signaling the presence of the desired sequence.

Solid- and solution-phase techniques were used to prepare a series of ruthenated oligonucleotides containing either a 5' hexamethylene phosphodiester attachment or a 5' carbamate attachment with linker arms composed of either six carbons or nine carbons. The emission properties of these conjugates, both in their single-stranded and duplex forms, were examined in order to determine which features might be further exploited for application as novel, luminescent probes for nucleic acids.

One point which should be kept in consideration when attempting to evaluate the obtained luminescence results is the effect of the covalent attachment on the binding of the ruthenium complex. $[\text{Ru}(\text{phen})_2\text{dppz}]^{2+}$ has a binding constant for double-helical DNA of at least 10^7 M^{-1} . Although the linker attachment to the ancillary phenanthroline is at the position least likely to hinder intercalative binding, alterations in the depth of intercalation or the extent of stacking may occur which would affect binding of the covalently tethered intercalator.

The steady state luminescence of the duplex containing Ru-NH(CH₂)₉NHCO₂AGTCTAGGCCTATCGT-3' was measured under conditions of varying salt alongside its noncovalently bound analogue (Table 4.1). The binding of covalently attached ruthenium to its duplex in the presence of 10 mM magnesium is strongly affected as is evidenced by the almost 25% decrease in the luminescence intensity. The lack of a corresponding decrease in the noncovalently bound duplex serves as evidence that the binding of the covalently attached ruthenium complex is adversely affected by the high salt concentration. It appears that, at least for the nonane carbamate, the presence of the linker weakens the binding affinity of the ruthenium complex for the duplex although a lowered binding affinity for that particular site can not be ruled out. Certainly this result

Table 4.1. Effect of Salt Concentration on the Steady-state Luminescence of Duplex Containing Ru-NH(CH₂)₉NHCO₂AGTCTAGGCCCTATCGT-3'.^a

	<u>50 mM Na⁺/5 mM Tris</u>	<u>50 mM Na⁺/10 mM Mg²⁺/10 mM Tris</u>	
Ru + === d	<u>R.L.I.</u> ^{b,c}	<u>R.L.I.</u> ^{b,c}	0.23
Ru=== e	0.22	0.43	0.33

^aAll samples are 5 μM in metal and duplex.

^bThe luminescence intensity is reported relative to a solution of 10 μM [Ru(bpy)₃]²⁺. Excitation is at 440 nm.

^cThe wavelength at the emission maximum is not affected by the increase in salt concentration.

^dRu + === represents [Ru(phen)₂dppz]²⁺ noncovalently bound to oligonucleotide duplex.

^eRu=== represents ruthenated duplex.

indicates that the dissociation constant for this covalently tethered intercalator must be on the order of 10^{-6} M.

Single-stranded Ruthenium Complex Versus Ruthenated Duplex. Table 4.2 documents the steady-state intensities and the luminescence lifetimes for all prepared ruthenium conjugates, both in the single-stranded and duplex forms. Although substantial enhancements are observed with the conjugates Ru-NH(CH₂)₉NHCO₂AGTGCGAAG-3' and Ru-NH(CH₂)₆OPO₂AGTGCCAAGCTTGCA-3', the magnitude of the luminescence enhancement upon hybridization for the majority of the constructed ruthenated oligonucleotides is much less than that observed for the parent ruthenium molecule on addition of double-stranded DNA ($> 10^3$).^{1a} In every case, the single-stranded ruthenium complexes luminesce to some extent. In some samples, the luminescence intensity displayed by the single-stranded complex is higher than that observed for the metalated duplex. The luminescence of the noncovalently bound complex does not appear to be an appropriate analogue for predicting the behavior of the covalently bound sample upon hybridization; the emission changes of the covalently modified strand on annealing to its complement do not always parallel those of the noncovalently bound sample. In addition, binding of the ruthenium complex in the two different duplexes is rarely analogous due to the structural confinement of the ruthenium complex in the covalently modified duplex caused by the linker.

A biexponential decay in the emission is detected for each ruthenated oligonucleotide. Biexponential decays of the excited state are also a characteristic feature of the parent [Ru(phen)₂dppz]²⁺ bound to nucleic acids.² The two lifetime components are believed to result from differential stacking of the dppz ligand within an intercalation site, which is a conclusion supported by ¹H-NMR studies.⁴ It is not clear that the structural basis for the two lifetimes will be similar for the ruthenated single strand. That the single-stranded ruthenium complex luminesces is not surprising given the hypochromicity in the dppz intraligand band observed for each carbamate-containing sequence synthesized,

Table 4.2. Comparison of Luminescence Properties for Single-stranded Ruthenated Oligonucleotides, Ruthenated Duplexes, and Their Noncovalently Bound Analogues.

<u>Sample^a</u>	<u>Single-stranded</u>			<u>Double-stranded</u>		
	<u>R.L.I.^b</u>	<u>$\lambda_{\max}(\text{nm})$</u>	<u><math>\tau(\text{ns})^c</math></u>	<u>R.L.I.^b</u>	<u>$\lambda_{\max}(\text{nm})$</u>	<u><math>\tau(\text{ns})^c</math></u>
4 μM Ru + AGTGCCAAGCTTGCA				0.15	610	420 (35) 90 (65)
4 μM Ru-NH(CH ₂) ₆ PO ₂ AGTGCCAAGCTTGCA ^e	0.019 ^d			0.17	598	500 (60)
2 μM Ru + AGAAGCCTGGT	0.17	615	300 (23) 65 (77)	0.09	616	110 (40) 275 (17)
2 μM Ru-NH(CH ₂) ₆ NHCO ₂ AGAAGCCTGGT ^g	0.10	606	390 (23) 108 (77)	0.14	610	68 (83) 340 (33)
2 μM Ru + TCTAAGCCATCCGCT	0.07	611	295 (37) 60 (63)	0.21	607	103 (67) 574 (25)
2 μM Ru-NH(CH ₂) ₆ NHCO ₂ TCTAAGCCATCCGCT ^{e,g}	0.16	602	478 (29) 109 (71)	0.19	608	103 (75) 402 (31)
2 μM Ru-NH(CH ₂) ₆ NHCO ₂ TCTAAGCCATCCGCT	0.11	604	518 (20) 106 (80)	0.12	606	31 (69) 463 (29)
2 μM Ru-NH(CH ₂) ₆ NHCO ₂ TCTAAGCCATCCGCT	0.14	603	454 (27) 106 (73)	0.17	606	113 (71) 419 (42)
2 μM Ru + AGTGCGAAG	0.025	611		0.16	609	133 (58)
2 μM Ru-NH(CH ₂) ₉ NHCO ₂ AGTGCGAAG ^{e,g}	0.034	608	251 (42) 17 (58)	0.13	603	240 (45) 50 (55)
2 μM Ru-NH(CH ₂) ₉ NHCO ₂ AGTGCGAAG	0.04	612	225 (45) 20 (55)	0.27	602	379 (52) 164 (48)

<u>Sample</u>	<u>R.L.I.</u>	<u>$\lambda_{max}(nm)$</u>	<u>$\tau(ns)$</u>	<u>R.L.I.</u>	<u>$\lambda_{max}(nm)$</u>	<u>$\tau(ns)$</u>
2 μM Ru + AGTGCGAAGGCC	0.22	610	680 (55) 100 (45)	0.10	614	420 (26) 80 (74)
2 μM Ru-NH(CH ₂) ₉ NHCO ₂ AGTGCGAAGGCC ^{e,g}	0.59	600	760 (66) 110 (34)	0.33	603	530 (39) 120 (61)
2 μM Ru-NH(CH ₂) ₉ NHCO ₂ AGTGCGAAGGCC	0.37	601	720 (52) 80 (48)	0.32	601	620 (36) 110 (64)
2 μM Ru + AGTGCGAAGGCCGTGGAACGT	0.12	613	420 (27) 70 (73)	0.09	615	290 (27) 70 (67)
2 μM Ru-NH(CH ₂) ₉ NHCO ₂ AGTGCGAAGGCCGTGGAACGT ^{e,g}	0.29	601		0.24	602	640 (39) 110 (61)
2 μM Ru-NH(CH ₂) ₉ NHCO ₂ AGTGCGAAGGCCCTGGAACGT	0.40	601	680 (47) 110 (53)	0.33	602	590 (38) 110 (62)
2 μM Ru + AGTGCATATATAAAGTACGT	0.11	613		0.21	609	
2 μM Ru-NH(CH ₂) ₉ NHCO ₂ AGTGCATATATAAAGTACGT ^h	0.10	607		0.15	604	
2 μM Ru-NH(CH ₂) ₉ NHCO ₂ AGTGCATATATAAAGTACGT ⁱ	0.22	604		0.22	605	
2 μM Ru + AGTGTATATAAACGT	0.14	619		0.19	617	
2 μM Ru-NH(CH ₂) ₉ NHCO ₂ AGTGTATATAAAGTACGT ^f	0.29	602		0.21	604	
2 μM Ru + AGTCATGTGGCCTAGTCCGT	0.15	614		0.11	611	

<u>Sample</u>	<u>R.L.I.</u>	<u>$\lambda_{\text{max}}(\text{nm})$</u>	<u>$\tau(\text{ns})$</u>	<u>R.L.I.</u>	<u>$\lambda_{\text{max}}(\text{nm})$</u>	<u>$\tau(\text{ns})$</u>
2 μM Ru-NH(CH ₂) ₉ NHCO ₂ AGTCATGTGGCCTAGTCCG ^f	0.18	601	0.18	0.18	601	601
5 μM Ru + AGTCTAGGCCCTATCGT	0.16	625	0.22	0.22	617	617
5 μM Ru-NH(CH ₂) ₉ NHCO ₂ AGTCTAGGCCCTATCGT ^{e,g,i}	0.31	612	0.43	0.43	604	604
5 μM Ru-NH(CH ₂) ₉ NHCO ₂ AGTCTAGGCCCTATCGT	0.37	614	0.42	0.42	602	602
5 μM Ru + AGTCTGTTAACATCGT	0.20	620	0.36	0.36	619	619
5 μM Ru-NH(CH ₂) ₉ NHCO ₂ AGTCTGTTAACATCGT ^{e,g,i}	0.34	612	0.45	0.45	604	604
5 μM Ru-NH(CH ₂) ₉ NHCO ₂ AGTCTGTTAACATCGT	0.34	610	0.43	0.43	602	602

^aRu in samples represents [Ru(phen)₂dppz]²⁺.

^bThe luminescence intensity is reported relative to a solution of 10 μM [Ru(bpy)₃]²⁺. Excitation is at 440 nm.

^cEmission was monitored at 610 nm, with excitation at 480 nm. The numbers in parentheses denote the pre-exponential factor and indicate the relative contribution of that particular component to the lifetime decay.

^dIntensity also includes contributions from buffer background. For this particular sample, the single-stranded intensity is essentially negligible.

^eConjugate prepared from isomer of C₁ symmetry.

^fConjugate prepared from late eluting metal isomer.

^gCovalently bound ruthenium samples were isolated from the same reaction mixture and have been analyzed by ESI-MS.

^hConjugate prepared from early eluting metal isomer.

ⁱDifficulty was encountered when purifying conjugates by HPLC. Although samples were characterized by ESI-MS, quantitative phosphate analysis, and enzymatic digest, analytical HPLC chromatograms of purified material still showed the presence of minor contaminants which may influence the luminescence properties of the conjugates.

clearly demonstrating interaction between the oligonucleotide and the appended metal complex in solution. Significant hypochromicity in the dppz intraligand band was not observed for the conjugate containing the hexamethylene phosphodiester linker.

The luminescence shown by the ruthenated single strand clearly indicates limited water accessibility of the dppz ligand. However, the structural basis for the interaction between the oligonucleotide and the covalently tethered complex responsible for the luminescence is not obvious. Dilution experiments suggest that it is an intramolecular interaction although gel electrophoresis shows that in some cases, the luminescence may result from intermolecular effects. Perhaps the extended aromatic surface of the dppz ligand which enables the complex to bind so avidly to double-helical DNA through stacking also permits stacking in the single strand or possibly folding of the oligonucleotide around the metal complex such that the dppz ligand is protected from water, thereby resulting in the luminescence. It is known that if bases are linked to each other in oligo- and polynucleotides, stacking interactions between adjacent bases occur and give rise to stable, single-stranded, helical structures.⁶ The stability of these single-stranded stacks is related to the purine content of the strand which is most likely due to the greater surface area available for stacking for the purine bases; of the different single-stranded polynucleotides, poly(A) is mainly helical and poly(U) is predominately random coil at room temperature. It is not obvious that the purine content of the strand is related in any way to the luminescence intensity of the single-stranded ruthenated oligonucleotide. It is apparent, however, that distinct differences exist among the various sequences and in order to utilize the ruthenium luminescence as a marker for sequence-specific detection, a systematic analysis should be performed to elucidate the sequence contributions to the luminescence of the single-stranded ruthenium complex.

Using the Intercalation Site to Dictate Luminescence Properties. By using the same base sequence for the 5' terminus, the ruthenated oligonucleotides can be designed such that the intercalating environment is the same. In this manner, the steady-state and

time-resolved emission of the covalently attached ruthenium complex can be compared for a series of modified oligonucleotide duplexes. If the ruthenium intercalation site is the same across a series, then the ruthenium luminescence properties should also be similar due to the sensitivity of ruthenium emission to its environment. Variations in the ruthenium luminescence, provided that features such as linker length, linker attachment, and ruthenium isomer used are identical, will then reflect structural perturbations of the oligonucleotide duplex itself.

This notion is best illustrated in the comparison of the luminescence properties for the first three ruthenated oligonucleotides listed in Table 4.3, all of which possess the same nine base sequence at their 5' termini. The relative luminescent intensities and the wavelengths of maximum emission are similar for the 12mer and 20mer duplexes containing equivalent intercalation sites; the slight variations observed in the excited state lifetimes are within the error of the measurements. Parallel steady-state emission properties are also displayed by ruthenated oligonucleotide duplexes containing the 5' terminus AGTC (Table 4.2). The luminescent intensities and the emission lifetimes for the 9mer duplex containing an equivalent binding site (5' AGTG) are significantly lower than those observed for the 12mer and the 20mer duplexes.⁷ This decreased emission is most likely due to greater dynamic flexibility of the ruthenated 9mer due to its short length. At room temperature, fraying of the duplex at the terminus opposite the ruthenium complex may occur, resulting in the observed decrease in the luminescence intensity. The localized melting of the duplex terminus opposite the ruthenium complex observed in the thermal denaturation profile of this ruthenated duplex is fully consistent with the luminescence result.

The greater dynamic fluxionality of shorter length oligonucleotide duplexes is clearly demonstrated by incubation of an oligonucleotide duplex containing Ru-NH(CH₂)₉-NHCO₂AGTCTAGGCCTATCGT-3' sequence with the restriction enzyme *Hae* III. *Hae* III generates a blunt ended cut in the center of its 5'-GGCC-3' recognition site to produce

Table 4.3. Comparison of Luminescence Properties for Ruthenated Oligonucleotide Duplexes Containing Analogous 5' Termini.

<u>Sample</u> ^a	<u>R.L.I.</u> ^b	<u>λ_{max}</u> (nm)	<u>τ</u> (ns) ^c
Ru-NH(CH ₂) ₉ NHCO ₂ AGTGCCGAAG ^d	0.27	602	110 (40) 379 (52) 164 (48)
Ru-NH(CH ₂) ₉ NHCO ₂ AGTGCCGAAGGCC ^d	0.32	601	620 (36) 110 (64)
Ru-NH(CH ₂) ₉ NHCO ₂ AGTGCCGAAGGCCCTGGAAACGT ^d	0.33	602	590 (38) 110 (62)
Ru-NH(CH ₂) ₉ NHCO ₂ AGTGCATATATAAGTACGT ^e	0.22	605	
Ru-NH(CH ₂) ₉ NHCO ₂ AGTGTATATAAACGT ^e	0.21	604	

^aAll samples are *duplexes* containing the indicated strands. Although all samples listed in the table were prepared using different isomers of the metal complex, it is believed that all samples correspond to the product obtained from coupling of the late eluting metal isomer. Measurements were conducted with 2 μ M solutions of ruthenated duplex.

^bThe luminescence intensity is reported relative to a solution of 10 μ M [Ru(bpy)₃]²⁺. Excitation is at 440 nm.

^cEmission was monitored at 610 nm with excitation at 480 nm. The numbers in parentheses denote the pre-exponential factor and indicate the relative contribution of that particular component to the lifetime decay.

^dConjugate prepared from isomer of C₁ symmetry. Two major fractions were isolated from the reaction mixture. Based upon their HPLC chromatograms, it is believed that the sample shown corresponds to the product obtained from coupling of the late eluting metal isomer.

^eConjugate prepared from late eluting metal isomer.

two 8mer duplexes; the luminescence decreases by 9% upon incubation with the enzyme which is consistent with greater fluxionality of the 8mer duplex relative to the parent 16mer oligonucleotide duplex due to partial melting as a result of the shorter length.

As seen in Table 4.3, increased dynamic flexibility may also contribute to the lower luminescent intensities observed for the 5'-AGTG duplexes containing a central 5'-TATATAAA-3' sequence. AT-rich regions are known to be unusually flexible⁸; work performed in our laboratory suggests that this particular sequence is intrinsically unwound as a result of its flexibility.⁹ The ruthenated duplexes containing a central 5'-TATATAAA-3' may be partially melted in the center due to the inherent fluxionality of that particular sequence, an effect which is manifested in the decreased luminescent intensities for the two duplexes.

Although the ruthenated duplex containing the hexamethylene phosphodiester linkage also contains the 5'-AGTG terminus, its emission intensity is substantially lower than those observed for the nonane carbamate linkage duplexes (Table 4.4). In addition, the contributions to the excited-state decay for the short and long lifetime components are reversed for the phosphodiester, with contains a higher percentage of the long lifetime component, indicating at least a different orientation of the metal complex in the site. The decreased intensity displayed here is most likely caused by decreased flexibility in the linker, rather than changes in duplex structural stability. Comparison of the effects of different linker lengths on the ruthenium luminescence suggests that shorter length linkers are more rigid with lower apparent emission intensities (*vide infra*).

Detailed information about the intercalation site for oligonucleotides covalently modified by rhodium complexes containing a phi ligand can be obtained due to the photochemical properties of the rhodium complex.¹⁰ Is it possible to obtain analogous information about the ruthenium binding site from the emission properties of the intercalated metal? Photophysical studies performed on noncovalent $[\text{Ru}(\text{phen})_2\text{dppz}]^{2+}$ bound to AT- and GC-containing synthetic polynucleotides showed sequence-dependent

Table 4.4. Comparison of Luminescence Properties for Ruthenated Oligonucleotide Duplexes Containing Similar Sequences at the 5' Terminus but with Different Linkers.

<u>Sample</u> ^a	<u>R.L.I.</u> ^b	<u>λ_{max}</u> (nm)	<u>τ</u> (ns) ^c
4 μ M Ru-NH(CH ₂) ₆ OPO ₂ AGTGCCAAGCTTGCA ^d	0.17	598	500 (60) 110 (40)
2 μ M Ru-NH(CH ₂) ₉ NHCO ₂ AGTGCGAAGGCC ^d	0.32	601	620 (36) 110 (64)

^aAll samples are *duplexes* containing the indicated strands.

^bThe luminescence intensity is reported relative to a solution of 10 μ M [Ru(bpy)₃]²⁺. Excitation is at 440 nm.

^cEmission was monitored at 610 nm with excitation at 480 nm. The numbers in parentheses denote the pre-exponential factor and indicate the relative contribution of that particular component to the lifetime decay.

^dConjugate prepared from isomer of C₁ symmetry.

variations in the ruthenium luminescence.² The greatest distinctions between the two polymers were in the time-resolved lifetimes and the wavelengths of maximum emission intensity. The excited state lifetimes for ruthenium complex bound to poly d(AT)-poly d(AT) are significantly longer (740 ns versus 290 ns) and the emission maximum is red-shifted compared to complex bound to poly d(GC)-poly d(GC) (620 nm versus 606 nm). No large differences were observed between the steady-state luminescence intensities.

Even with the data on noncovalently bound oligomers as a reference, conclusions about the details of the ruthenium intercalation site in the covalently modified duplexes can not be readily made. Using the nine carbon carbamate 5'-AGTG sequences as an example, the lifetimes for the 12mer and 20mer duplexes appear to be intermediate between exclusively GC-containing and exclusively AT-containing polymers. Although the excited state lifetimes and their relative percentages are closer to those of the AT sequence, no corresponding red shift in the emission wavelength consistent with intercalation into an AT rich site occurs. The wavelength of the intercalated ruthenium complex for most of the constructed ruthenated duplexes are actually blue-shifted from purely GC-containing duplexes. It is possible that slight differences in stacking of the intercalating ligand due to the presence of the linker may alter the energetics of emission without severely affecting the luminescence lifetimes. A better noncovalent analogue for luminescence comparison might be the starting ruthenium isomer rather than the unmodified $[\text{Ru}(\text{phen})_2\text{dppz}]^{2+}$. In order to more thoroughly address the issue of binding site characterization using the photophysical properties of the ruthenium complex, the effects of totally different sequences at the metal intercalation site should be examined.

Effect of Complex Orientation on the Ruthenium Luminescence. In addition to variations in the sequence, the influence of slight perturbations in the structure of the ruthenated oligonucleotide itself was studied. To examine the influence of the linker orientation on the ruthenium luminescence, the sequence 5'-AGTGCATATATAAAGTACGT-3' was coupled to both the early eluting metal isomer

(isomer 1) and the late eluting metal isomer (isomer 3). These two isomers vary in the displacement of the nonsymmetric modified phenanthroline ligand about the metal center as described in Chapter 3. The results are shown in Table 4.5. More substantial changes in the luminescence occur for the ruthenated oligonucleotide synthesized with isomer 1.

Also included in Table 4.5 are the differences in luminescence observed for ruthenated duplexes prepared using the isomer of C_1 symmetry (isomer 2). The coupling reactions for the sequences 5'-AGTGCGAAGGCC-3' and 5'-AGTGCGAAGGCCTGGAACGT-3' yielded two well-resolved peaks of equivalent areas. These peaks most likely represent products differing in linker orientation, or coupling to the positional analogues of isomer 1 and isomer 3. The two fractions, for both sequences, have emission characteristics which vary significantly, in both the single-stranded and duplex forms. Further study here is warranted; the exact effect caused by the difference in linker orientation is unknown. In addition, the results may not be independent of the 5' terminal sequence.

Effects of Linker Length on the Ruthenium Luminescence. On comparing the steady-state luminescence properties for both the nine carbon and the six carbon carbamate linkers (Table 4.6), it appears that the longer linker provides greater flexibility to the attached ruthenium complex, resulting in larger differences in the emission properties between single-stranded and duplex forms. These differences are more apparent in the time-resolved data. Upon hybridization to the complementary sequence, the accompanying changes in the excited-state lifetimes are of substantially greater magnitude with the nine carbon linker (Table 4.2).

Table 4.6 shows the differences in luminescence observed for ruthenated duplexes containing linkers of different lengths. Caution must be exercised, however, in the interpretation of this data due to the absence of equivalent samples; because the ruthenium emission is highly sensitive to its environment, comparison of the two linkers using different binding sites may not be the optimal means of evaluation. Inspection of the

Table 4.5. Comparison of Luminescence Properties for Ruthenated Oligonucleotide Duplexes Containing Variations in Linker Orientation on Metal Complex.

<u>Sample</u> ^a	<u>R.L.I.</u> ^b	<u>I_{duplex}/I_{single}</u>
Ru-NH(CH ₂) ₉ NHCO ₂ AGTGTATATAAACGT ^c	0.15	1.50
Ru-NH(CH ₂) ₉ NHCO ₂ AGTGTATATAAACGT ^d	0.22	no change
Ru-NH(CH ₂) ₉ NHCO ₂ AGTGCGAAGGCC ^e	0.33	0.56
Ru-NH(CH ₂) ₉ NHCO ₂ AGTGCGAAGGCC	0.32	0.86
Ru-NH(CH ₂) ₉ NHCO ₂ AGTGCGAAGCCCTGGAACGT ^e	0.24	0.83
Ru-NH(CH ₂) ₉ NHCO ₂ AGTGCGAAGCCCTGGAACGT	0.33	0.83

^aAll samples are *duplexes* containing the indicated strands. Measurements were conducted with 2 μM solutions of ruthenated duplex.

^bThe luminescence intensity is reported relative to a solution of 10 μM [Ru(bpy)₃]²⁺. Excitation is at 440 nm.

^cConjugate prepared from early eluting metal isomer.

^dConjugate prepared from late eluting metal isomer.

^eCovalently bound ruthenium samples have been isolated from the same reaction mixture and have been analyzed by ESI-MS. Conjugates were prepared from the isomer of C₁ symmetry. Based upon the HPLC chromatograms of the reaction mixtures, isolated fractions are believed to be products differing in linker orientation, or coupling to the positional analogues of isomer 1 (first sample) and isomer 3 (second sample).

Table 4.6. Comparison of Luminescence Properties for Ruthenated Oligonucleotide Duplexes Containing Variations in Linker Length.

<u>Sample</u> ^a	$I_{\text{duplex}}/I_{\text{single}}$	$\lambda_{\text{(duplex)}} - \lambda_{\text{(single)}}$ ^b
Ru-NH(CH ₂) ₆ NHCO ₂ AGAAGGCCCTGGT ^c	1.4	1 nm (red)
Ru-NH(CH ₂) ₆ NHCO ₂ TCTAAGCCATCCGCT ^c	1.2	6 nm (red)
Ru-NH(CH ₂) ₉ NHCO ₂ AGTGCCGAAG ^c	3.8	5 nm (blue)
Ru-NH(CH ₂) ₉ NHCO ₂ AGTCTAGGCCCTATCGT ^{c,d}	1.4	8 nm (blue)
Ru-NH(CH ₂) ₉ NHCO ₂ AGTGCCGAAGCCCTGGAACGT ^c	0.83	1 nm (red)
Ru-NH(CH ₂) ₉ NHCO ₂ AGTGATATAAACGT ^c	0.72	2 nm (red)

^aAll samples are *duplexes* containing the indicated strands. Comparisons conducted on 2 μM concentrations of ruthenated duplex unless otherwise stated.

^bIndicates difference in the maximum emission wavelength between duplex and single-stranded forms. Red or blue states the direction of the wavelength shift upon annealing.

^cConjugate prepared from isomer of C₁ symmetry.

^dComparisons conducted on 5 μM duplex solutions.

^eConjugate prepared from late eluting metal isomer.

steady-state data shows that for both ruthenated duplexes containing the hexamethylene carbamate linker, the luminescence of both samples increases upon duplex formation, along with a red shift in the emission maximum. The behavior of the nonane linker contrasts that of the six carbon linker; an enhancement in the luminescence on hybridization yields a blue shift in the emission maximum whereas a decrease in the luminescence results in a red shift. The variations observed between the two linkers most likely reflect differences in the stacking interaction of the ruthenium complex with the single-strand and with the duplex. That the two lengths produce substantially different effects upon complex binding and the resulting emission properties is evident; the shorter linker appears to restrain the conformational mobility of the attached ruthenium, leading to smaller changes in the emission properties upon hybridization compared to the longer linker. A decreased luminescent intensity for the duplex relative to intensities displayed by the nine carbon carbamate-containing duplexes is also observed for the hexamethylene phosphodiester linker. Due to the extreme sensitivity of the ruthenium emission to its environment, the photophysical properties of ruthenated duplexes containing *only variations in the linker* should be performed. At the present time, it is not obvious which linker features are more suitable for diagnostic applications. For instance, the increased flexibility of the nonane linker may lead to higher emission of the ruthenated single strand. The most desirable situation is presumably reproducible emission properties upon binding to equivalent 5' terminal duplex sequences.

Temperature Dependence of Single-stranded Ruthenium and Ruthenium Modified Duplex. The luminescence characterization of the constructed ruthenated oligonucleotides, in both their single-stranded and duplex forms, effectively demonstrates the extreme sensitivity to even subtle alterations in sequence or structure. One luminescence feature which appears to be general and may prove extremely valuable for diagnostic applications is the temperature dependence of these metalated oligonucleotides.

The change in luminescence of solutions of Ru-NH(CH₂)₆NHCO₂-AGAAGGCCTGGT-3', single-stranded and duplex form, upon variation of the temperature was explored (Figure 4.7). A 10° C increase in the temperature produces a decrease in the luminescence of the single-stranded ruthenium complex while the emission of the covalently modified duplex is unaffected. Identical behavior upon increasing the temperature is found for the noncovalently bound analogues, confirming the generality of this feature. Normally, loss of luminescence with increasing temperature is observed due to increased vibrational deactivation; the luminescence of [Ru(bpy)₃]²⁺ decreases by 11% upon raising the temperature from 26° C to 36° C. Although the luminescence of the single-stranded ruthenium oligonucleotide is not completely eliminated upon raising the temperature, the luminescence of the duplex form has always been found to be significantly higher than that of the single strand. By destabilizing the single-stranded form, perhaps by using a pyrimidine sequence near the intercalation site, the discrimination upon increasing the temperature may be greatly increased. The maintenance of luminescence provided by binding to duplex DNA could prove to be extremely advantageous in solution phase hybridization experiments by allowing the discrimination of mismatched sequences from correctly annealed sequences by measuring the luminescence near the melting temperature.

4.3.3. Ru-NH(CH₂)₆OPO₂AGTGCCAAGCTTGCA-3' as a Novel Hybridization Probe

Luminescence Characterization of Duplex. Due to the favorable luminescence properties displayed by this particular conjugate, the metalated oligonucleotide Ru-NH(CH₂)₆OPO₂AGTGCCAAGCTTGCA-3' was chosen for further examination to address the suitability of these ruthenated oligonucleotides as novel hybridization probes for sequence-specific detection of single-stranded DNAs. Figure 4.8 displays the emission spectra of the ruthenium modified oligonucleotide in the absence and presence of different

Figure 4.7. Relative luminescent intensities of 2 μM solutions of Ru-NH(CH₂)₆NHCO₂AGAAGGCCTGGT-3' and hybridized duplex (top) and the noncovalently bound analogues (bottom) at 26° C and 37° C. Emission intensities are compared to a 10 μM [Ru(bpy)₃]²⁺ standard.

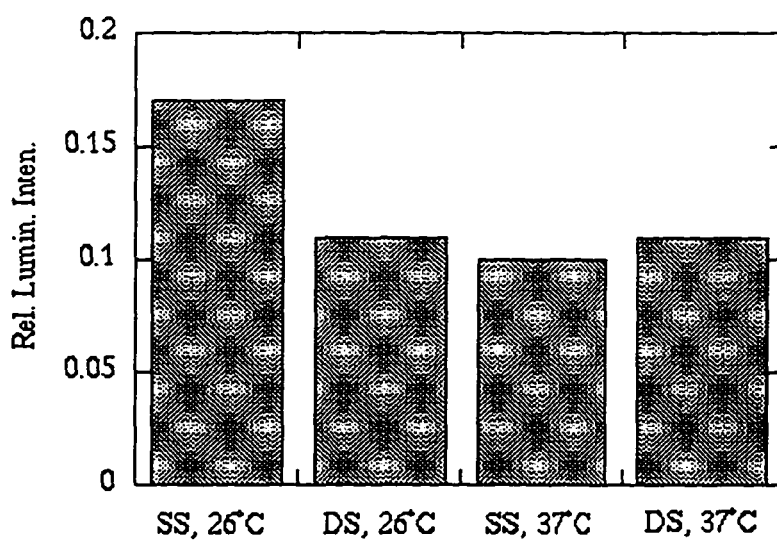
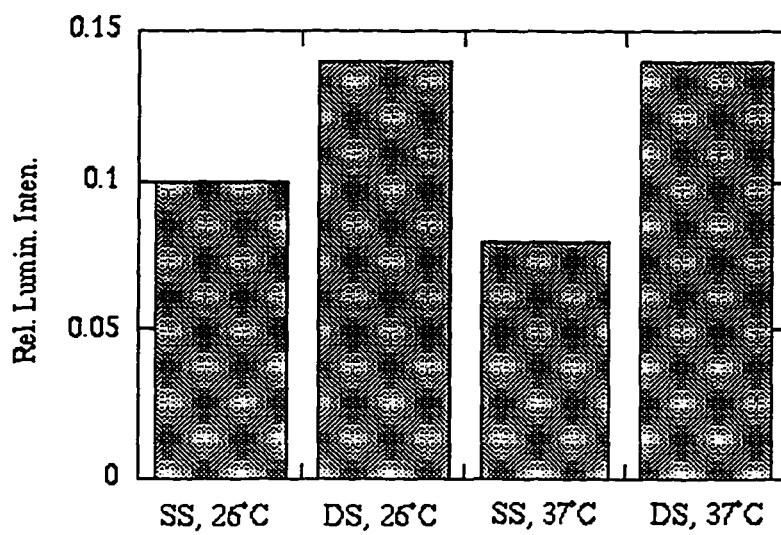
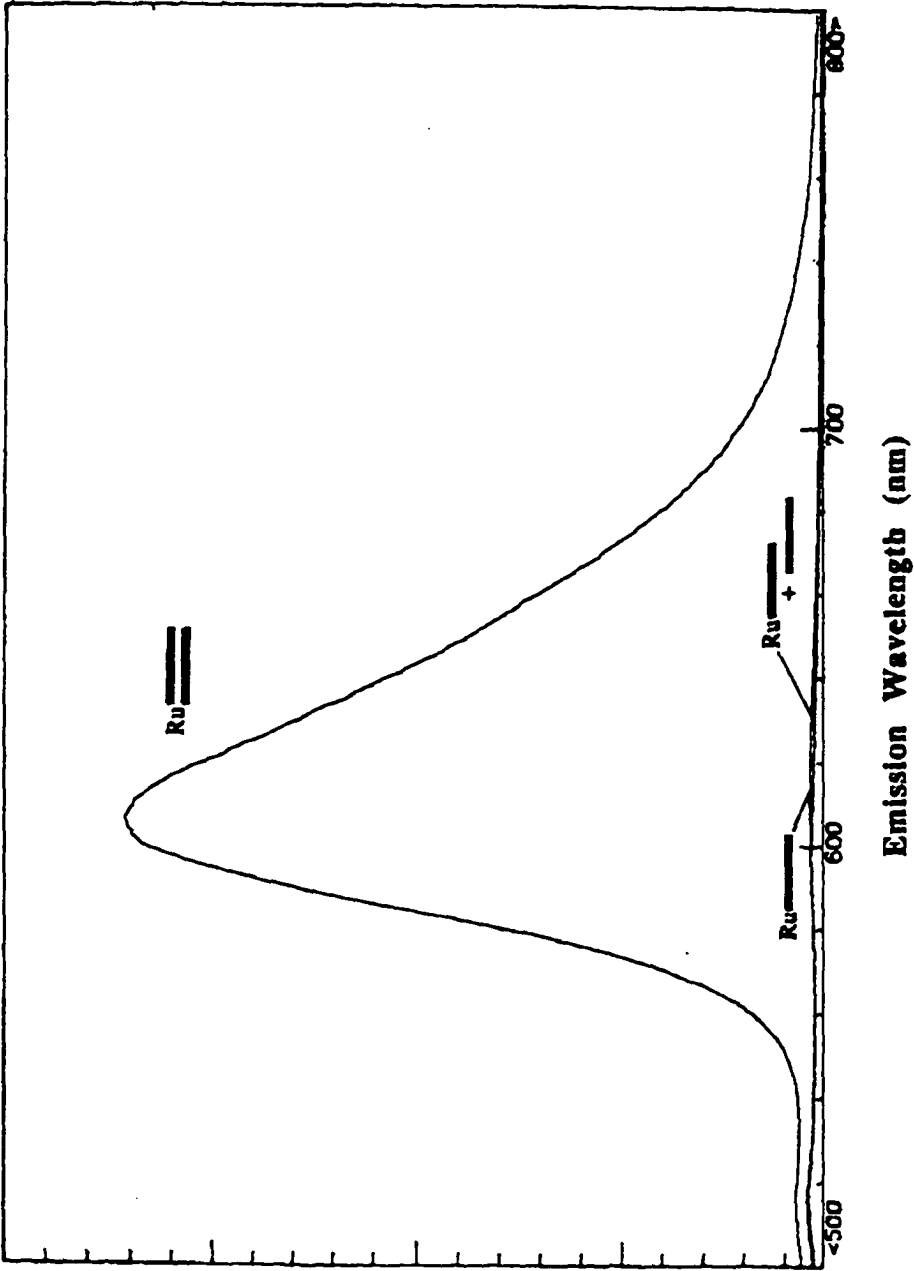


Figure 4.8. Emission spectra of the single-stranded metalated complex in the presence of its complementary strand (Ru=), in the absence of added oligonucleotide (Ru-), and in the presence of a noncomplementary strand (Ru- + -). Excitation is at 440 nm.



I

DNAs. By itself, the single-stranded metal complex shows little detectable luminescence. When annealed to its complementary strand bright photoluminescence is apparent. In contrast, in the presence of a noncomplementary strand, there is little emission enhancement. In effect, the oligonucleotide-derivatized metal complex can function as a sequence-specific molecular light switch, distinguishing it from other conjugates prepared with carbamate-based linkers.

Dilution experiments were performed to confirm the intramolecular nature of the ruthenium interaction; at $\leq 5 \mu\text{M}$ duplex, the luminescence is linear with concentration (Figure 4.9). Addition of unmodified duplex to the covalently bound duplex yields a $\leq 5\%$ change in the luminescence. As the amount of unmodified duplex is increased, a wavelength shift in emission maximum is observed as more intermolecular intercalation occurs. Addition of unmetalated duplex to the metalated single strand does lead to some luminescence and intermolecular intercalation.

The luminescence of the hybridized ruthenated duplex was used to characterize the molecular assembly. The comparative luminescence titrations for the ruthenium modified sequence 5'-AGTGCCAAGCTTGCA-3' are shown in Figure 4.10. Titration of free $[\text{Ru}(\text{phen})_2\text{dppz}]^{2+}$ into a solution containing unmetalated duplex results in a linear increase in the luminescence until the emission saturates at about three equivalents of ruthenium(II) per duplex. Competitive binding of ruthenium to the duplex is displayed with an average binding site of little more than four base pairs. The analogous experiment performed on the metalated duplex shows saturation of luminescence after addition of almost two equivalents of $[\text{Ru}(\text{phen})_2\text{dppz}]^{2+}$. The similarity in results obtained between the two duplexes demonstrates that the structural integrity of the duplex is maintained after covalent modification with the ruthenium.

Mismatch Experiments. Table 4.7 contains luminescence data for the metalated oligonucleotide annealed to a series of 15mers containing mismatches near or far from the intercalation site. The luminescence generally correlates with the relative stability of the

Figure 4.9. Dilution of a 10 μM solution of ruthenated 15mer oligonucleotide duplex. Luminescence intensity is measured relative to the luminescence of 10 μM ruthenated duplex.

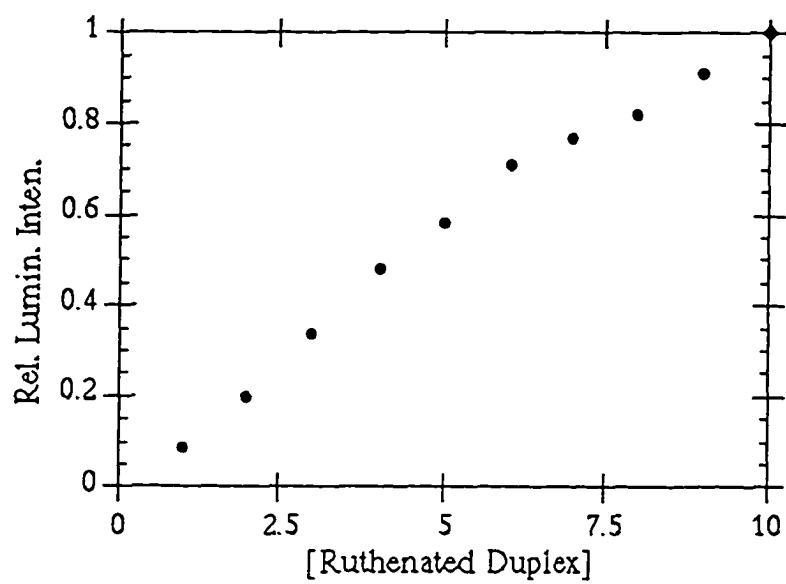


Figure 4.10. Luminescence titrations of free $[\text{Ru}(\text{phen}')_2\text{dppz}]^{2+}$ into oligonucleotide duplex containing Ru-NH(CH₂)₆OPO₂AGTGCCAAGCTTGCA-3' (right) and unmodified oligonucleotide duplex (left). The luminescence intensity for both duplexes saturates at a *total* ruthenium concentration of about three ruthenium complexes per 15 base pair duplex. Intensity is reported in arbitrary units.

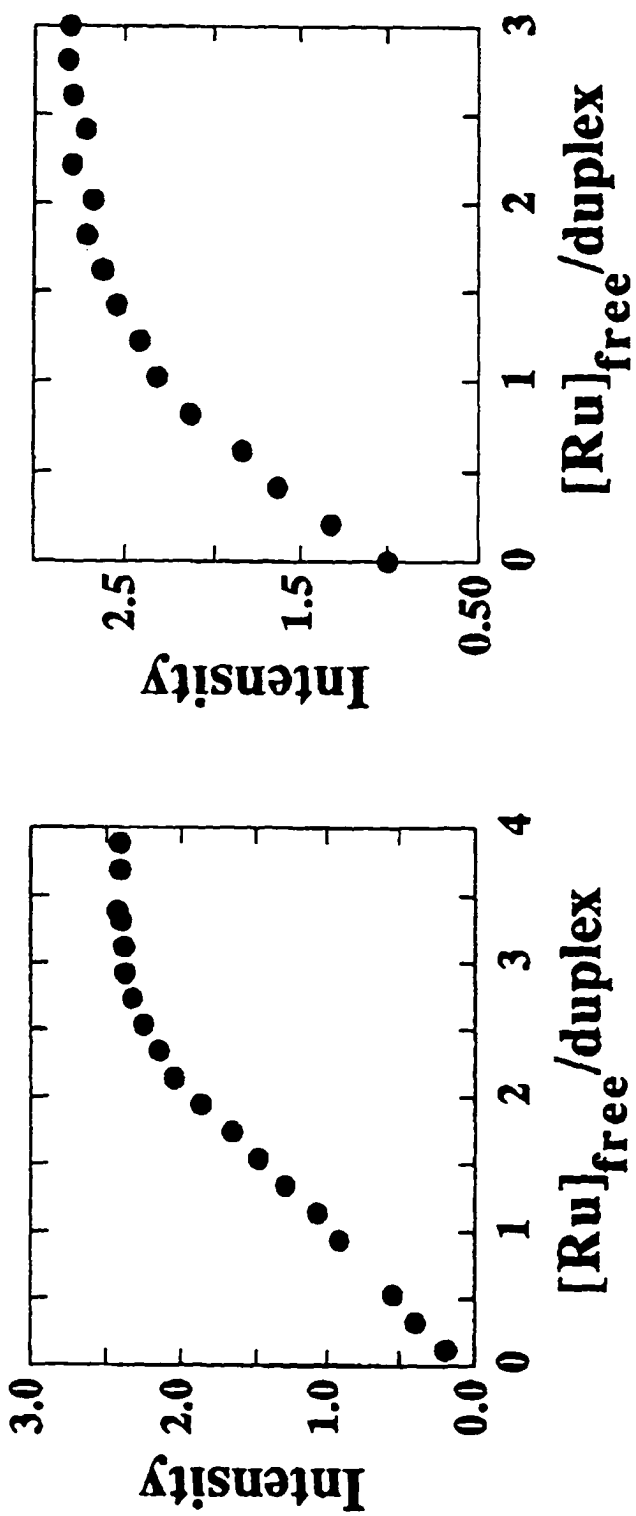


Table 4.7. Luminescence data for metalated oligonucleotides annealed to a series of 15mers containing various base mismatches.

<i>Sample</i>	<i>Number of base mismatches</i>	<i>R.I.</i>
ACGTTCGAACCGTGA + Ru TGCAAGCTTGGCACT	0	1
ACGTTCGAACCGTGA-(CH ₂) ₆ -NH ₂ -(Ru) TGCAAGCTTGGCACT	0	1.16
ACGTTCGAACCGTGA-(CH ₂) ₆ -NH ₂ -(Ru) TGCAAGCTTGGCCCT ↓	1	.68
ACGTTCGAACCGTGA-(CH ₂) ₆ -NH ₂ -(Ru) TGCCAGCTTGGCACT ↓	1	.37
ACGTTCGAACCGTGA-(CH ₂) ₆ -NH ₂ -(Ru) TGCCAGCTTGACACT ↓	2	.26
ACGTTCGAACCGTGA-(CH ₂) ₆ -NH ₂ -(Ru) TACCCGCCCTGACACT ↑ ↑ ↑ ↑	5	0.11

duplexes. As expected, the luminescence is decreased with a mismatch near the 5' terminus of the metalated strand, at a site where complex intercalation is likely. Not surprisingly, the luminescence is decreased to a substantially greater extent with a mismatch at the 3' terminus. This result is consistent with those obtained from the ruthenated duplexes discussed earlier which clearly illustrate how the duplex structure distal to the ruthenium binding site can affect the emission of the intercalated complex, reaffirming the unique sensitivity of the ruthenium complex.

The destabilizing effects of a base mismatch near the 5' end appear to be moderated by the stabilizing effect of complex intercalation, but a similar compensation is not available at the 3' end. The mismatch results, therefore, are consistent with intramolecular intercalation by the dppz complex tethered to the 5'-terminus. The stabilizing effect of complex intercalation upon base mismatches proximal to the complex binding site would be adverse for solution phase hybridization assays since the luminescence would not directly reflect proper duplex formation. By measuring the luminescence enhancement near the melting temperature of the ruthenated duplex, however, this temperature effect could be utilized to further discriminate between properly hybridized ruthenated duplexes and duplexes containing mismatches.

4.4. Implications for Diagnostic Application

Based upon the luminescence characterization of the above series of ruthenated duplexes, one area for further study comes to mind with respect to diagnostic applications. The highly sensitive nature of the ruthenium emission to its intercalating environment is a feature which should be exploited, but complete binding of the complex to its corresponding duplex must be ensured before this property can be utilized. It is apparent that, at least with the nonane carbamate linker, binding to the duplex has been weakened considerably relative to the noncovalently bound standard as evidenced by the dramatic decrease in emission intensity at high salt concentrations. An immediate solution might be

to use higher ruthenium concentrations. Unfortunately, the concentration range is limited due to the intermolecular interactions which occur at higher concentrations.

Because the binding sequences were not varied greatly due to the extreme sensitivity of the ruthenium emission, it is possible that an optimum binding site exists for the ruthenium complex. Although singlet oxygen-sensitized photocleavage studies suggested that no strong binding preferences existed for $[\text{Ru}(\text{phen})_2\text{dppz}]^{2+}$ binding (Chapter 2), other studies such as $^1\text{H-NMR}$ and luminescence measurements (section 4.3.1.) convincingly show that preferential binding does occur. The latter studies have an advantage in that those results are exclusively due to binding behavior and are not dependent on other extraneous factors such as base oxidation potentials and lifetimes of intermediate species. In addition to screening alternate ruthenium binding sequences, further investigations on the influences of linker length and orientation off the metal complex on the emission properties should be performed. Studies performed on detection of fluorescein-labeled DNA duplexes using fluorescence anisotropy using linkers of different lengths (4, 6, 9, and 12 carbons) gave optimal results with a six carbon linker.¹¹

The propensity of the ruthenated single-strand to luminesce by itself and also of the ruthenium complex to stabilize mismatches within its binding site renders solution phase detection difficult. Although the results obtained using the conjugate containing the phosphodiester linker appear to be very encouraging, we have been limited in exploring its capabilities by our synthetic methods; in addition to its low reproducibility, the synthesis was also low yielding. Solid-phase methods for constructing conjugates containing the functionalized phenanthroline ligand, phen', are also low yielding, making subsequent analysis difficult.

The differential effects of temperature upon the ruthenated single-strand and ruthenated duplexes may be valuable in solution phase detection by augmenting the observed discrimination. In addition, complex derivatives containing the bipyridine ligand may be used to construct the metalated oligonucleotides. Due in part to the increased

flexibility and the decreased hydrophobicity of the bipyridine ligand relative to the phenanthroline ligand, the emission of $[\text{Ru}(\text{bpy})_2\text{dppz}]^{2+}$ bound to nucleic acids appears more sensitive to conformational differences.² The increased sensitivity imparted by the bipyridine ligand combined with the increased luminescence enhancement from using a dipyrrophenazine derivative methylated at the 14' position on the phenazine ring (DPPX)¹² may result in a ruthenium complex with a lower affinity for single-stranded oligonucleotides and, consequently, greater luminescence enhancement upon hybridization.

4.5. Conclusion

A series of ruthenated oligonucleotides was constructed and the luminescence properties of their duplexes characterized in order to evaluate their utility as novel nucleic acid probes. Biochemical studies conducted on the ruthenated duplexes confirmed the absence of any significant structural perturbations caused by the 5' terminal modification. The structural integrity of these modified oligonucleotide duplexes was also confirmed using the unique spectroscopic features imparted by the ruthenium center. From photophysical studies, it was determined that even subtle alterations in the structure of these ruthenated strands significantly affected their luminescence properties due to the extreme sensitivity of the ruthenium complex to the nature of its binding environment. The photophysical properties of $\text{Ru-NH}(\text{CH}_2)_6\text{OPO}_2\text{AGTGCCAAGCTTGCA-3'}$ have been described in detail. The overall results of this investigation suggest that an oligonucleotide functionalized with a dppz complex of ruthenium may be used to target single-stranded DNA in a sequence-specific fashion and that this derivative could be extremely valuable in the development of novel hybridization probes for both heterogeneous and homogeneous assays.

References

- ^{1a}Friedman, A.E.; Chambron, J.-C.; Sauvage, J.-P.; Turro, N.J.; Barton, J.K., *J. Am. Chem. Soc.*, **1990**, *112*, 4960. ^{1b}Holmlin, R.E.; Barton, J.K., *Inorg. Chem.*, **1995**, *34*, 7.
- ²Jenkins, Y.; Friedman, A.E.; Turro, N.J.; Barton, J.K., *Biochemistry*, **1992**, *31*, 10809.
- ^{3a}Kumar, C.V.; Asuncion, E.H., *J. Am. Chem. Soc.*, **1993**, *115*, 8547. ^{3b}Tarui, M.; Doi, M.; Ishida, T.; Inoue, M.; Nakaike, S.; Kitamura, K. *Biochem. J.*, **1994**, *304*, 271-279.
- ^{4a}Dupureur, C.M.; Barton, J.K., *J. Am. Chem. Soc.*, **1994**, *116*, 10286. ^{4b}Dupureur, C.M., unpublished results.
- ^{5a}Hjort, C.; Lincoln, P.; Norden, B., *J. Am. Chem. Soc.*, **1993**, *115*, 3448. ^{5b}Haq, I.; Lincoln, P.; Suh, D.; Norden, B.; Chowdhry, B.Z.; Chaires, J.B., *J. Am. Chem. Soc.*, **1995**, *117*, 4788.
- ⁶Saenger, W. in *Principles of Nucleic Acid Structure*; Cantor, C. (Ed.); Springer-Verlag: New York; 1984.
- ⁷The isomer of C_1 symmetry was used to prepare these three sequences. Each synthesis yielded two major fractions of equivalent peak areas. It is believed, based upon the HPLC chromatograms of the reactions, that the 12mer and the 20mer fractions correspond to orientational isomers (differing in the position of linker orientation with respect to the metal center). The 9mer fractions are either resolved diastereomers or orientation isomers similar to the 12mer and the 20mer products. No CD spectra were measured to rule out resolved diastereomers.
- ⁸Drew, H.R.; Weeks, J.R.; Travers, A.A., *Embo J.*, **1985**, *4*, 1025.
- ⁹Terbrueggen, R.H.; Barton, J.K., *Biochemistry*, **1995**, *34*, 8227.
- ¹⁰Murphy, C.J.; Arkin, M.A.; Jenkins, Y.; Ghatlia, N.C.; Bossman, S.H.; Turro, N.J.; Barton, J.K., *Science*, **1993**, *262*, 1025.
- ¹¹Kumke, M.U.; Li, G.; McGown, L.B.; Walker, G.T.; Preston Linn, C., *Anal. Chem.*, **1995**, *67*, 3945.

¹²Hartshorn, R.M.; Barton, J.K., *J. Am. Chem. Soc.*, 1992, 114, 5919.